NEW WIENER SYSTEM BASED MODELING AND SIGNAL PROCESSING METHOD FOR CHARACTERIZATION OF VASCULAR FUNCTION

By

AMIT PATEL

A Dissertation submitted to the

Graduate School-New Brunswick

Rutgers, The State University of New Jersey

In partial fulfillment of the requirements

For the degree of

Doctor of Philosophy

Graduate Program in Electrical and Computer Engineering

Written under the direction of

John K-J. Li

And approved by

_____

_____

_____

_____

New Brunswick, New Jersey

October, 2017

ABSTRACT OF THE DISSERTATION

New Wiener System Based Modeling and Signal Processing Method

for Characterization of Vascular Function

By AMIT PATEL

Dissertation Director:

John K-J. Li

Central aortic blood pressure waveform ($\boldsymbol{P_a}$) is a critical determinant of the state of overall cardiovascular function, but it cannot be measured directly by noninvasive means. Numerous attempts were made to derive $\boldsymbol{P_a}$ from noninvasively measured peripheral pressure ($\boldsymbol{P_p}$) using mathematical transformations, transfer function or arterial system modeling approaches. These techniques, in general, do not account for inter-subject or intra-subject variability. A few methods have recently been proposed to generate personalized adaptive transfer function employing arterial system modeling. However, these personalized models have to be calibrated across different patients at different times and the model algorithms are very sensitive to calibration technique and calibration error. More recently, multi-channel blind system identification (MBSI) have been implemented on these systems to mathematically derive common source $\boldsymbol{P_a}$ based on multiple $\boldsymbol{P_p}$ inputs. This method seems to afford self-calibrating and minimizes estimation error. In

general, MBSI approaches are more convenient and practical for aortic pressure estimation, but have not been widely adopted.

In this thesis, the arterial system is proposed to be modeled as a Weiner System with linear finite impulse response (FIR) filter accounting for larger arteries transmission channel and non-linear memoryless function block accounting for all nonlinearities due to narrowing of arteries, branching and visco-elastic forces. This model is then experimentally validated with seven human blood pressure datasets. Single input and multiple output (SIMO) or aortic-to-radial arterial transmission channel and aortic-to-femoral arterial transmission channel are established. To model the nonlinear memoryless monotonic function in the Wiener System model a correlation study is performed for linear finite impulse response (FIR) filter simulated peripheral pressure vs. measured peripheral pressure waveform. Each of this correlation curves were fitted to linear, quadratic and cubic polynomial equation. It was found that Wiener model with 3^{rd} order polynomial function yielded better modelling accuracy than that from 2^{nd} order polynomial function which in turn was better than mere linear FIR filter.

$\boldsymbol{P_a}$ estimation technique is then presented by modeling arterial system as Multi-channel Weiner System. With this structure when pressure waveforms are measured from two distinct peripheral locations, multichannel blind system identification (MBSI) technique can be used to estimate common input pressure signal or $\boldsymbol{P_a}$. Nonlinear MBSI method was employed on human blood pressure waveforms (7 datasets). Results show $\boldsymbol{P_a}$ can be accurately derived. This method by nature is self-calibrating to account for any inter-personal, along with intra-personal, vascular dynamics inconstancy. Besides $\boldsymbol{P_a}$ estimation, the proposed MBSI method also allows extraction of system dynamics for

vascular channels. Initially, linear finite impulse response (FIR) filter is assumed to be of fixed 10^{th} order in the Wiener System model across all patient dataset. To further improve performance of this aortic pressure estimation method, a new and improved method is developed which estimates channel order preceding arterial system identification. By using effective channel order, system identification is optimized which then enhances aortic pressure estimation. Results showed significant improvement over our earlier method with far more accurate aortic pressure estimation. The outcome of the novel method as presented by this dissertation has the potential to enhance clinical diagnostic accuracy and subsequent treatment efficacy assessment.

Acknowledgements

I am grateful to Professor John K-J. Li for his advice, encouragement, trust and support over my Ph.D. years. He has been an excellent advisor and always directed me toward doing fundamental research that will make a difference. He also exposed me to infinite possibilities by doing research in Aortic Pressure Estimation, Reflection Coefficient, Augmentation Index, Apparent Phase Velocity, Attenuation Constant, etc.

I would also like to thank Dr. Michael McMurtry and Dr. Barry Finegan from the Department of Anesthesiology & Pain Medicine at the University of Alberta for their technical contributions to the data collection that was used to study and validate human arterial system model.

Dedication

This thesis is dedicated to my new born girl Yashvi, wife Akanksha Patel, and to my parents, Mahendra and Kailash Patel, who have supported me all the way since the beginning of my studies. Also, this thesis is dedicated to all those who value and aspire creativity.

Table of Contents

Chapter 1: Introduction

1.1 Background

Knowledge about the magnitude and shape of the central aortic pressure wave provide very important information regarding cardiac function and heart-blood vessel interaction. Furthermore, aortic pressure waveform can be used to derive valuable clinical information particularly in hypertension an in patients with coronary arterial disease (Li, 2000) regarding vascular stiffness, wave reflections, augmentation index, aortic flow, ventricular ejection duration, arterial compliance and systolic load and other features useful in the clinical examination (Li, 2000; Li, 2004; O'Rourke et al., 1992; Murgo et al., 1980; Wesseling et al., 1993; Li et al., 1990; Li and Zhu, 1994). Thus, analysis of aortic pressure waveform morphology has recognized significance during patient assistance and also to monitor drug-cardiovascular system interaction.

Despite the vast usefulness of aortic pressure waveform, its routine utilization is hampered due to invasiveness of aortic pressure measurement procedures through catheterization (Li et al., 1976). This is not a preferred method for routine screening, diagnosis or therapy follow-up, because of its invasiveness and large underlying cost. Noninvasive continuous monitoring of peripheral artery pressure with photoplethysmography and applanation tonometry (Imholz et al., 1998; Kelly et al., 1989; Söderström et al., 2002) are preferred. For the latter, radial artery is the most common application site as its underlying bony tissue aids more optimal applanation as flat artery walls features transmural forces to be perpendicular to blood vessel surface (Drzewiecki et al., 1983).

Aortic pressure wave encounters complex wave reflection in arterial network as it travels from aorta to peripheral sites (Li, 2004). These wave reflections result in amplification of systolic and pulse pressures with their magnitudes depending on arterial network properties and its corresponding transmission path (Karamanoglu et al., 1995). Systolic pressure in radial arteries becomes significantly larger than in central aorta. So, cardiac afterload and perfusion has to be derived from aortic pressure or more central arterial pressure rather than calculating them directly from peripheral arterial pressure waveforms (Waddell et al., 2001).

Above mentioned clinical significance of central aortic pressure waveform warrants investigation on noninvasive estimation of aortic pressure. Numerous research activities have been undertaken to transform non-invasive peripheral pressure data (such as carotid artery (Chen et al., 1996), brachial artery (Karamanoglu et al., 1995), and radial artery pressure (Chen et al., 1997) to central aortic pressure waveform using mathematical transformations and/or mathematical models (Karamanoglu et al., 1995). Most of these methods, generally, involve peripheral-to-aortic pressure transfer function derivation, averaged over group of patients (Söderström et al., 2002). This transfer function is then used to convert peripheral pressure wave to aortic pressure wave. The "generalized transfer function" techniques are based on the primary assumption that heart and arterial tree properties are consistent between all patients and at all times. It is well known that these properties differ with different subjects, age and medical condition. Thus, a few techniques have been proposed for personalized transfer function employing arterial system modeling (Stergiopulos et al., 1998; Karamanoglu and Feneley, 1997; Segers et

al., 2000; Sugimachi et al., 2001; Swamy et al., 2009; Stok, 2016; Xiao et al., 2017; Guala et al., 2017).

Some of Medical Devices currently available in the market that provide non-invasive aortic pressure estimation solution are: 1. SphygmoCor designed and developed by an Australian-headquartered company, AtCor Medical Limited. 2. Mobil-O-Graph designed and developed by a German-headquartered company I.E.M. GmbH. (Papaioannou et al., 2016)

Several studies have focused on the estimation of central aortic pressure from more easily available peripheral pressure waveforms. Lack of standardization, pressure waveforms were recorded at different peripheral arterial sites, such as the femoral, carotid, radial and finger arteries and transfer function/model is subsequently applied to derive estimated aortic pressure waveform. Many of these approaches can broadly be classified into three different categories; these are summarized in the following sections:

1.2 Black Box System Identification or Generalized Transfer Function

These types of aortic pressure estimation method normally convert peripheral pressures to aortic pressure using a general/ generic transfer function. Hence, this type of approach does not account for inter-subject as well as intra-subject variability.

1.2.1 Autoregressive Exogenous (ARX) Method

Mathematical transformation was applied by Chen et at. (Chen et al., 1997) from recorded radial arterial pressure waveform to estimate aortic pressure noninvasively, while invasive aortic pressure was measured simultaneously at different hemodynamic conditions (steady state, Valsalva maneuver, abdominal compression, nitroglycerin and

vena caval obstruction). For each of this case, individual transfer function between radial pressure and its corresponding aortic pressure was calculated using linear Auto-regressive exogenous model. According to the linear ARX (autoregressive exogenous) Model a causal linear system can be expressed in terms of input (current and past) and output data (past)

$$T(t) = -a_1T(t-1) - a_2T(t-2) - \cdots - a_{na}T(t-na) + b_1P(t-1) + \cdots + b_{nb}P(t-nb) \quad (1\text{-}1)$$

where $T(t-x), 0 \leq x \leq na$ represent present and past output while $P(t-x), 1 \leq x \leq na$ are previous input. Here, a_y, $1 \leq y \leq na$ and b_z, $1 \leq z \leq nb$ are weights for respective terms and hence they are characteristics of the model.

Linear ARX model was found to result in better estimation for a given length of data set as compared to Fourier transform based method. These individual transfer functions were then averaged to obtain general transfer function. Because of averaging any particular difference among individual transfer functions was lost. Albeit this, central aortic pressure estimated using generalized transfer function was comparable to measured aortic pressure with ≤0.2±3.8 mmHg error, arterial compliance to 6±7% accuracy, and augmentation index to within −7% (30±45% accuracy) (Chen et al., 1997). This ARX based generalized transfer function method yielded reasonable estimation for aortic pressure and arterial compliance. But augmentation index estimation from this method was unacceptable as augmentation index would need higher precision aortic pressure wave re-construction.

1.2.2 Neural Network Nonlinear ARX (NNARX) Method

Neural network-based autoregressive exogenous model (NNAW model) was proposed by Varanini et al. (Varanini et al., 2003) for central aortic pressure derivation from peripheral pressure. This method first trains a neural network based nonlinear model, which is later used to reconstruct central arterial pressure (output) from radial pressure waveform (input). A generalized nonlinear autoregressive exogenous (NARX) model can be represented by following equation

$$y(t) = f(y(t-1), \dots, y(t-n_a), x(t-d), \dots, x(t-d-n_b+1)) + \varepsilon(t) \quad (1\text{-}2)$$

where t is time, $y(t)$ is model output, $x(t)$ is model input, $\varepsilon(t)$ is white noise and $f(.)$ is a nonlinear function. The $f(.)$ is nonlinear function of past input and out values of the model. The problem was defined to estimate the unknown function $f(.)$ using training data set (x, y) with objective to minimize the estimation error $e(t)$; i.e. is disparity between measured output y and estimated $\hat{y}$.

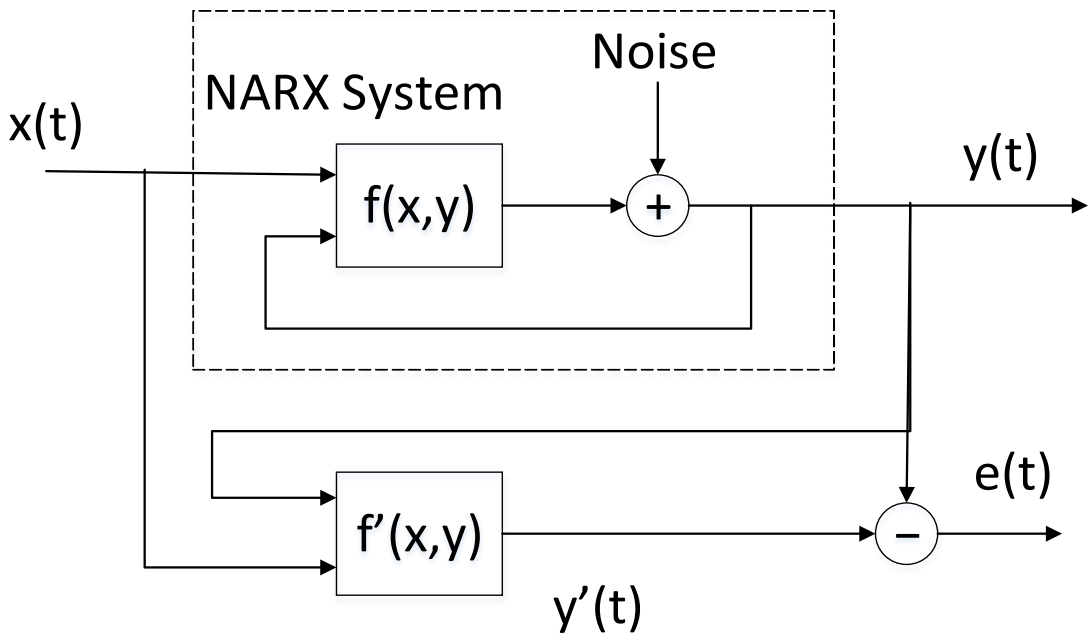

Fig. 1-1. Neural Network Auto-regressive exogenous model proposed by Varanini et al. for central aortic pressure (input) derivation from peripheral pressure (output)

Radial tonometry pressure along with invasive aortic pressure was measured in 20 patients. Out of these 10 patients data set was used to train the model parameter and rest 10 patients data set was used to test/ validate the model. It was found that NNARX model resulted in more accurate aortic wave reconstruction (especially more detailed dicrotic notch and systolic inflexion pressure) as compared to linear ARX model. Thus, augmentation index calculated from NNARX method was more accurate than one from ARX estimated aortic pressure. (Varanini et al., 2003)

1.3 Gray Box System Identification (Personalized Transfer function)

Generalized transfer function initially gained popularity owing to its simplicity; same generic transfer function or model is applied to derive aortic pressure curve from peripheral pressure for all patients irrespective of their medical condition. Nonetheless, as

noted previously, cardiovascular properties are different from patient to patient and can also vary for a given patient depending on his/her physiological state. Hence generalized transfer function does not rationalize either inter-subject or intra-subject variability. Generalized transfer function estimated aortic pressure is normally biased depending on training set. Having personalized or adaptive transfer function or model will be far more valuable as it can accommodate inter-subject and temporal variability of arterial tree. The tube model and wave separation method are excellent example of individualized peripheral-to-aortic pressure transformation technique.

1.3.1 The Wave Separation Method

Resolution of blood pressure waveform into its forward ($\boldsymbol{P_f}$) and reflected ($\boldsymbol{P_r}$) or backward ($\boldsymbol{P_b}$) waves in the time domain was first proposed by Li (Li, 1986). Time domain method is efficient and can be easily visualized. An example of this methodology is shown below in Figure 1-2.

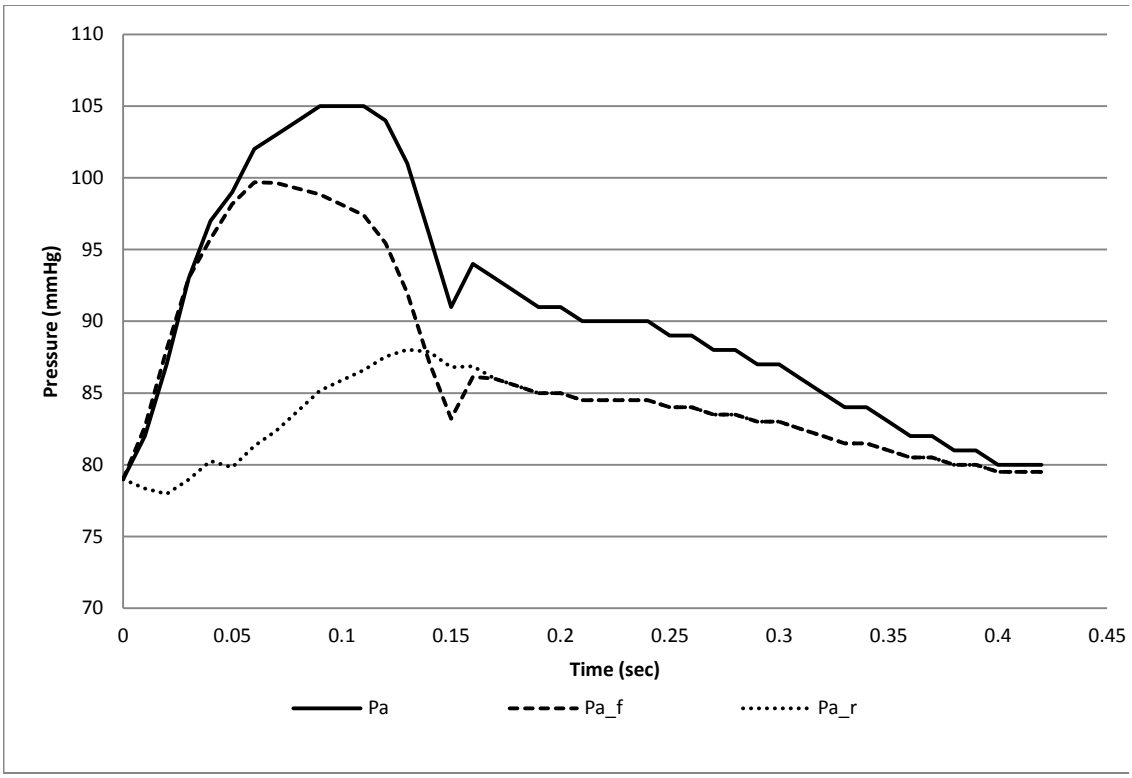

Fig. 1-2. Aortic pressure waveforms resolved into its forward ($\boldsymbol{P}_f$) and reflected ($\boldsymbol{P}_r$) components by Li's time-domain method. It can be seen that forward and reflected pressures undergo constructive addition to result in the measured aortic pressure.

Stergiopulos et al. (Stergiopulos et al., 1998) proposed a time domain approach to estimate aortic pressure curve from tonometer measured peripheral pressure and flow velocity curve. This method first decomposes measured peripheral pressure P_p (and velocity V_p) into their forward and backward counterparts:

$$P_f = Z_c.V_f(t) = [P_p(t) + Z_c.V_p(t)]/2 \quad (1\text{-}3)$$

and

$$P_b = Z_c.V_b(t) = [P_p(t) - Z_c.V_p(t)]/2 \quad (1\text{-}4)$$

where subscripts f and b denote forward and backward waves, respectively, and Z_c is the characteristic impedance of the artery. It is noted here that noninvasive flow velocity can be commonly measured with an ultrasound Doppler probe.

In the equations above, characteristic impedance Z_c was calculated as average slope of pressure-velocity curve in early systole, as shown by Li (Li, 1986). After separation, forward pressure wave is delayed (by time T_d) to account for the time it takes for travelling from aorta to peripheral site. On the other hand, reflected wave is advanced in time as this wave component is approaching toward central aorta. These time shifted wave counterparts are summed to recreate aortic pressure. When tested, this method was able to estimate aortic systolic pressure, diastolic pressure and complete waveform with mean squared error of 0.1, 1.0 and 1.56 mmHg respectively. As this wave separation method utilized parameters Z_c and T_d obtained on per-patient basis, aortic pressure estimated using this personalized transfer function is better predictor of true aortic pressure as compared to one derived from generalized transfer function.

1.3.2 The Tube Model Method

Characterizing the tube load in order to obtain transfer function was first utilized by Sugimachi et al. (Sugimachi et al., 2001) and Westerhof et al. (Westerhof et al., 2007). The frequency (ω) dependent impedance $Z_i(\omega)$ of terminal load can be characterized by two parameters (see equation below; Ai and Bi, where 0<Ai<Bi). The values of these parameters depend on the peripheral resistance and compliance. The resultant pressure signal $p_{art}(t)$ {or flow signal $q_{art}(t)$} at any arterial tube site can be written in terms of forward and backward pressure (or flow) signals after accounting for wave propagation

delay (T_d) between signal probe site (peripheral artery) and signal originating site (aorta) by proper time shifting of forward/reflected signal.

$$p_{art}(t) = p_f(t + T_d') + p_b(t - T_d') \quad (1\text{-}5)$$

$$q_{art}(t) = q_f(t + T_d') + q_b(t - T_d') \quad (1\text{-}6)$$

Swamy et al. modelled arterial tree as parallel tube of pressure and flow (Swamy et al., 2009). As shown in Figure 1-3, the arterial system is represented as parallel m tubes along with series terminal load elements. Here the aorta is connected to i^{th} peripheral artery through i^{th} tube with constant characteristic impedance Z_{ci}. This tube allows pressure wave to propagate from aorta through peripheral arterial end site with a constant time delay T_{di}. The i^{th} terminal load implies arterial bed distal to i^{th} peripheral artery. As shown in the arterial tree tube model figure below, peripheral artery pressure ($p_{pi}(t)$) can be derived from aortic pressure [$p_a(t)$] using transfer function (Stergiopulos et al., 1998). Here, the model parameters T_{di}, A_i and B_i are unknown and are characteristic to individual subjects transfer function for a given time.

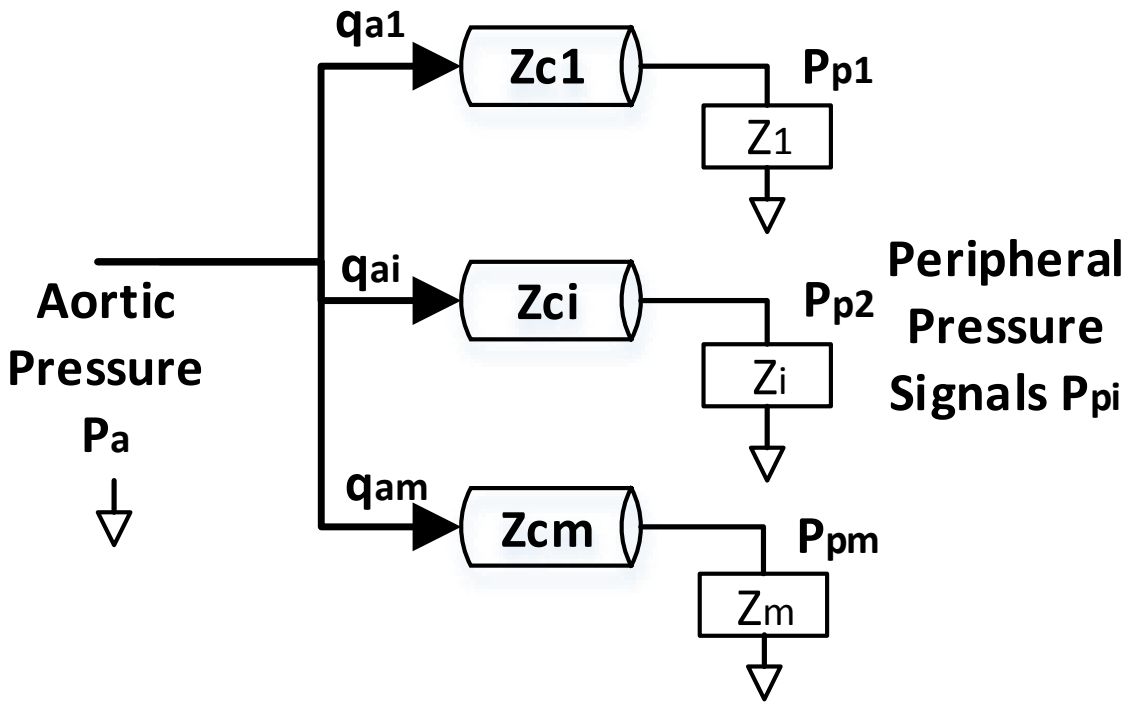

Fig. 1-3. Parallel tube model of pressure and flow in the arterial tree on which the aortic pressure estimation technique is based. Here, Z_{ci} is characteristic impedance and $Z_i(\omega)$ is terminal load.

Where characteristic impedance Z_{ci} corresponding to ith tube with constant is given by

$$Z_i(\omega) = \frac{Z_{ci}(j\omega + B_i)}{j\omega + A_i} \tag{1-7}$$

where i=1,2,…m

Transfer function relating a peripheral pressure waveform $p_{pi}(t)$ to the aortic pressure waveform $p_a(t)$ in terms of the unknown parameters of the model

$$TF_{ppi2pa} = \frac{\left(\frac{B_i + A_i}{2} + j\omega\right) e^{j\omega T_{di}} + \frac{B_i - A_i}{2} e^{-j\omega T_{di}}}{B_i + j\omega} \quad (1\text{-}8)$$

Transfer function relating $p_{pi}(t)$ to the arterial flow waveform at the corresponding tube entrance $q_{ai}(t)$ in terms of the same parameters.

$$TF_{ppi2qai} = \frac{\left(\frac{B_i + A_i}{2} + j\omega\right) e^{j\omega T_{di}} - \frac{B_i - A_i}{2} e^{-j\omega T_{di}}}{Z_{ci}(B_i + j\omega)} \quad (1\text{-}9)$$

For T_{di} calculation carotid artery pressure was measure using non-invasive tonometry. T_{di} is estimated a time difference between beginning of systole in carotid pressure and measured tonometry peripheral arterial pressure (Sugimachi et al., 2001). T_{di} does not normally vary frequently; T_{di} measurement once a week or even month is generally sufficient for re-calibrating the tube model parameters (Swamy et al., 2009). Subsequently, the tube model parameters are computed iteratively using 15 cycles of measured peripheral waveform and previously measured T_{di}. Different values of parameters are guessed; for each of these value aortic pressure waveforms are derived using the tube model peripheral pressure-to-aortic pressure transfer function shown above. Only those pairs of parameters that yield physiologically feasible pressure waveforms are used to derive flow waveform from peripheral waveform using tube model peripheral pressure-to-aortic flow transfer function shown above. Assuming that aortic valve closes completely during diastole, blood flow through aorta (and thus peripheral artery) during this period can be approximated as negligible. With this assumption, the parameters that provide minimum aortic flow during diastole are chosen.

Ultimately, the trained transfer function with optimized parameters is applied to transform measured peripheral pressure wave to aortic pressure wave. As these parameters are calibrated for each of the patients, the tube model is capable of adapting to inter-subject and intra-subject variation. To validate this method, it was applied on the 6 healthy dogs for which simultaneous aortic and peripheral pressure signals were acquired. Aortic pressure waveforms were constructed from measured peripheral pressure waveforms using this method and then compared with measure aortic pressure waveforms. RMS error between derived and measured aortic pressure for complete waveform, systolic and pulse pressure were 3.7, 4.3 and 3.4 mmHg, respectively. This was an improvement over ARX based generalized transfer function with errors of 4.8, 6.1 and 6.7 mmHg, respectively.

1.4 Blind System Identification

More recently, blind system identification are been implemented to predict aortic pressure wave from two or more of peripheral arterial pressure wave. These methods generally model arterial tree as single input, multiple output (SIMO) system. Multichannel blind system identification is applied on these systems to mathematically derive common source aortic pressure which, in multichannel system, caused multiple outputs (i.e. peripheral pressure).

1.4.1 Multichannel Blind System Identification (MBSI) Method

Multichannel blind system identification using eigenvector algorithm based FIR filter identification technique was proposed by Swamy et al. (Swamy et al., 2007),utilizing previously established signal processing methodology (Abed-Meraim et al., 1997), for aortic pressure estimation from two or more peripheral pressure signals.

Arterial tree is modeled as single-input, multiple-output system with peripheral pressure signals $p_{pi}(t)$ (where i≥2) as system output and aortic pressure signal $p_a(t)$ as system input. Pressure wave transmission channel are modeled by linear time invariant (LTI) system impulse responses $h_i(t)$; this $h_i(t)$ is believed to preserve cardiovascular dynamic properties of i^{th} transmission channel (arteries). It is assumed that these LTI channels can be well defined by finite impulse response and they are coprime with each other (i.e. their Z transforms don't have any common zeros or poles).

As seen in the diagram below (Figure 1-4), mathematically peripheral pressure measured at different peripheral artery can be expressed as convolution of their respective transmission channel impulse response $h_i(t)$ and aortic pressure signal $p_a(t)$:

$p_{pi} = h_i \otimes p_a$, where terms with "i" suffix denotes quantities for i^{th} peripheral arterial system

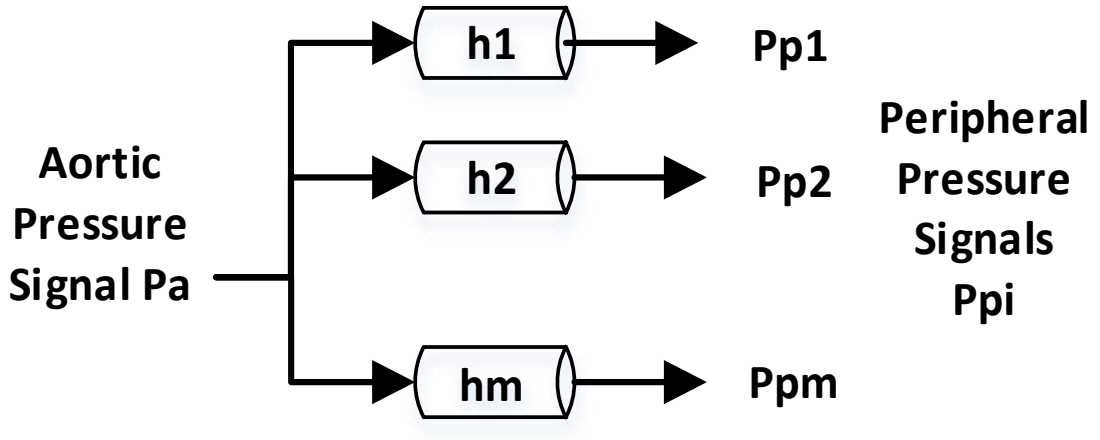

Fig. 1-4. The single-input, multi-output model of the arterial tree with peripheral pressure signals $p_{pi}(t)$ (where i≥2) as system output and aortic pressure signal $p_a(t)$ as system input. This is used for multichannel blind system identification to estimate aortic pressure

Also, every peripheral arterial channel impulse response can be expressed in terms of any of other peripheral arterial channel impulse response, i.e.

$$p_{pi}(t) \otimes h_j(t) = [p_a(t) \otimes h_i(t)] \otimes h_j(t) \tag{1-10}$$

$$= h_i(t) \otimes \left[p_a(t) \otimes h_j(t)\right]$$

$$= h_i(t) \otimes p_{pj}(t), where\ i \neq j$$

For proof of concept, this method was implemented using two peripheral artery pressure as two channel blind system identification. Above equation involving convolution can be written as convolution sum and also account for measurement noise and/or modeling error e(t):

$$\sum_{k=0}^{L-1} h_1(k)p_{p2}(t-k) - \sum_{k=0}^{L-1} h_2(k)p_{p1}(t-k) = e(t) \quad (1\text{-}11)$$

tϵ[L-1,N-1]

here L and N are number of FIR filter order and sample size of acquired discrete peripheral pressure wave respectively. This equation can also be represented in cascaded matrix form using Hankel Matrix:

$$\underbrace{[P_{p2} - P_{p1}]}_{P}\underbrace{\begin{bmatrix} h_1 \\ h_2 \end{bmatrix}}_{h} = e \quad (1\text{-}12)$$

Hankel Matrix P_{pi} is defined as:

$$P_{pi} = \quad (1\text{-}13)$$

$$\begin{bmatrix} p_{pi}(0) & p_{pi}(1) & \cdots & p_{pi}(L-1) \\ p_{pi}(1) & p_{pi}(2) & \cdots & p_{pi}(L) \\ \vdots & \vdots & \ddots & \vdots \\ p_{pi}(N-L) & p_{pi}(N-L+1) & \cdots & p_{pi}(N-1) \end{bmatrix}, i \in [1,2]$$

Above equation is essentially an optimization problem to minimize error e which can be solved using linear algebra concept of null space. The nullspace of matrix P is made up of vectors h for which $\boldsymbol{Ph} = \mathbf{0}$. Once computed, h_i are then used to reconstruct aortic pressure $p_a(t)$.

Each of the measured peripheral pressure and aortic pressure relation can be written in form of convolution sum:

$$p_{pi}(t) = \sum_{k=0}^{L-1} h_i(k) p_a(t-k) + n_i(t) \tag{1-14}$$

Where $n_i(t)$ represents noise/ error in measurement or system modelling. The set of two peripheral pressure equations can laid out in matrix form using Toeplitz matrices H_i.

$$\underbrace{\begin{bmatrix} p_{p1} \\ p_{p2} \end{bmatrix}}_{P_p} = \underbrace{\begin{bmatrix} H_1 \\ H_2 \end{bmatrix}}_{H} p_a + \underbrace{\begin{bmatrix} n_1 \\ n_2 \end{bmatrix}}_{n} \tag{1-15}$$

Toeplitz matrix H_i is defined as:

$$H_i = \begin{bmatrix} h_i(L-1) & \cdots & h_i(0) & \cdots & 0 \\ \vdots & \cdots & \vdots & \cdots & \vdots \\ 0 & \cdots & h_i(L-1) & \cdots & h_i(0) \end{bmatrix} \tag{1-16}$$

Above mentioned matrix equation is basically optimization problem to minimize noise n which can be solved (to a scale factor) using least square estimation (Abed-Meraim et al., 1997):

$$p_a = (H^T H)^{-1} H^T P_p \tag{1-17}$$

Finally, the reconstructed aortic pressure was scaled such that mean peripheral pressure is same as mean aortic pressure. This step is justified by Poiseuille's law (Noordergraaf, 1978). Thus scaled aortic pressure $p_a^s(t)$ can be computed as follows:

$$p_a^s(t) = p_a(t).\frac{Mean(p_{pi}(t))}{Mean(p_a(t))} \tag{1-18}$$

Thus this method calculates personalized arterial system model transfer function and does not resort to generalized transfer function. Swamy et al. (Swamy et al., 2007) applied their method using two peripheral (femoral and radial) pressure data from four

swine which was then validated against respective measured aortic pressure. From estimated aortic pressure waveform the root mean squared error was found to be 4.6mmHg, 6.1mmHg and 7.1mmHg for total waveform, Systolic pressure and Pulse pressure respectively.

1.4.2 Laguerre-Model MBSI Method

A Laguerre-Model based multichannel blind system identification method was shown by McCombie et al. (McCombie et al., 2005) to estimate common system input (aortic flow) from multiple system output (peripheral arterial pressures). This method first models the hemodynamics of each branch in form of Laguerre functions as Laguerre orthonormal basis functions are known to help reduce number of FIR filter coefficients to precisely characterize arterial system irrespective of its slow decaying dynamics. A normal Laguerre expansion series is expressed as

$$V_k(z) = \frac{K}{(z-a)}\left(\frac{1-az}{z-a}\right)^{k-1} ; with\ K = \sqrt{(1-a^2)T} \tag{1-19}$$

Here parameter "a" serve as slowest decaying system pole and T is the sampling period. With this Laguerre function representation, arterial system FIR filter can be written as

$$\widehat{H}_i(z) = \sum_{k=1}^{L_i} b_k^{(I)} \frac{K}{(z-a)}\left(\frac{1-az}{z-a}\right)^{k-1} \tag{1-20}$$

where i denotes ith channel dynamic arterial system. Consider two channel MBSI equality condition with Y_1 and Y_2 being measured peripheral arterial pressures (which are input to MBSI model):

$$H_1 Y_2(n) = H_2 Y_1(n) \tag{1-21}$$

Rewriting above equation with Laguerre function representation of FIR filters:

$$\left(\sum_{k=1}^{L_2} b_k^{(2)} \frac{K}{(z-a)}\left(\frac{1-az}{z-a}\right)^{k-1}\right) Y_1(n) \tag{1-22}$$

$$= \left(\sum_{k=1}^{1} b_k^{(1)} \frac{K}{(z-a)}\left(\frac{1-az}{z-a}\right)^{k-1}\right) Y_2(n)$$

Or

$$\sum_{k=1}^{L_2} b_k^{(2)} x_k^{(1)}(n) = \sum_{k=1}^{L_2} b_k^{(1)} x_k^{(2)}(n)\,; with\ x_k^{(i)} \tag{1-23}$$

$$= \frac{K}{(z-a)}\left(\frac{1-az}{z-a}\right)^{k-1} Y_i(n)$$

$x_k^i(n)$ are k[th] order filter coefficients of i[th] channel system for a given n[th] time series of observed n[th] output series $Y_i(n)$. Above mentioned summation equation can written in matrix multiplication form:

$$\underbrace{\begin{bmatrix} x_1^{(1)}(n) & \cdots & x_{L_2}^{(1)}(n) \\ \vdots & \ddots & \vdots \\ x_1^{(1)}(n-N & \cdots & x_{L_2}^{(1)}(n-N) \end{bmatrix}}_{X_1} \underbrace{\begin{bmatrix} b_1^{(2)} \\ \vdots \\ b_{L_2}^{(2)} \end{bmatrix}}_{B_2} \tag{1-24}$$

$$- \underbrace{\begin{bmatrix} x_1^{(2)}(n) & \cdots & x_{L_1}^{(2)}(n) \\ \vdots & \ddots & \vdots \\ x_1^{(2)}(n-N & \cdots & x_{L_1}^{(2)}(n-N) \end{bmatrix}}_{X_2} \underbrace{\begin{bmatrix} b_1^{(1)} \\ \vdots \\ b_{L_1}^{(1)} \end{bmatrix}}_{B_1} = \begin{bmatrix} 0 \\ \vdots \\ 0 \end{bmatrix}$$

Or

$$[X_1 \quad -X_2].\begin{bmatrix} B_1 \\ B_2 \end{bmatrix} = 0 \tag{1-25}$$

In order to solve for B_1 and B_2 in above equation, null space of $[X_1 \quad -X_2]$ was computed using singular value decomposition.

Thereafter, with thus computed channel dynamics B_1 and B_2 the input cardiac output u(t) is estimated from measured peripheral pressure by de-convolving one of the transfer function from its corresponding channel output. For this a deconvolution method, based on Gurelli and Nikias (Gürelli and Nikias, 1995), was used.

This algorithm was applied to swine data for validation. Catheterization of left radial artery and right iliac artery and cardiac output flow were measured to assess the performance of the Laguerre based MSBI method. They first compared measured peripheral pressures against model estimated peripheral pressures. Two peripheral pressure waveforms were used to train the Laguerre model, i.e. two arterial system transfer functions. Using these estimated FIR filters along with measured Cardiac output, respective radial and iliac arterial pressure data were reproduced. These simulated radial and iliac arterial pressures $\widehat{y_i}$(t) were correlated with corresponding measured signals y_i(t) using mean absolute percent error MAPE:

$$MAPE = \left(\frac{1}{N}\sum_{n=1}^{N}\frac{\widehat{y_i}(n) - y_i(n)}{y_i(n)}\right) \times 100 \tag{1-26}$$

For fair comparison simulated data were scaled and also delayed w.r.t to its measured counterpart. The MAPE quality was calculated for estimated radial and iliac arterial pressure to be 3.3% and 3.2% respectively. Also, the deconvolution algorithm

was validated by comparing estimated cardiac output with measured one. Inverse transfer functions of these two Laguerre based arterial system FIR filters were computed by deconvolution operation. These inverse filters along with two measured peripheral pressure signals were later used to estimate the common input cardiac output flow. Visually estimated cardiac output was found to closely match with measured one.

Chapter 2: Aims and Significance of the Thesis

2.1 Specific Aims

The generalized transfer function approaches, despite their simplified implementation, renders rather less useful aortic pressure estimation as it does not account for inter or intra-subject differences. Gray box system identification models on the other hand can be tuned on per-patient basis and also at different times. Hence, it can adapt with any patient-to-patient variation and also any changes in time. But, these models substantially depend on tuning parameters or calibration techniques. Even a small error in calibration parameters can result in to significant modelling error. This constraint renders this approach rather impractical despite of its high performance and adaptive nature. On the contrary, Blind system identification approach for aortic pressure estimation does not require any explicit calibration or personalized measurements. Hence, this method by nature is self-calibrating to account for any inter-person along with intra-person vascular dynamics inconstancy. Besides the application of aortic pressure estimation, MBSI method extracts the system dynamics for vascular channels. Thus, MBSI approaches for aortic pressure estimation are more convenient and practical. All of the MBSI approaches, so far, have assumed the arterial system to be linear time invariant (LTI) system. Nonetheless, neglecting nonlinearity of hemodynamics to entertain modelling simplicity can result in estimation error.

A novel Wiener system based arterial channel model is first presented in Chapter 3. Human hemodynamic data is used to validate this model. In the model a linear finite impulse response (FIR) filter represents pulse transmission in large arteries and a non-

linear memoryless function block accounts for non-uniform arterial geometric and viscoelastic properties (Patel and Li, 2017; Patel et al., 2017). Employing this architecture two or more exclusive peripheral pressure signals can be measured and multichannel blind system identification (MBSI) technique can be used to estimate common source i.e. aortic pressure $\boldsymbol{P_a}$; Chapter 4 introduces this method and demonstrates aortic pressure estimation performance. This methodology is self-calibrating in that any inter-personal or intra-personal vascular dynamics inconstancy can be accounted for. The simulation results showed that nonlinear multichannel blind system identification (MBSI) provides much better accuracy than linear approach. One could also derive dynamic behavior of the individual pulse transmission paths, i.e. from aorta to the two peripheral arterial sites (Patel and Li, 2017; Patel et al., 2017). In Chapter 5, this method is further improved by estimating channel order preceding arterial system identification. By using effective channel order, system identification is optimized which then enhances aortic pressure estimation.

2.2 Significance of the Thesis

A well-modelled arterial system can be key in understanding the physical properties of arterial wall which in turn could provide insights to cardiovascular function. Potentially, this could help identify and monitor or manage cardiovascular disease. It has been clearly proven that an elevated arterial blood pressure is an important risk factor for cardiovascular pathology ([No, 1999). Being able to identify arterial channel system could be a great asset when studying epidemiology when treating common cardiovascular diseases like hypertension (MacMahon et al., 1990; Collins et al., 1990). More recently several research groups have been investigating the dynamic relation between different

arterial mechanical properties and pulse wave transmission phenomenon. For instance, the degree of wave reflection is assessed by the augmentation index, as well as vascular stiffness and arterial compliance. (O'Rourke et al., 1992; Waddell et al., 2001; Marchais et al., 1993; Mohiaddin et al., 1989; Salomaa et al., 1995; Leeson et al., 2000; Martin et al., 2000; Li, 2000)

As an example of the application of this method, two or more peripheral pressure can be continuously monitored non-invasively for patient bed side diagnostics. This can be then fed in to presented non-linear MBSI based algorithm (implemented in a computer) to estimate aortic pressure. As this algorithm is self-calibrating, it is very robust and adaptive approach for aortic pressure estimation. Also, this will provide personalized solution for human arterial system modelling, i.e. system dynamics identification for vascular channels. This accurately estimated aortic pressure waveform can be used to derive valuable clinical information to aid patient bed side assistance.

Chapter 3: A Novel Nonlinear Black Box Wiener System Model for Arterial Pulse Transmission

3.1 Nonlinearity of Arterial Channels

The vascular channels through which the pressure wave propagates originating from central aorta to the peripheral arteries are inherently nonlinear. The linear approximation can result in mismatch in shape of pressure waveform especially peak systolic pressure which is crucial for Augmentation Index calculation (Varanini et al., 2003; Stergiopulos et al., 1998). It has been shown that when modeling arterial system with a nonlinear system yields higher modeling accuracy than when using linear system model. (Varanini et al., 2003),(Qasem et al., 2001; Gao et al., 2016). Change in physiological properties of arterial system has direct impact on the proper function of the left ventricle (Murgo et al., 1980; Shimizu and Kario, 2008; Boutouyrie et al., 2010).

Overall coupling between left ventricle and arterial network is well described by prescribing the arterial system as a 3 element Windkessel model with passive circuit elements: series resistance Z_0 representing characteristic aortic impedance, resistor for peripheral resistance/ viscosity and capacitor for arterial compliance. It is known that arterial compliance is inversely proportional to the pressure exerted on its wall and so using constant arterial compliance could significantly and negatively impact modelling accuracy. Li et al. (Li, 1998; Li et al., 1990; Berger and Li, 1992; Li et al., 1997) proposed a nonlinear pressure dependent compliance model in lieu of constant compliance in the Windkessel model. When simulated this modified Windkessel model

(with non-linear compliance) demonstrated better performance than conventional model (Fogliardi et al., 1996).

Complex physiological mechanisms in cardiovascular system aspire to maintain arterial blood pressure for biological homeostasis. There are different feedback signals such as baroreflex that regulate blood pressure (Karaaslan et al., 2005). Arterial system can be speculated as dynamic control systems with various feedback loops and nonlinear functions (2017). Hence, by employing system theory to model arterial channels can provide knowledge which might not be accessible to measurement.

3.2 Proposed Arterial System Model

When cardiovascular transmission channel is modelled across two different arterial sites (say aortic-to-peripheral) the system is intrinsically nonlinear. Especially, when peripheral arterial pressure waveform is measured at distant peripheral sites, e.g. femoral arteries, the effect of narrowing of arteries, branching and visco-elastic force become more significant. In this case, the non-linearity of arterial behavior may not be negligible. With this consideration the cardiovascular system may be modelled as Wiener system with linear filter and memoryless non-linear function block, as shown in Figure 3-1. The linear filter can account for larger arteries transmission channel and the non-linear memoryless function block can account for all nonlinearities due to tapering of arteries, branching and visco-elastic properties.

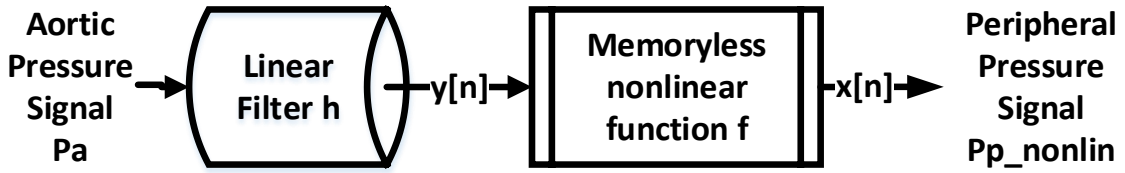

Fig. 3-1. Proposed black box Wiener System model for arterial channel with linear filter and memoryless non-linear function block

The input-output relation of this system can be represented as

$$P_p = f(\underbrace{h \otimes P_a}_{y}) \tag{3-1}$$

Here, P_a and P_p are aortic and peripheral pressure signals respectively, h is linear FIR filter, y is h filtered P_a with $\otimes$ representing convolution operation between h and P_a and $f(.)$ is a memoryless nonlinear function. For present study, nonlinear function $f(.)$ is assumed to be second f_2 or third f_3 order polynomial. To demonstrate modeling error caused by neglecting nonlinearity, f is also estimated as linear function f_1. These linear f_1, quadratic f_2 and cubic f_3 polynomial functions are defined as:

$$f_1 = \mathrm{a}_1 \times y + \mathrm{a}_2 \tag{3-2}$$

$$f_2 = \mathrm{a}_3 \times y^2 + \mathrm{a}_4 \times y + a_5 \tag{3-3}$$

$$f_3 = \mathrm{a}_6 \times y^3 + \mathrm{a}_7 \times y^2 + \mathrm{a}_8 \times y + a_9 \tag{3-4}$$

Where $a_{i=1:9}$ are coefficients of respective linear, quadratic and cubic polynomial fitting equation. Hence, arterial transmission channel is modelled and compared as Wiener System for three different cases using FIR filter h and series linear f_1, quadratic f_2 and cubic f_3 polynomial functions.

$$P_{p1} = g_1(P_a) = f_1(h \otimes P_a) \tag{3-5}$$

$$P_{p2} = g_2(P_a) = f_2(h \otimes P_a) \tag{3-6}$$

$$P_{p3} = g_3(P_a) = f_3(h \otimes P_a) \tag{3-7}$$

It can be seen that g_1 corresponds to linear transfer function similar to one referred in the previous studies as individual transfer function ITF (Jeon, 2007; Chen et al., 1997; Fetics et al., 1999). Hence, g_1 (with linear f_1) serves as baseline comparison to ascertain improvement in modeling accuracy by introducing nonlinear function block f_2 and f_3 in Wiener system g_2 and g_3 respectively.

3.3 Validation of Weiner System based Arterial Pulse Transmission Channel Model

3.3.1 Experimental Data

In order to validate proposed Wiener system model arterial channel, a correlation study was performed on previously acquired hemodynamic measurements (7 datasets with University of Alberta IRB approval) which are described in detail elsewhere

(Rashedi et al., 2013). Here, these hemodynamic signals relevant to our study are summarized. First group (Group 1) of data was compiled with seven different dataset of simultaneous central aortic (P_a) and radial (P_r) pressure waveform recorded for 2 min at sampling rate of 1kHz from patients undergoing cardiac surgery with cardiopulmonary bypass. Table 3-1 lists mean aortic pressure (MBP), systolic pressure (SBP) and diastolic pressure (DBP) from aortic as well as radial pressure of seven datasets that were used to validate proposed approach.

Table 3-1. Group 1: Hemodynamic measures of pressure signals included in the study

Data ID	Aortic Pressure			Radial Pressure	
	MBP (mmHg)	SBP (mmHg)	DBP (mmHg)	SBP (mmHg)	DBP (mmHg)
1	62.28	84.38	45.94	84.11	48.74
2	70.49	96.46	48.52	100.30	50.74
3	68.60	89.06	52.56	90.38	54.76
4	61.38	82.91	48.83	82.14	51.22
5	77.99	96.67	56.84	99.82	57.97
6	58.85	75.39	45.04	77.50	47.75
7	72.64	92.27	54.38	95.77	55.85

Similarly, second group (Group 2) of data was compiled with seven different dataset of simultaneous central aortic (P_a) and femoral (P_f) invasively recorded for 2 min at sampling rate of 1kHz from patients undergoing cardiac surgery with cardiopulmonary bypass. Table 3-2 lists these pressure data for the aorta as well femoral artery of seven datasets that were used to validate proposed approach.

Table 3-2. Group 2: Hemodynamic measures of pressure signals included in the study

Data ID	Aortic Pressure			Femoral Pressure	
	MBP (mmHg)	SBP (mmHg)	DBP (mmHg)	SBP (mmHg)	DBP (mmHg)
8	85.55	126.96	57.07	131.01	58.05
9	70.49	104.42	51.30	111.41	51.10
10	82.63	118.13	59.28	129.56	59.14
11	90.20	117.09	67.61	125.62	66.56
12	72.32	103.91	57.31	111.87	56.53
13	65.98	94.85	46.39	117.24	44.82
14	86.24	107.41	62.88	122.35	61.16

Note that MBP was computed as average of total central aortic pressure waveform. It can be seen that the physiologic conditions of the datasets analyzed are diverse. Specifically, SBP varied significantly between different datasets. Thus, this wide range of hemodynamic signals allowed us to validate model at distinct physiological conditions.

3.3.2 Signal pre-processing/ signal conditioning

From each of the 2min long dataset recorded 35 second segments were extracted such that these segments were free from any signal corruption. Also, each of datasets: for Group 1 with synchronous aortic and radial pressure waveform; and for Group 2 with synchronous aortic and femoral pressure waveform was down-sampled to 100Hz. These 35 sec segments were then used for analysis. From these 35 sec segments first 25 sec waveforms (training dataset) were used for training Wiener Model and rest of 10 sec waveforms (test datasets) were used to test validity of the fitted model. Figure 3-2 shows

sample waveforms for Group 1 with simultaneous P_a and P_r. Figure 3-3 shows sample waveforms for Group 2 with simultaneous P_a and P_f.

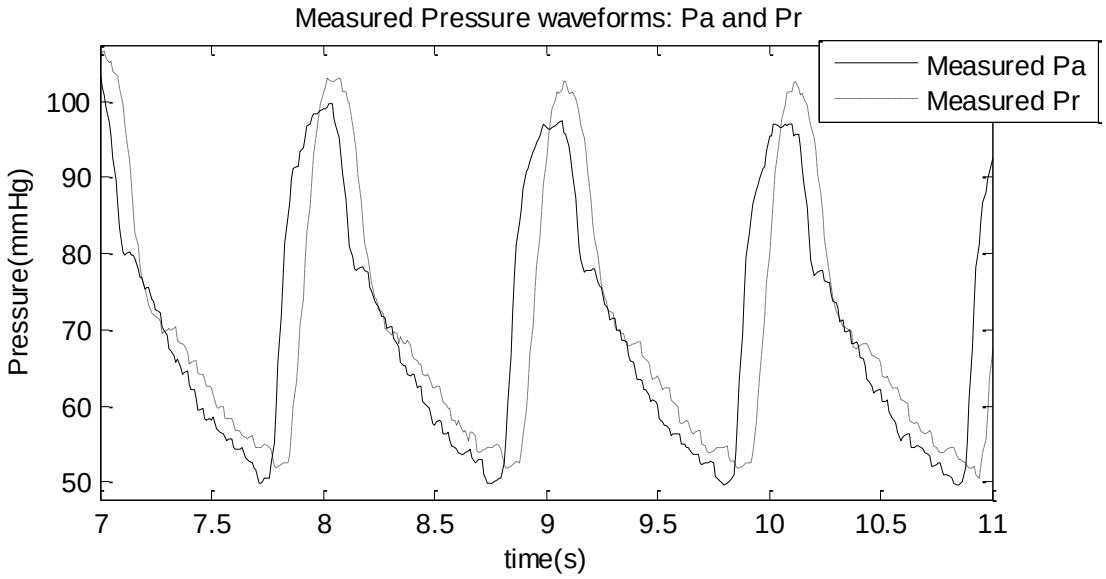

Fig. 3-2. Sample of simultaneously measured aortic and radial pressure waveform (Group 1)

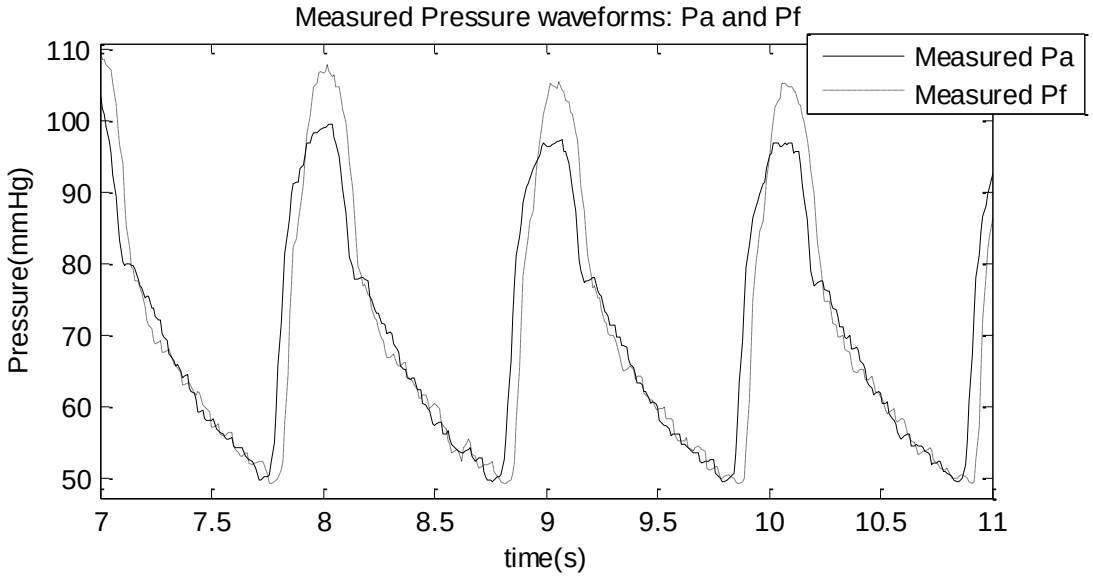

Fig. 3-3. Sample of simultaneously measured aortic and femoral pressure waveform (Group 2)

3.3.3 Cardiovascular Wiener System model

3.3.3.1 Arterial linear channel identification

To validate the Cardiovascular Wiener System model each of the training datasets (i.e. first 25 sec of waveforms) for Group 1 and Group 2 were fitted to Wiener System. Linear FIR filter h was estimated on individual basis as aortic-to-radial pressure (using Group 1 training dataset) and aortic-to-femoral pressure (using Group 2 training dataset) transfer function by assuming nonlinearity to be unity. To compute transfer function MATLAB function "tfest" was used with P_a as input signal and P_r as output signal for aortic-to-radial pressure transfer function for each of the Group 1 training datasets. Similarly, "tfest" was used with P_a as input signal and P_f as output signal for aortic-to-femoral pressure transfer function for each of the Group 2 training datasets. Figure 3-4 shows example of linear system identification for aortic-to-radial arterial channel and Figure 3-5 is an example of for aortic-to-femoral arterial channel linear system identification. In the Wiener System model linear transfer function was assumed to be finite impulse response (FIR) filter of order 10.

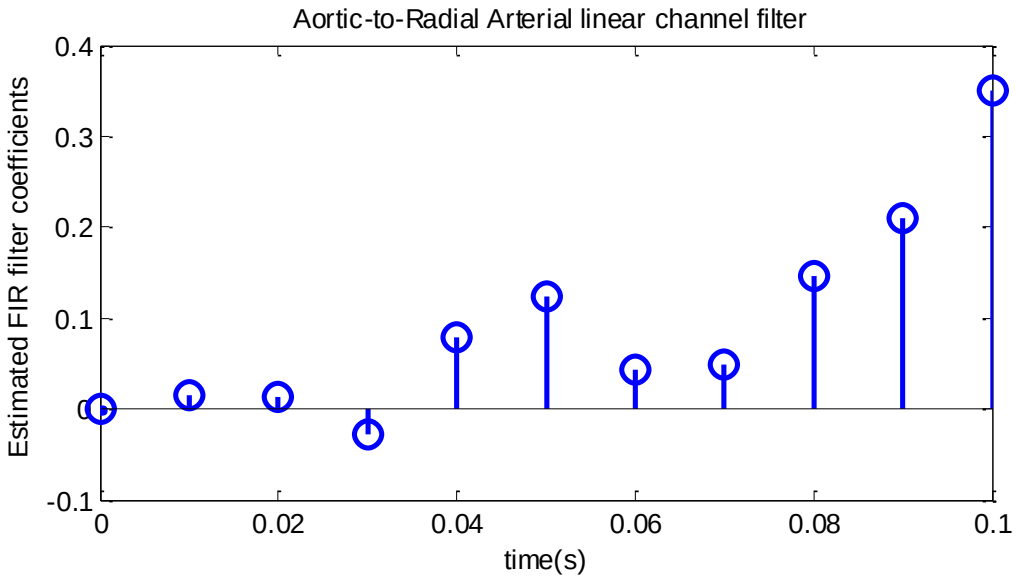

Fig. 3-4. Aortic-to-radial pressure signal transmission channel Arterial channel FIR filter identification.

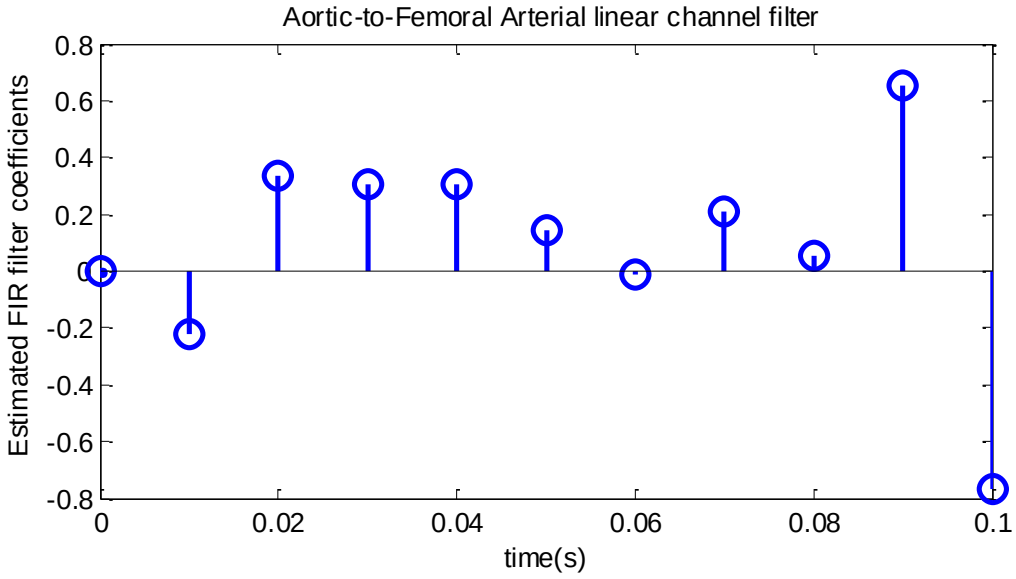

Fig. 3-5. Aortic-to-femoral pressure signal transmission channel Arterial channel FIR filter identification.

3.3.3.2 Modelling Non-linear function

To model the nonlinear memoryless monotonic function in the Wiener System model for aortic-to-radial artery (or aortic-to-femoral artery) a correlation study was performed for linear FIR filter simulated radial (or femoral) pressure vs. measured radial (or femoral) pressure waveform from 25 sec training datasets. Radial (or femoral) arterial pressure was simulated by convolving individualized FIR filter $h(t)$ with respective aortic pressure signal P_a. This simulated radial $P_r^{simulated}$ (or femoral $P_f^{simulated}$) pressure waveforms were then compared against measured radial $P_r^{measured}$ (or femoral $P_f^{measured}$) pressure waveforms. Each of this correlation curves were fitted to linear f_1, quadratic f_2 and cubic f_3 polynomial equation.

As measure of fitting accuracy Pearson r-value squared (r^2) was calculated along with fitted linear, quadratic and cubic polynomial equations. This correlation analysis was carried out using 2500 data points. Figure 3-6 and 3-7 show the correlation for each of seven training datasets from Group 1.

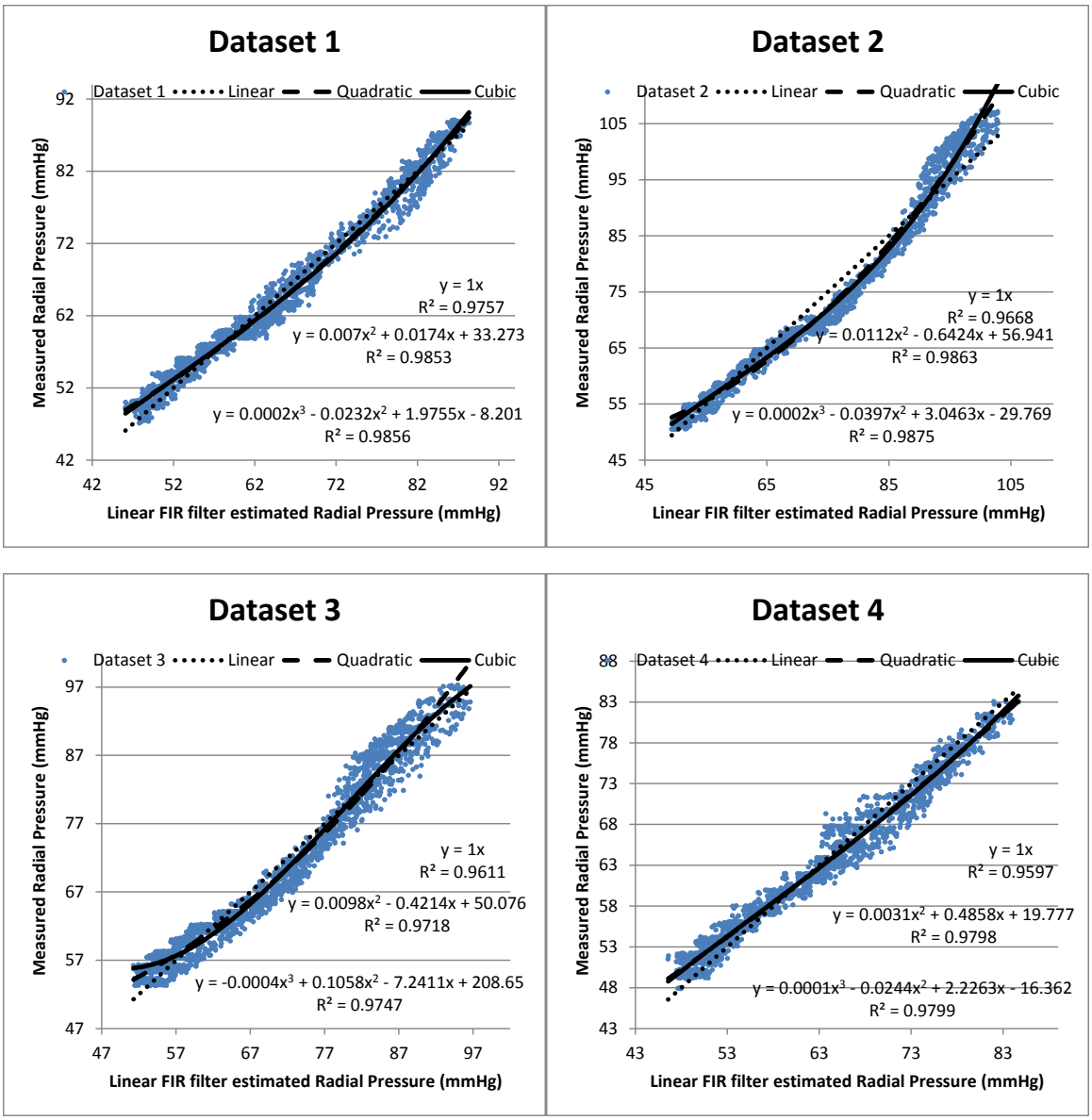

Fig. 3-6. Correlation graphs for linear FIR filter simulated radial pressure vs. measured radial pressure waveform from seven different datasets (Group 1) of simultaneously measured aortic and radial pressure waveforms.

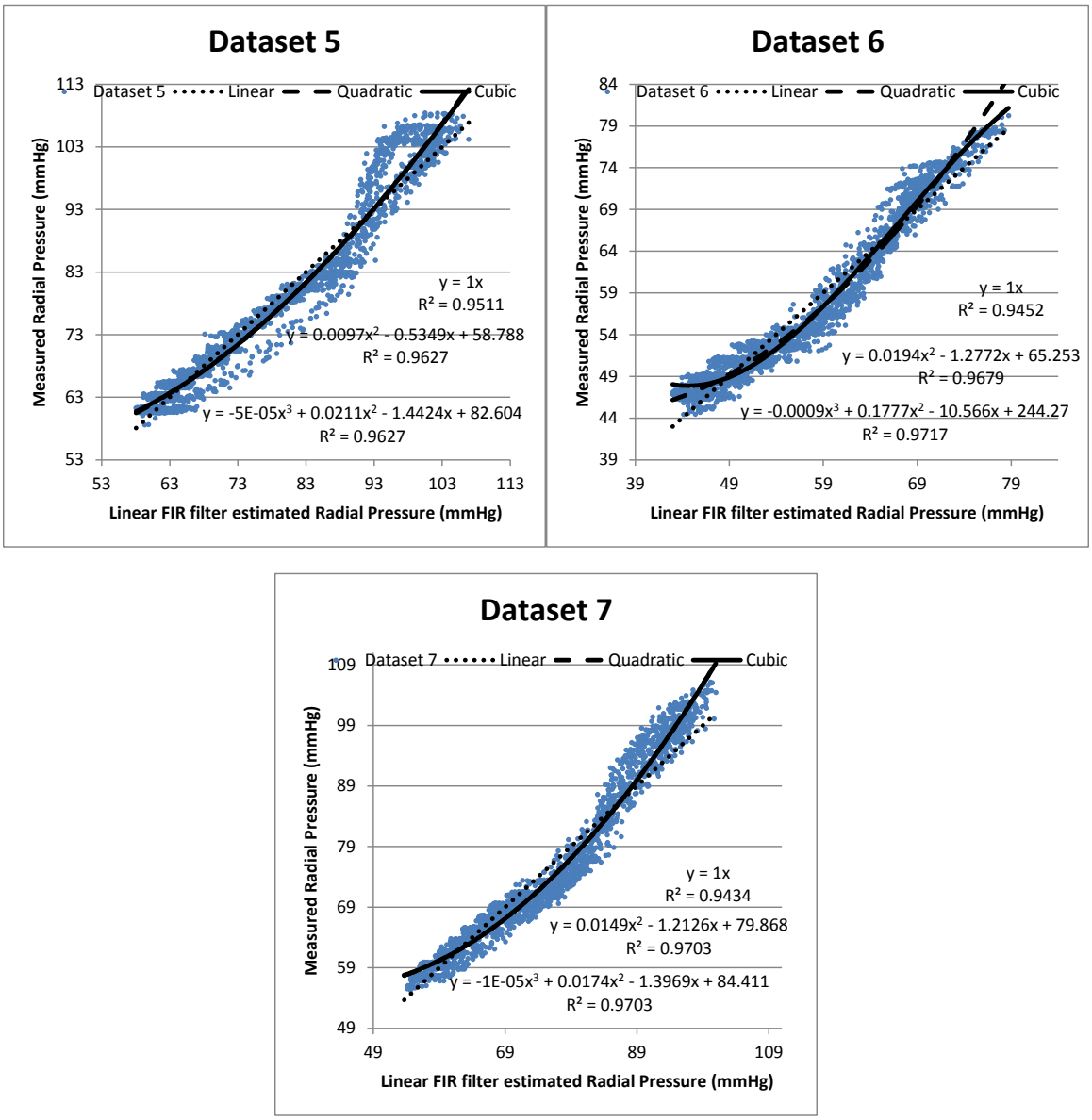

Fig. 3-7. Correlation graphs for linear FIR filter simulated radial pressure vs. measured radial pressure waveform from seven different datasets (Group 1) of simultaneously measured aortic and radial pressure waveforms.

Similarly, correlation curves between $P_f^{simulated}$ and $P_f^{measured}$ were fitted to linear, quadratic and cubic polynomial equations. Figure 3-7, 3-8 shows the correlation for each of seven training datasets from Group 2.

It can be seen from Figure 3-6, 3-7, 3-8 and 3-9 that f_3 fitted curves resulted in lower r^2 value than f_2 fitted curves and f_2 fitted curves produced lower r^2 value than f_1 fitted curves. That is fitting between $P_p^{simulated}$ and $P_p^{measured}$ is improved for higher order polynomial as compared to lower order polynomial.

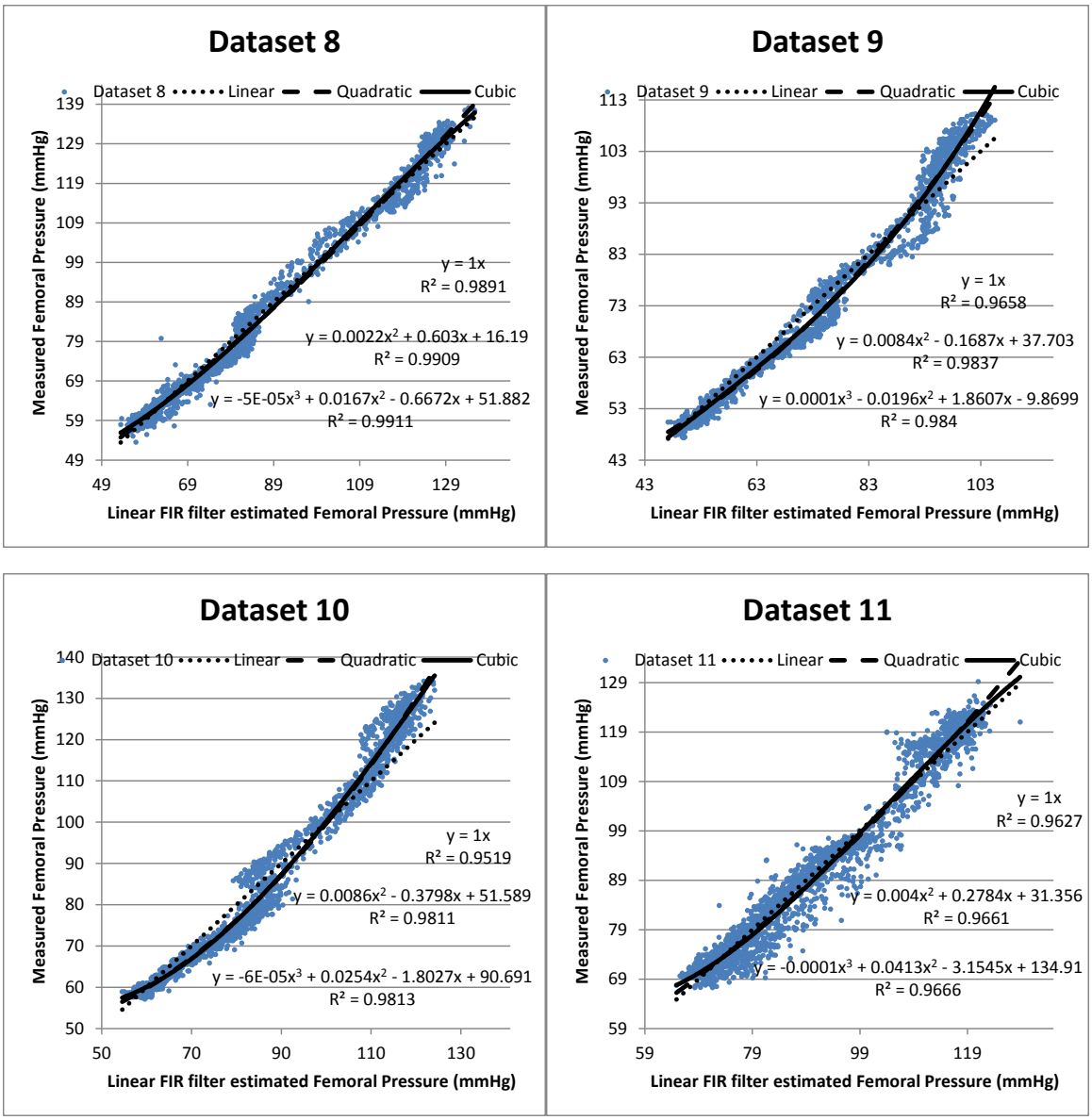

Fig. 3-8. Correlation graphs for linear FIR filter simulated femoral pressure vs. measured femoral pressure waveform from seven different datasets (Group 2) of simultaneously measured aortic and femoral pressure waveforms.

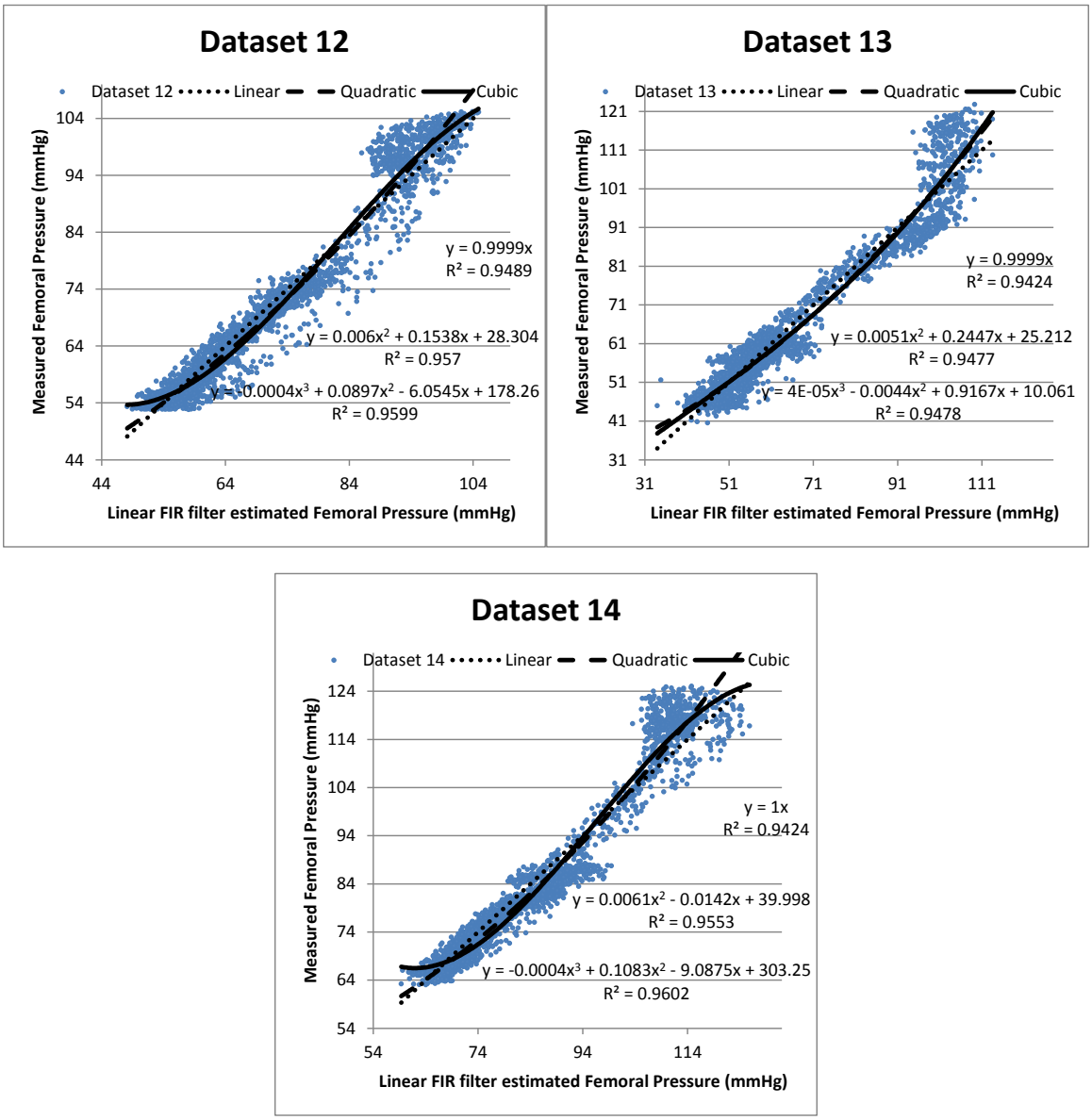

Fig. 3-9. Correlation graphs for linear FIR filter simulated femoral pressure vs. measured femoral pressure waveform from seven different datasets (Group 2) of simultaneously measured aortic and femoral pressure waveforms.

3.3.4 Simulated Waveforms

Experiment was carried out to study the performance of the Wiener system based arterial channel model for P_r (or P_f) estimation on each of seven datasets. For each of the

datasets (from Group 1 as well as Group 2) Wiener System model was simulated for three different cases using estimated individual FIR filter h along with respective P_a (test datasets, i.e. last 10 sec waveforms) and series linear f_1, quadratic f_2 and cubic f_3 polynomial functions. Radial pressure (or femoral pressure) was generated as P_{r1} (or P_{f1}), P_{r2} (or P_{f2}) and P_{r3} (or P_{f3}) using Wiener system g_1, g_2 and g_3 with nonlinear functions f_1, f_2 and f_3 respectively.

For comparison, corresponding $P_r^{measured}$ and $P_f^{measured}$ were plotted alongside Wiener model simulated signals. Figure 3-10 illustrates reconstructed P_r signals using g_1, g_2 and g_3 Wiener model along with measured $P_r^{measured}$.

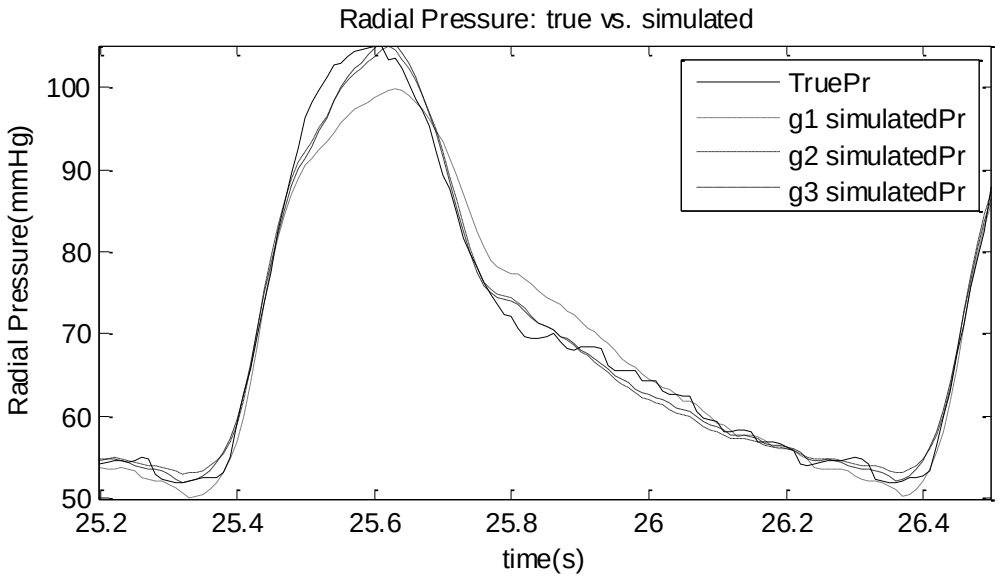

Fig. 3-10. Sample waveform of reconstructed P_r signals using g_1, g_2 and g_3 Wiener model along with measured $P_r^{measured}$

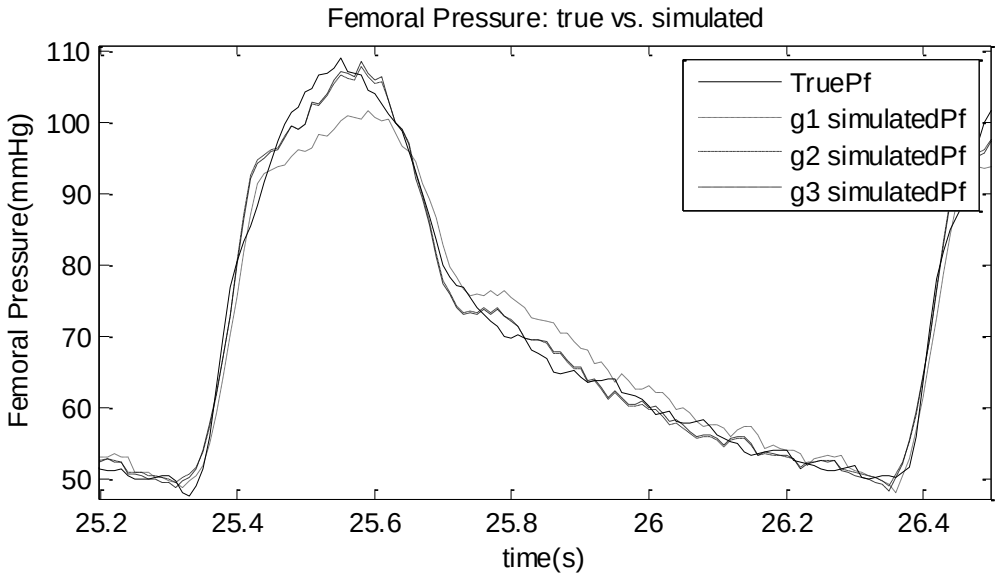

Fig. 3-11. Sample waveform of reconstructed P_f signals using g_1, g_2 and g_3 Wiener model along with measured $P_f^{measured}$

Likewise, P_f signals were reconstructed using g_1, g_2 and g_3 Wiener model along with measured $P_f^{measured}$; Figure 3-11 demonstrates an example of these waveforms. It can be seen that g_2 constructed P_r (and P_f) better aligns with measured $P_r^{measured}$ (and $P_f^{measured}$) as compared to g_1 constructed P_r (and P_f). Also, g_3 simulated P_r (and P_f) better coheres with measured $P_r^{measured}$ (and $P_f^{measured}$) as compared to g_2 simulated P_r (and P_f); see Figure 3-10 and 3-11.

3.3.5 Accuracy of Wiener System model for arterial channel

Besides visual comparison between the measured vs. simulated P_p (i.e. P_r and P_f) waveforms among different Wiener models g_1, g_2 and g_3 with test datasets P_a, root mean squared error were computed for each case and used as figure of merit. $RMSE$ was computed for the total 10 sec test dataset waveform. Lower the root mean squared error implied higher correlation between measured and estimated P_p. $RMSE$ is computed as

sample-by-sample difference between measured $P_r^{measured}$ (or $P_f^{measured}$) and estimated P_{r1} (or P_{f1}) for g_1, g_2 and g_3 Wiener models. Data analysis from above mentioned all experiments are summarized in the Table 3-3 (for aortic-to-radial arterial channel) and Table 3-4 (for aortic-to-femoral arterial channel).

Table 3-3. Root mean squared error for radial pressure estimated using Wiener models g_1, g_2 and g_3. P_{r1}, P_{r2} and P_{r3} are simulated radial pressure signals using g_1, g_2 and g_3 Wiener model

Dataset ID	RMSE (mmHg)		
	$\boldsymbol{P_{r1}}$	$\boldsymbol{P_{r2}}$	$\boldsymbol{P_{r3}}$
1	1.971	1.589	1.581
2	3.209	2.564	2.502
3	2.618	2.498	2.336
4	1.823	1.382	1.372
5	2.966	2.649	2.647
6	2.739	2.433	2.313
7	2.901	2.579	2.560

Table 3-4. Root mean squared error for femoral pressure estimated using Wiener models g_1, g_2 and g_3. P_{f1}, P_{f2} and P_{f3} are simulated femoral pressure signals using g_1, g_2 and g_3 Wiener model

Dataset ID	RMSE (mmHg)		
	$\boldsymbol{P_{f1}}$	$\boldsymbol{P_{f2}}$	$\boldsymbol{P_{f3}}$
8	3.837	3.706	3.628
9	3.795	2.975	2.909
10	5.839	4.617	4.558
11	5.661	5.405	5.369
12	4.615	4.563	4.321
13	5.437	5.304	5.292
14	4.483	3.915	3.893

Chapter 4: Aortic Pressure Estimation using Blind Identification Approach on Single Input Multiple Output (SIMO) Non-linear Wiener Systems

4.1 Proposed Multi-Channel Arterial Tree Model

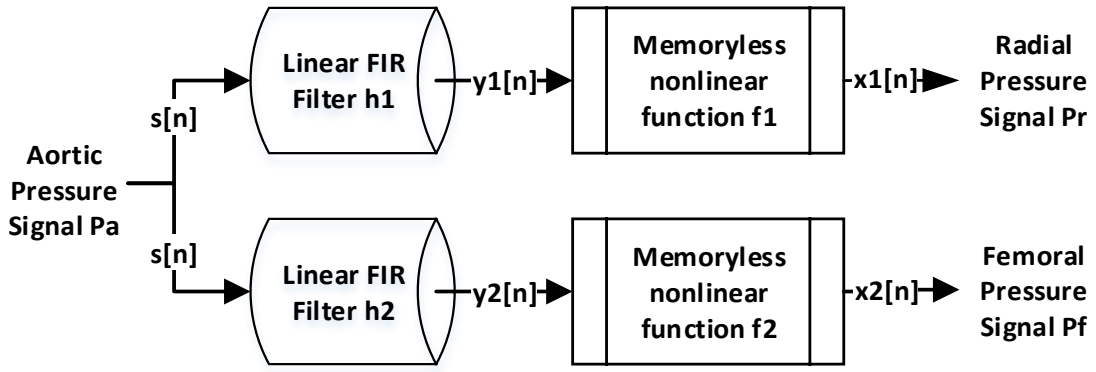

Fig. 4-1. Proposed Single Input Multiple Outputs Wiener System model for the arterial system. FIR finite impulse response filter.

By modeling arterial system as single-input multiple-output (SIMO) MBSI can be employed to estimate common source aortic pressure P_a. When MBSI technique is implemented using distal peripheral measurement sites, e.g. femoral arteries, the effect of narrowing of arteries, branching and visco-elastic force become more significant. In this case, the non-linearity of arterial behavior (especially at distal termination) may not be negligible. With this consideration, cardiovascular system may be modelled as Wiener system with linear finite impulse response or FIR filter and memoryless non-linear function block, as shown in Figure 4-1. The linear FIR filter can account for larger arteries transmission channel and non-linear memoryless function block can account for

all nonlinearities due to non-uniformities in the arterial system, such as narrowing of arteries, branching and visco-elastic forces. To facilitate multi-channel blind system identification second Wiener system segment for another cardiovascular transmission channel can be modelled. With this structure if pressure waveforms are measured from two distinct peripheral locations MBSI technique can be used to characterize the linear FIR filters along with non-linear functions for each of the two transmission channels. Thus computed linear filter and non-linear functions can be then de-convolved from measured output pressure signals to estimate common input pressure signal, in this case P_a signal.

4.2 Aortic Pressure Estimation Method

A relatively flexible multi-channel blind system identification method for SIMO system was proposed by Van Vaerenbergh et al. (Van Vaerenbergh et al., 2013). This Alternating Kernel Canonical Correlation Analysis (AKCCA) method, in specific, targets SIMO system with nonlinear Wiener systems.

To be consistent with the convention, the following notation is used for the analysis that follows: lowercase letters x are used for scalar variables, lower case boldface letters $\boldsymbol{x}$ represent vectors, uppercase boldface letters $\boldsymbol{X}$ stand for matrices, discrete time elements are depicted using square bracket $x[n]$ and caret superscript designate estimated value $\hat{x}$.

4.2.1 Blind Identification of Linear SIMO Systems

This method first formulates blind identification of a linear system with two channels. For a given SIMO system with two output signals $\boldsymbol{x_1}$ and $\boldsymbol{x_2}$ at linear channels $\boldsymbol{h_1}$ and $\boldsymbol{h_2}$ respectively that are excited by same input signal $s[n]$ can be written as

$$x_i[n] = \sum_{l=0}^{L-1} h_i[l]s[n-l] = h_i[n] * s[n] \tag{4-1}$$

where $h_i = [h_i[0], \ldots., h_i[L-1]]^T$ is the impulse response vector of the i-th channel, L is the maximal channel length (which is assumed to be known), and $h_i[n] * s[n]$ is the convolution between h_i and the input signal $s[n]$. Channels, $\widehat{\boldsymbol{h}}_{\boldsymbol{1}}$ and $\widehat{\boldsymbol{h}}_{\boldsymbol{2}}$ can be estimated by minimizing the following cost function

$$\underset{\widehat{\boldsymbol{h}}_{\boldsymbol{1}},\widehat{\boldsymbol{h}}_{\boldsymbol{2}}}{\textbf{minimize}} \frac{\mathbf{1}}{\mathbf{2}} \left\| \boldsymbol{X_1}\widehat{\boldsymbol{h}}_{\boldsymbol{2}} - \boldsymbol{X_2}\widehat{\boldsymbol{h}}_{\boldsymbol{1}} \right\|^{\mathbf{2}} \tag{4-2}$$

$$\boldsymbol{Subject\ to} \left\| \boldsymbol{X_2}\widehat{\boldsymbol{h}}_{\boldsymbol{1}} \right\|^{\mathbf{2}} = \left\| \boldsymbol{X_1}\widehat{\boldsymbol{h}}_{\boldsymbol{2}} \right\|^{\mathbf{2}} = \mathbf{1}$$

Equation (4-2) is called canonical correlation analysis (CCA) problem (Xu et al., 1995), which is solved as principal eigenvector of generalized eigenvalue problem (GEV) (Hotelling, 1936) shown below

$$\begin{bmatrix} \mathbf{0} & \boldsymbol{X_2^T X_1} \\ \boldsymbol{X_1^T X_2} & \mathbf{0} \end{bmatrix} \underbrace{\begin{bmatrix} \boldsymbol{h_1^T} \\ \boldsymbol{h_2^T} \end{bmatrix}}_{\widehat{\boldsymbol{h}}} = \boldsymbol{\rho} \begin{bmatrix} \boldsymbol{X_2^T X_2} & \mathbf{0} \\ \mathbf{0} & \boldsymbol{X_1^T X_1} \end{bmatrix} \underbrace{\begin{bmatrix} \boldsymbol{h_1^T} \\ \boldsymbol{h_2^T} \end{bmatrix}}_{\widehat{\boldsymbol{h}}} \tag{4-3}$$

Here $\boldsymbol{X_i}$ is the data matrix defined as

$$\boldsymbol{X_i} = \begin{bmatrix} x_i[n+L-1] & \dots & x_i[n] \\ \vdots & \ddots & \vdots \\ x_i[n+N-1] & \dots & x_i[n+N-L] \end{bmatrix}, where\ i = 1,2 \tag{4-4}$$

Full characterization of $\widehat{\boldsymbol{h_i}}$ is only possible if the two channels are co-prime or in other words don't have common zeros (Xu et al., 1995). When solving for $\widehat{\boldsymbol{h_i}}$ a constraint has to be applied so as to neglect trivial solution $\widehat{\boldsymbol{h_i}} = \mathbf{0}$.

4.2.2 Blind Identification and Equalization of SIMO Wiener Systems

Consider a nonlinear SIMO system with each of the channels modeled as Wiener system as shown in the Figure 4-1. The input-output relation of this system can be represented as

$$x_i[n] = f_i\left(\sum_{l=0}^{L-1} h_i[l]s[n-l]\right) \tag{4-5}$$

The nonlinearities $f_i(.)$ have to be restricted to monotonous and invertible to allow calculating inverse nonlinearities in identification problem. Based on previous study, in case of arterial system the nonlinearities due to distal peripheral arteries can be approximated as monotonous invertible nonlinear functions without hysteresis. (Stergiopulos et al., 1999)

4.2.2.1 Outline of the AKCCA Method

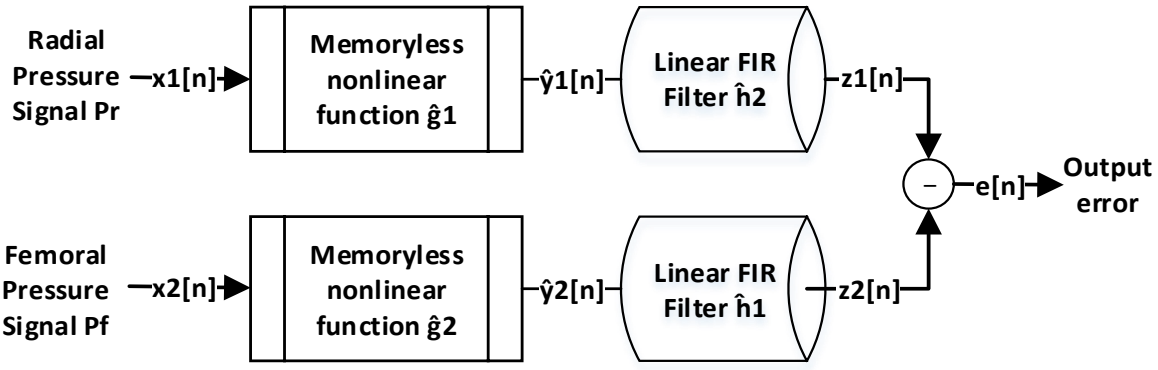

Fig. 4-2. Multiple inputs single output or MISO Hammerstein System model for blind identification

For given two-channel SIMO Wiener system shown in Figure 4-1 the proposed identification method can be modeled as two-channel MISO Hammerstein system, see Figure 4-2. First, cost function is defined that needs to be minimized

$$J = \frac{1}{2}\sum_{n=1}^{N} |z_1[n] - z_2[n]|^2 = \frac{1}{2}\sum_{n=1}^{N} |e[n]|^2 \tag{4-6}$$

Where $\boldsymbol{z_1}$ and $\boldsymbol{z_2}$ are the identification model outputs

$$z_i[n] = \sum_{l=0}^{L-1} \hat{h}_j[l]\hat{g}_i(x_i[n-l]), \tag{4-7}$$

*w*here $i, j = 1,2$ and $i \neq j$

4.2.2.2 Kernel Methods

Using Kernel Methods a nonlinear problem of data x can be transformed into high-dimensional reproducing kernel Hilbert space (RKHS), in which transformed data can be

separated linearly. Applying Representer theorem (Schölkopf et al., 2001), a nonlinear function $g(.)$ can be modeled as shown by equation (4-8).

$$y = g(x) = \sum_{n=1}^{N} \alpha[n]\kappa(x, x[n]) \tag{4-8}$$

where $\{x[n] \mid n = 1, \ldots, N\}$ are the training data.

Equation (4-8) can be represented in matrix form as

$$\underbrace{\begin{bmatrix} y[1] \\ \vdots \\ y[nN] \end{bmatrix}}_{\boldsymbol{y}} = \boldsymbol{K} \underbrace{\begin{bmatrix} \alpha[1] \\ \vdots \\ \alpha[N] \end{bmatrix}}_{\boldsymbol{\alpha}} \tag{4-9}$$

Here $y[n]$ are system outputs corresponding to $x[n]$ and $\boldsymbol{K} \in \mathbb{R}^{N \times N}$ is the kernel matrix defined as

$$\boldsymbol{K}[i, j] = \kappa(\boldsymbol{x}[i], \boldsymbol{x}[j]) \tag{4-10}$$

4.2.2.3 Optimization Problem

Incorporating kernel expansion equation (4-7), the identification model output vector $\boldsymbol{z_i}$ of i-th channel can be written as

$$\underbrace{\begin{bmatrix} z_i[1] \\ \vdots \\ z_i[N] \end{bmatrix}}_{z_i} = \bar{\boldsymbol{K}}_{\boldsymbol{i}} \boldsymbol{r}_{\boldsymbol{j}}, \tag{4-11}$$

where $i, j = 1,2$ and $i \neq j$. The elements of $\bar{\boldsymbol{K}}_{\boldsymbol{i}} \in \mathbb{R}^{N \times (LM)}$ are defined in terms of K_i, the kernel matrix of the available data $x_i[n]$ of corresponding branch as

$$\bar{K}_i[n, lM + m] = K_i[n - l, m], \tag{4-12}$$

and r_j represents the Kronecker product

$$r_j = \underbrace{\begin{bmatrix} \hat{h}_j[1] \\ \vdots \\ \hat{h}_j[L-1] \end{bmatrix}}_{\hat{\boldsymbol{h}}_j} \otimes \underbrace{\begin{bmatrix} \hat{\alpha}_i[1] \\ \vdots \\ \hat{\alpha}_i[N] \end{bmatrix}}_{\hat{\boldsymbol{\alpha}}_i} \tag{4-13}$$

Using kernel expression of two channels for SIMO Wiener the optimization problem (equation (4-2)) can be reformed to

$$\underset{\boldsymbol{r_1}, \boldsymbol{r_2}, \hat{\boldsymbol{h}}_1, \hat{\boldsymbol{h}}_2, \hat{\boldsymbol{\alpha}}_1, \hat{\boldsymbol{\alpha}}_2}{\textbf{minimize}} \| \bar{\boldsymbol{K}}_1 \boldsymbol{r}_2 - \bar{\boldsymbol{K}}_2 \boldsymbol{r}_1 \|^2 \tag{4-14}$$

$$\boldsymbol{Subject\ to}\ \| \bar{\boldsymbol{K}}_1 \boldsymbol{r}_2 \|^2 = \| \bar{\boldsymbol{K}}_2 \boldsymbol{r}_1 \|^2 = \boldsymbol{1}$$

$$\boldsymbol{r_2} = \hat{\boldsymbol{h}}_2 \otimes \hat{\boldsymbol{\alpha}}_1$$

$$\boldsymbol{r_1} = \hat{\boldsymbol{h}}_1 \otimes \hat{\boldsymbol{\alpha}}_2$$

This expression can be simplified to

$$\underset{\boldsymbol{r_1}, \boldsymbol{r_2}, \hat{\boldsymbol{h}}_1, \hat{\boldsymbol{h}}_2, \hat{\boldsymbol{\alpha}}_1, \hat{\boldsymbol{\alpha}}_2}{\textbf{minimize}} \| \boldsymbol{z_1} - \boldsymbol{z_2} \|^2 \tag{4-15}$$

$$\boldsymbol{Subject\ to}\ \| \boldsymbol{z_1} \|^2 = \| \boldsymbol{z_2} \|^2 = \boldsymbol{1}$$

4.2.2.4 Alternating Optimization Procedure

Equation (4-15) being non-convex optimization problem an iterative strategy is used that alternates between estimating linear channels $\hat{\boldsymbol{h}}_i$ and the nonlinearity estimates $\hat{\boldsymbol{\alpha}}_i$ so that the solution converges to minimize estimation error

- Iteration 1: Initial $\widehat{\boldsymbol{\alpha}}_{\boldsymbol{i}}$ is guessed and used to compute $\widehat{\boldsymbol{h}}_{\boldsymbol{i}}$. With this $\widehat{\boldsymbol{\alpha}}_{\boldsymbol{i}}$ the $\widehat{\boldsymbol{y}}_{\boldsymbol{i}}[\boldsymbol{n}]$ can be calculated using Equation (4-9). With this $\widehat{\boldsymbol{y}}_{\boldsymbol{i}}[\boldsymbol{n}]$ identification model output $\boldsymbol{z}_{\boldsymbol{i}}[\boldsymbol{n}]$ can be found using Equation (4-3)

$$z_i[n] = \sum_{l=0}^{L-1} \hat{h}_j[l]\hat{y}_i[n-l], \tag{4-16}$$

*w*here $i, j = 1,2$ and $i \neq j$

Matrix representation of equation (4-16) can be given by

$$\boldsymbol{z}_{\boldsymbol{i}} = \widehat{\boldsymbol{Y}}_{\boldsymbol{i}}\widehat{\boldsymbol{h}}_{\boldsymbol{j}} \tag{4-17}$$

Using this relation equation (4-17) the minimization problem equation (4-15) becomes

$$\underset{\widehat{\boldsymbol{h}}_{\boldsymbol{1}},\widehat{\boldsymbol{h}}_{\boldsymbol{2}}}{\mathbf{minimize}} \left\|\widehat{\boldsymbol{Y}}_{\boldsymbol{1}}\widehat{\boldsymbol{h}}_{\boldsymbol{2}} - \widehat{\boldsymbol{Y}}_{\boldsymbol{2}}\widehat{\boldsymbol{h}}_{\boldsymbol{1}}\right\|^{\boldsymbol{2}} \tag{4-18}$$

$$\boldsymbol{Subject\ to} \left\|\widehat{\boldsymbol{Y}}_{\boldsymbol{1}}\widehat{\boldsymbol{h}}_{\boldsymbol{2}}\right\|^{\boldsymbol{2}} = \left\|\widehat{\boldsymbol{Y}}_{\boldsymbol{2}}\widehat{\boldsymbol{h}}_{\boldsymbol{1}}\right\|^{\boldsymbol{2}} = \mathbf{1}$$

Equation (4-18) is identical to the CCA problem (equation (4-2)) which can be solved using the GEV (equation (4-3)) (Hardoon et al., 2004)

- Iteration 2: With $\widehat{\boldsymbol{h}}_{\boldsymbol{i}}$ estimated from step 1, obtain $\widehat{\boldsymbol{\alpha}}_{\boldsymbol{i}}$**.** Using $\widehat{\boldsymbol{h}}_{\boldsymbol{1}}$ and $\widehat{\boldsymbol{h}}_{\boldsymbol{2}}$ computed from step 1 we can find identification output

$$z_i[n] = \sum_{m=1}^{N} W_i[n,m]\hat{\alpha}_i[m], \tag{4-19}$$

Where auxiliary variable W_i is defined as

$$W_i[n,m] = \sum_{l=0}^{L-1} \hat{h}_j[l] K_i[n-l,m] \tag{4-20}$$

Equation (4-19) can be expressed using matrix operation as

$$\boldsymbol{z_i} = \boldsymbol{W_i}\hat{\boldsymbol{\alpha}}_{\boldsymbol{i}} \, , with \, \boldsymbol{W_1} \in \mathbb{R}^{N \times N} \tag{4-21}$$

With above mentioned derivation minimization problem (equation (4-15)) is converted to

$$\underset{r_1, r_2, \hat{h}_1, \hat{h}_2, \hat{\alpha}_1, \hat{\alpha}_2}{\textbf{minimize}} \|\boldsymbol{W_1}\hat{\boldsymbol{\alpha}}_{\boldsymbol{1}} - \boldsymbol{W_2}\hat{\boldsymbol{\alpha}}_{\boldsymbol{2}}\|^2 \tag{4-22}$$

$$\boldsymbol{Subject\ to} \ \|\boldsymbol{W_1}\hat{\boldsymbol{\alpha}}_{\boldsymbol{1}}\|^2 = \|\boldsymbol{W_2}\hat{\boldsymbol{\alpha}}_{\boldsymbol{2}}\|^2 = \mathbf{1}$$

As in step 1 equation (4-22) formulates kernel CCA problem to estimate nonlinear $g_i(.)$.which can be solved using the GEV (equation (4-3)). For initialization, assume initial nonlinear function as identity function $g_i(x) = x$, then solve linear CCA problem (equation (4-9)) to compute the initial estimate of the linear channels $\hat{\boldsymbol{h}}_{\boldsymbol{i}}$ for given system outputs $x_i[n]$. Figure 4-3 summarizes AKCCA algorithm.

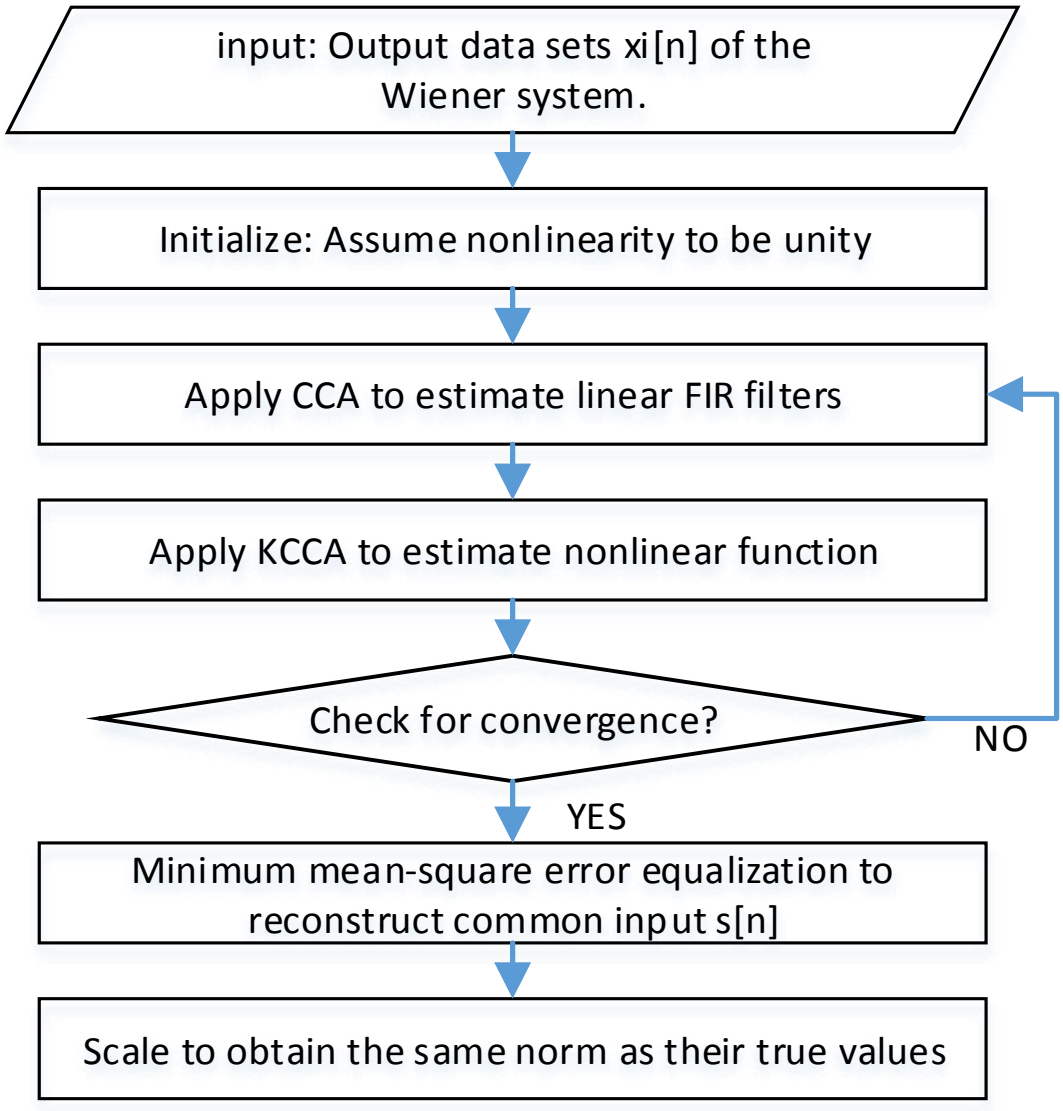

Fig. 4-3. Flowchart of alternating kernel canonical correlation analysis or AKCCA

4.3 Experimental Results

4.3.1 Experimental Data

In order to study the performance of nonlinear blind system identification for P_a estimation (nonlinear MBSI) AKCCA method was employed on previously acquired (with University of Alberta IRB approval) hemodynamic measurements (7 datasets)

which are described in detail elsewhere (Rashedi et al., 2013). Here, experimental setup to measure these hemodynamic signals is summarized. Simultaneous central aortic (P_a), radial (P_r) and femoral (P_f) artery pressures were invasively recorded for 2 min at sampling rate of 1kHz from patients undergoing cardiac surgery with cardiopulmonary bypass. Table 4-1 lists systolic pressure (sBP), diastolic pressure (dBP), mean pressure (mean BP), aortic-to-femoral artery pulse transit time (PTT_{af}) and aortic-to-radial artery pulse transit time (PTT_{ar}) of the datasets that were used to validate proposed approach. It can be seen that the physiologic conditions of the datasets analyzed are diverse. Specifically, PTT_{af} and PTT_{ar} varied significantly between different datasets. It has been previously studied that PTT deviation has considerable influence on the arterial channel dynamics (Sugimachi et al., 2001; Westerhof et al., 2007). Thus, wide range of hemodynamic signals allowed us to validate our method at distinct physiological conditions.

Table 4-1. Hemodynamic measures of pressure signals included in the study

Data ID	PTT_{af} (ms)	PTT_{ar} (ms)	Mean BP (mmHg)	dBP (mmHg)	sBP (mmHg)
1	60	50	55.91	44.35	76.48
2	50	80	61.38	52.77	87.20
3	80	110	49.53	49.46	75.66
4	60	110	58.58	46.41	97.85
5	50	80	65.98	47.78	96.27
6	50	130	59.10	49.64	80.05
7	60	80	62.28	47.28	90.58

Note that MeanBP was computed as average of total central aortic pressure waveform, dBP and sBP was computed as average of diastole and systole aortic pressure respectively measured at each cardiac cycle for 35 sec, PTT_{af} was computed as average of femoral pressure foot-to-aortic pressure foot time difference measured at each cardiac cycle for 35 sec, PTT_{ar} was computed as average of radial pressure foot-to-aortic pressure foot time difference measured at each cardiac cycle for 35 sec.

4.3.2 Signal pre-processing/ signal conditioning

From each of the 2min long dataset recorded 35 second segments were extracted such that these segments were free from any signal corruption. Also, each of aortic, femoral and radial pressure waveforms was downsampled to 100Hz. In order to decouple the aortic pressure estimation error due to error in arterial channel identification and error due to time separation among P_a, P_r and P_f these signals were time aligned. Particularly, P_r and P_f were advanced by PTT_{ar} and PTT_{af} respectively w.r.t. P_a. These 35 sec segments were then used for analysis. Figure 4-4, 4-5 and 4-6 shows sample waveforms P_a, P_r and P_f respectively; bottom graph displays full waveform of 35 sec length and top graph is zoomed for 7-10 sec to demonstrate details of recorded signals.

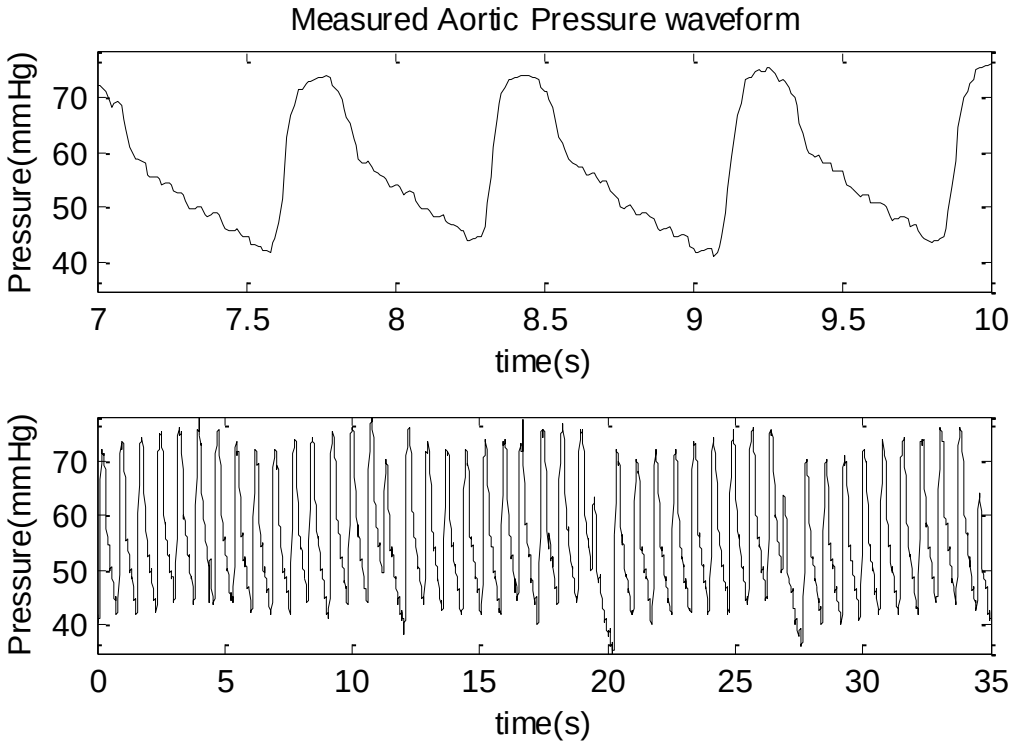

Fig. 4-4. Sample of measured aortic pressure waveform. Top: zoomed-in to 7-10 sec. Bottom: full 35 sec segment

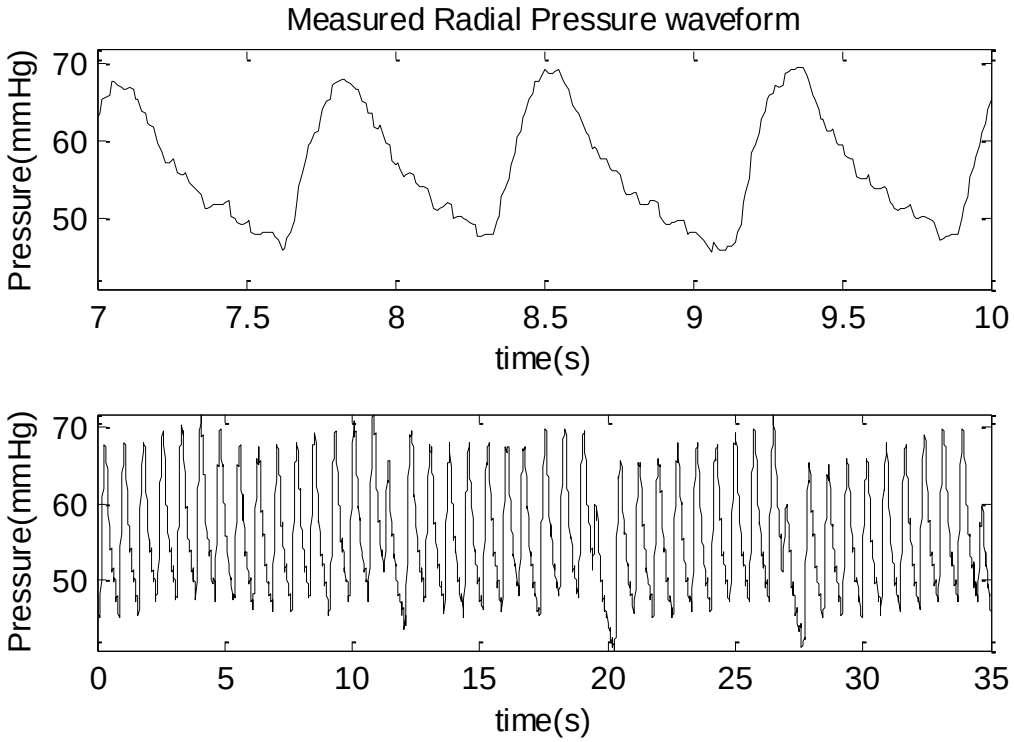

Fig. 4-5. Sample of measured radial pressure waveform. Top: zoomed-in to 7-10 sec. Bottom: full 35 sec segment

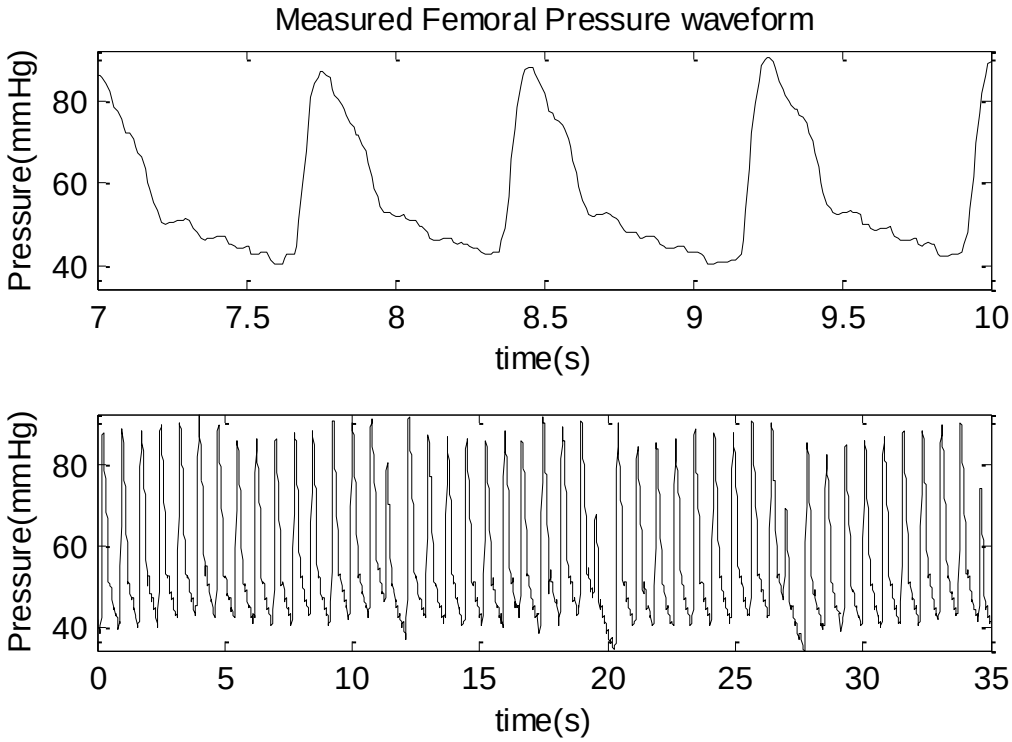

Fig. 4-6. Sample of measured femoral pressure waveform. Top: zoomed-in to 7-10 sec. Bottom: full 35 sec segment

4.3.3 Aortic pressure estimation

4.3.3.1 Measured vs. Estimated Aortic pressure waveform

Experiment was carried out to study the performance of the SIMO Wiener system based blind system identification for P_a estimation on each of seven datasets. For comparison, SIMO linear system based blind system identification for P_a estimation was applied on each dataset as well. In the Wiener System model linear transfer function was assumed to be finite impulse response (FIR) of order 10. First, AKCCA algorithm was applied for nonlinear blind system identification. Then same dataset was used as input to CCA algorithm for linear blind system identification. Thus, P_a signals were estimated using AKCCA and CCA methods. These estimates were then compared against measured

aortic pressure signals. AKCCA and CCA reconstructed aortic pressure waveforms were found to be noisy; they were low-pass filtered using three tap average FIR filter to filter high frequency noise. Figure 4-7 illustrates reconstructed P_a signals using AKCCA and CCA along with measured P_a for one of the seven pressure signal datasets. Figure 4-7 top-left shows nonlinear MBSI AKCCA estimated P_a against measured P_a, top-right is the filtered version of AKCCA estimated P_a. Similarly, Figure 4-7 bottom-left shows linear MBSI CCA estimated P_a against measured P_a, bottom-right is the filtered version of CCA estimated P_a. It can be seen that AKCCA constructed P_a better aligns with measured P_a as compared to CCA constructed P_a. Also, when estimated aortic pressure is smoothened the correlation is improved; see Figure 4-7.

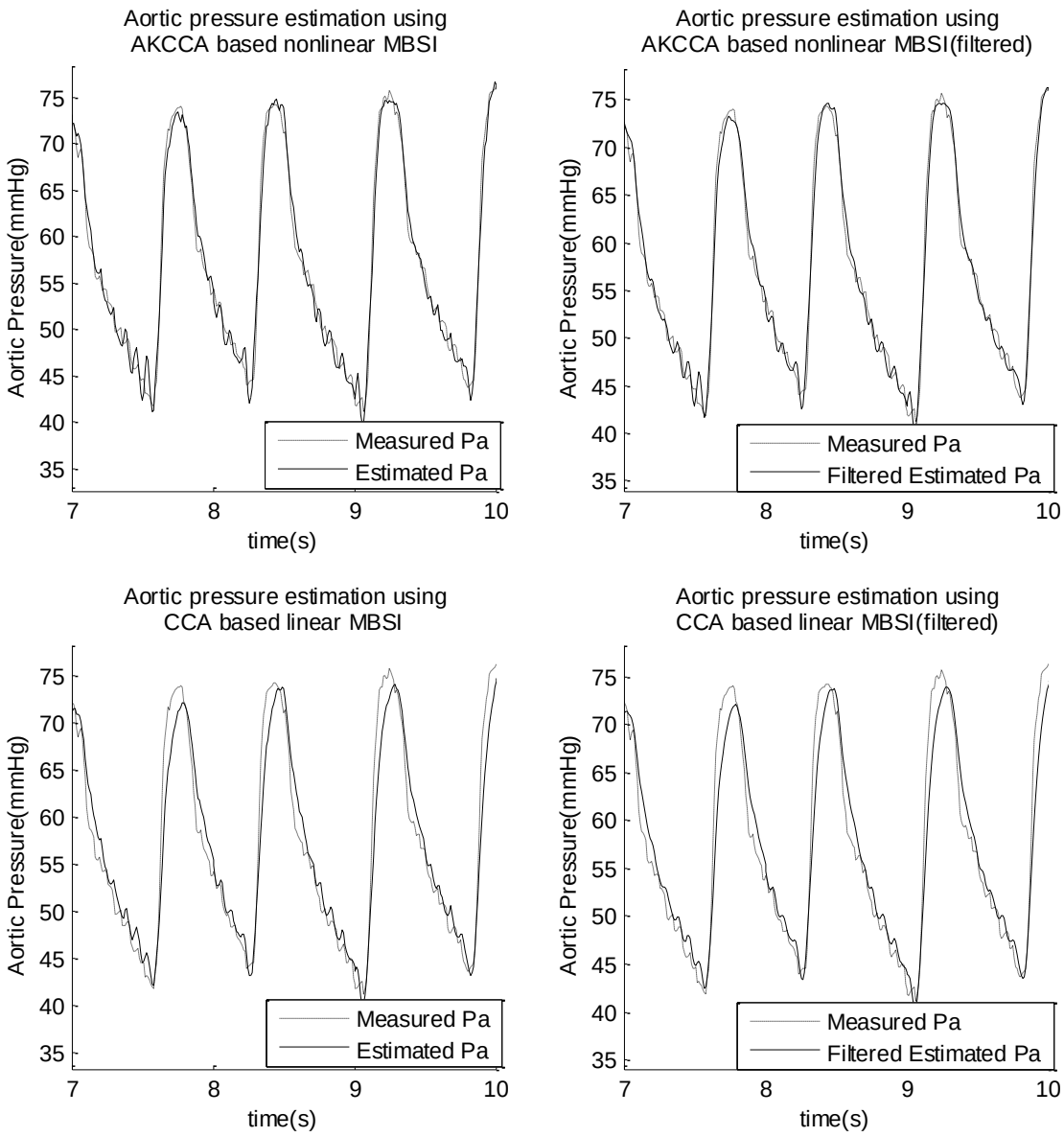

Fig. 4-7. Measured vs. estimated aortic pressure waveform using AKCCA based nonlinear MBSI and CCA based linear MBSI. Top-left: AKCCA generatedP_a. Top-right: filtered AKCCA generated P_a. Bottom-left: CCA generatedP_a. Bottom-right: filtered CCA generated P_a.

4.3.3.2 Arterial linear channel identification

Figure 4-8 shows example of linear arterial channel identification using nonlinear MBSI and linear MBSI approach. Figure 4-8 left displays FIR channels estimation using

AKCCA method and right one presents channels estimation using CCA method. Here, h_1 represents aortic-to-radial pressure signal transmission channel and h_2 represents aortic-to-femoral pressure signal transmission channel.

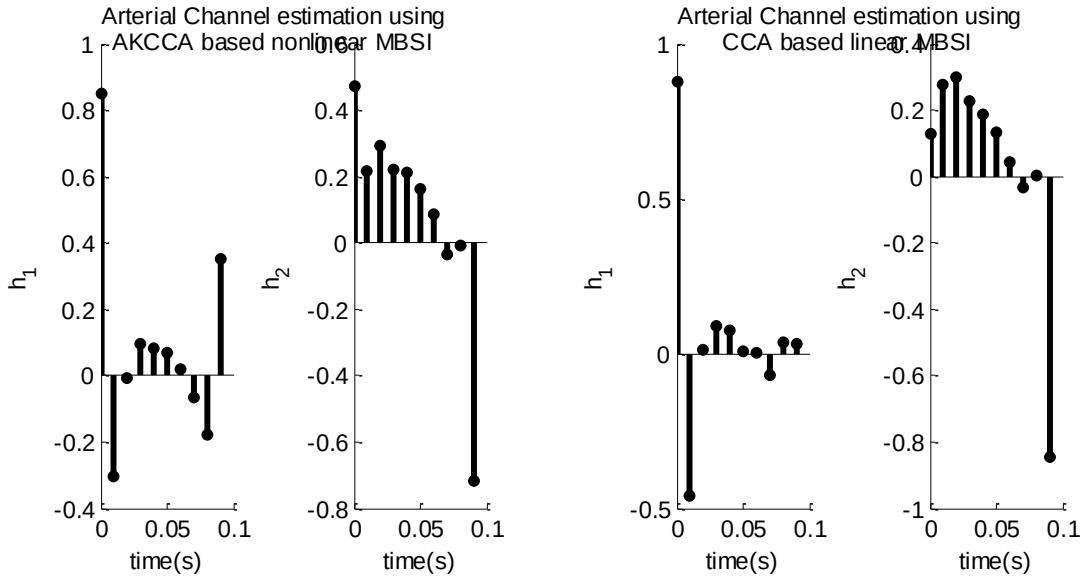

Fig. 4-8. Arterial channel identification using AKCCA based nonlinear MBSI (left) and CCA based linear MBSI (right). h_1: aortic-to-radial pressure signal transmission channel. h_2: aortic-to-femoral pressure signal transmission channel.

4.3.3.3 Correlation graph and Bland–Altman plot

The efficacy of nonlinear blind system identification for aortic pressure estimation was further assessed by correlation graph and Bland-Altman plot (Figure 4-9) between measured versus estimated P_a. For comparison these plots were computed for P_a estimated using nonlinear MBSI as well as linear MBSI. In correlation graphs, linear fitting was implemented while forcing zero intercept. As measure of fitting accuracy Pearson r-value squared (r^2) was calculated along with slope of fitted line. Alongside,

root mean squared error between measured and estimated P_a was computed to appraise statistical significance in difference.

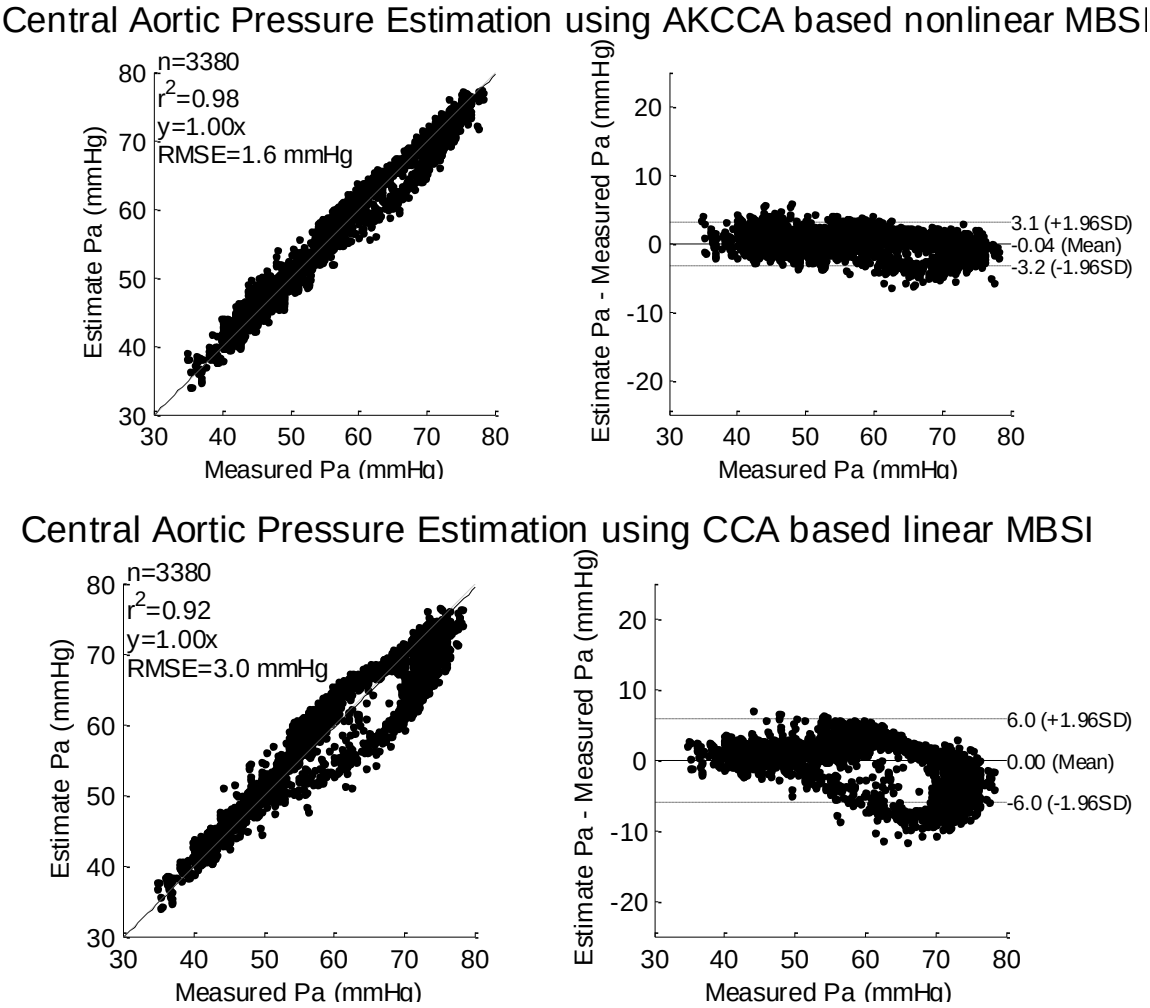

Fig. 4-9. Correlation graph for measured versus estimated P_a using nonlinear MBSI (top-left) and linear MBSI (bottom-left). Bland-Altman plots of P_a estimation error w.r.t. measured P_a for nonlinear MBSI (top-right) and linear MBSI (bottom-right). n: data points used for analysis, r^2: Pearson r-value squared, $RMSE$: root mean squared error, dashed line represents Coefficient of reproducibility ($\pm 1.96SD$) and solid line is mean of P_a estimation error.

Bland-Altman plots were obtained as sample-by-sample difference between measured and estimated aortic pressure waveform for nonlinear MBSI and linear MBSI. Coefficient of reproducibility (i.e. 1.96 times the standard deviation of the difference ($\pm 1.96SD$)) is displayed as dashed lines and solid line is mean of error in estimated P_a with respect to measured P_a. This correlation and Bland-Altman analysis was carried out using $n = 3380$ data point. Per correlation graphs, it was observed that nonlinear MBSI generated P_a versus measured P_a exhibited better line fitting ($r^2 = 0.98$) as compared to linear MBSI generated P_a versus measured P_a ($r^2 = 0.92$). $RMSE = 1.6mmHg$ in case of nonlinear MBSI produced P_a affirmed lower estimation error than in case of linear MBSI $RMSE = 3.0mmHg$. Coefficient of reproducibility ($1.96SD$) was computed lower for nonlinear MBSI ($\pm 3.1mmHg$) than for linear MBSI ($\pm 6.0mmHg$).

4.3.3.4 Data Analysis

Table 4-2. Root mean squared error for aortic pressure estimated using nonlinear MBSI and linear MBSI along with radial and femoral artery pressure with respect to measured aortic pressure

Data ID	Estimated Aortic Pressure RMSE (mmHg) using nonlinear MBSI			Radial Artery Pressure RMSE (mmHg)			Femoral Artery Pressure RMSE (mmHg)			Estimated Aortic Pressure RMSE (mmHg) using linear MBSI		
	TW	SP	DP	TW	SP	DP	TW	SP	DP	TW	SP	DP
1	1.61	0.78	0.68	5.06	5.75	4.19	5.59	12.68	1.73	3.05	1.79	0.93
2	1.30	0.93	1.08	5.10	1.90	2.68	5.05	12.47	1.52	1.37	0.94	1.97
3	2.18	2.28	2.11	5.36	5.32	2.80	3.68	10.49	2.81	2.19	2.32	2.17
4	2.18	1.34	0.88	9.73	4.47	3.28	5.87	12.95	1.31	2.64	2.24	1.46
5	2.25	3.11	0.81	8.68	10.39	6.08	8.95	20.86	1.73	7.20	10.46	2.53
6	2.59	2.71	1.45	7.74	6.45	5.46	9.07	25.37	1.96	3.06	2.78	1.83
7	3.39	4.24	1.36	6.11	4.81	2.80	8.46	26.55	2.00	4.08	4.30	3.74

Besides visual comparison between the measured vs. estimated P_a waveforms among nonlinear MBSI method and linear MBSI method, root mean squared error were computed for each case and used as figure of merit. $RMSE$ was computed for total waveform (TW), beat-to-beat systole pressure (SP) and beat-to-beat diastole pressure (BP). Lower the root mean squared error implied higher correlation between measured and estimated P_a. $TW\ RMSE$ is computed as sample-by-sample difference between measured P_a and estimated P_a for nonlinear and linear MBSI. Additionally, for

comparison these error metrics were computed for radial and femoral pressure waveforms with respect to measured aortic pressure waveforms. Data analysis from above mentioned all experiments is summarized in the Table 4-2. Based on the results, nonlinear MBSI demonstrated credible P_a estimation over variety of clinical dataset. Error metric computed on estimated P_a displayed far superior correlation with measured P_a as compared to unprocessed radial and femoral artery pressure waveforms. Furthermore, it can clearly be seen that P_a estimation using nonlinear MBSI outstands linear MBSI estimated P_a. Nonlinear MBSI estimated P_a was able to consistently reproduce TW, SP and DP of quality exceeding those from radial BP, femoral BP along with linear MBSI generated P_a. Linear MBSI generated P_a was observed to exhibit larger SP error than nonlinear MBSI based P_a. Lastly, three studied performance parameters of estimated aortic pressure were found to be broadly uncorrelated with corresponding reference values of these parameters.

4.3.4 Identification performance vs. data length

In this experiment, the influence of the number of data, N, on the aortic pressure estimation accuracy was studied. For reference, linear blind identification was performed on each data set for aortic pressure estimation as well. It can be seen from Table 4-3 that the root mean squared error decreases as data length used for non-linear blind identification increases; this is expected. Or in other words, performance of non-linear MBSI estimated P_a increases with increase in number of data points. On the other hand, the performance of linear MBSI estimated P_a decreases with increase in data length. This can be justified with following argument: linear blind identification assumes the system to be linear and hence estimates best linear fit for aortic pressure estimation. Nonlinear

aortic to peripheral pressure system can be assumed to be linear for short time. This assumption is violated more as the data length is increased. Hence, for linear MBSI estimated P_a with larger data length the error grows. This turns out to be one of the key drawbacks of using linear MBSI for P_a estimation. In order to favor linear assumption, very short data length has to be used for aortic pressure estimation. Adversely, shorter data length negatively impacts linear FIR filter estimation accuracy. Hence for linear MBSI there is trade of between FIR filter size (larger the order higher is filter accuracy) and nonlinear/ time invariance (larger the FIR filter length higher would be the error due to nonlinearity).

Table 4-3. Root mean squared error vs data length of non-linear MBSI and linear MBSI

Length of data N	Estimated Aortic Pressure TW Root Mean Squared error (mmHg)	
	Non-linear MBSI	Linear MBSI
1000	1.7152	2.9789
2000	1.6423	2.9060
3000	1.6197	3.0254
3400	1.6129	3.0502

Chapter 5: Reconstruction of Central Aortic Pressure from Varying Orders of Finite Impulse Response of Peripheral Arterial Blood Pressures

5.1 Limitation of previously proposed Aortic Pressure Estimation Technique

One drawback of using MBSI based estimation technique is that the arterial transmission channel order has to be known beforehand (E Moulines et al., 1995; Guanghan Xu et al., 1995; Lang Tong and Qing Zhao, 1999) . In the previously-mentioned aortic pressure estimation method linear finite impulse response (FIR) filter in the Wiener System model was assumed to be fixed 10^{th} order across all patient dataset. It is known that considerable degradation is observed if the channel order is under or overestimated (A P Liavas and P A Regalia, 2001; Liavas et al., ; S Karakutuk and T E Tuncer, 2011) by blind system identification. Especially, if the FIR filter coefficients of the channel being blind identified has negligible leading or trailing coefficients and the training data is noisy the system identification performance is further depreciated. SIMO MBSI performance is optimized if accurate channel order is used (S Karakutuk and T E Tuncer, 2011). Hence, it is desirable to estimate effective channel order in interest of better channel characterization (i.e. arterial channel identification) (A P Liavas et al., 1999; K Abed-Meraim et al., 1997) and equalization (i.e. P_a estimation) (Lang Tong and Qing Zhao, 1999). Here, a significantly improved technique to prior method is proposed by first estimating channel order for arterial transmission channel and then applying nonlinear MBSI for personalized aortic pressure estimation applications to cardiovascular diagnosis.

5.2 Improved Aortic Pressure Estimation Method

5.2.1 Blind order estimation

For sake of order estimation, the arterial system is assumed to be linear with no nonlinear function blocks. Figure 5-1 shows block diagram of SIMO linear model with outputs radial P_r and femoral P_f pressure signals and common input aortic pressure P_a. With this framework orders of linear FIR filters $\boldsymbol{h_{i=1,2}}$ can be estimated which then can be used for MBSI now with nonlinear function blocks $\boldsymbol{f_{i=1,2}}$ in SIMO Wiener model.

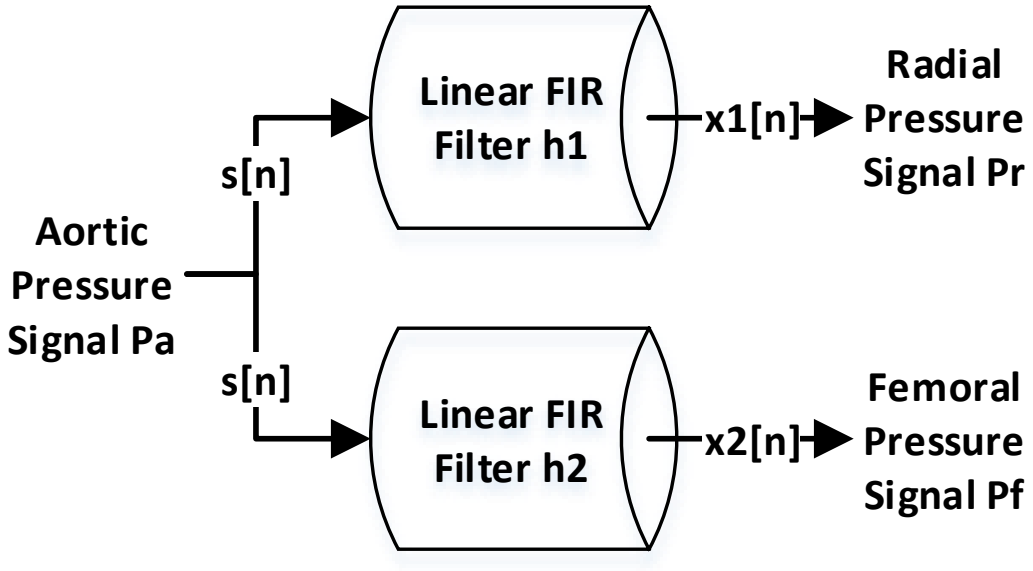

Fig. 5-1. The arterial system represented by the Single Input (aortic pressure) Multiple Outputs (radial and femoral arteries) Linear System model. FIR is the finite impulse response filter.

Several methods have been proposed for estimating either true channel order or its most significant part (which is effective channel order) (A P Liavas et al., 1999; A P Liavas and P A Regalia, 2001). A more flexible and robust method was presented for

SIMO channels order estimation with higher immunity to low signal-to-noise ratios and channels with negligible leading or trailing channel filter coefficients (Via et al., 2006). It is proved to be able to work with smaller datasets and colored (noisy) signals. This method was employed for channel order estimation prior to applying nonlinear MBSI for aortic pressure estimation. Here, this method is briefly summarized.

Consider SIMO system (two channels) with linear FIR filters a shown in Figure 5-1; here input signal $s[n]$ excites two distinct Lth order FIR filter channels $\boldsymbol{h_1}$ and $\boldsymbol{h_2}$ to produce two output signals $\boldsymbol{x_1}$ and $\boldsymbol{x_2}$ respectively. This can be expressed mathematically as

$$x_i[n] = \sum_{l=0}^{L-1} h_i[l]s[n-l] = h_i[n] * s[n] \tag{5-1}$$

Here $\boldsymbol{h_i} = [h_i[0], \dots., h_i[L-1]]^T$ is the impulse response vector of the i-th channel, L is the known channel length, and $h_i[n] * s[n]$ is the convolution between h_i and the input signal $s[n]$. Each of the two observations at the output can be compiled into data matrices:

$$\boldsymbol{X_i}(\hat{L}) = \begin{bmatrix} x_i[\hat{L}] & \dots & x_i[0] \\ \vdots & \ddots & \vdots \\ x_i[N-1] & \dots & x_i[N-\hat{L}-1] \end{bmatrix}, where\ i = 1,2 \tag{5-2}$$

where N is the number of data length, $\hat{L}$ is the estimated channel order.

In non-ideal conditions where measured output signals $\boldsymbol{x_1}$ and $\boldsymbol{x_2}$ are corrupted with noise channel identification, i.e. channel estimation $\widehat{\boldsymbol{h}}_{\boldsymbol{i}}(\hat{\boldsymbol{L}})$, can be performed blindly

using least square approach. This well-known least squares method, as introduced in (Guanghan Xu et al., 1995), minimizes following cost function:

$$J_{id}(\hat{L}) = \frac{\mathbf{1}}{\mathbf{2}} \left\| \boldsymbol{X_1}(\hat{L})\widehat{\boldsymbol{h}}_{\mathbf{2}}(\hat{L}) - \boldsymbol{X_2}(\hat{L})\widehat{\boldsymbol{h}}_{\mathbf{1}}(\hat{L}) \right\|^{\mathbf{2}} \tag{5-3}$$

$$\boldsymbol{Subject\ to} \left\| \boldsymbol{X_2}(\hat{L})\widehat{\boldsymbol{h}}_{\mathbf{1}}(\hat{L}) \right\|^{\mathbf{2}} = \left\| \boldsymbol{X_1}(\hat{L})\widehat{\boldsymbol{h}}_{\mathbf{2}}(\hat{L}) \right\|^{\mathbf{2}} = \mathbf{1}$$

These estimated channel filters $\widehat{\boldsymbol{h}}_{\boldsymbol{i}}(\hat{\boldsymbol{L}})$ can be deconvolved from their respective outputs $\boldsymbol{x_i}$ to retrieve the source signal $s[n]$. Another, more effective, method is to compute two equalizers $\boldsymbol{w_i}(\hat{\boldsymbol{L}})$ corresponding to each of $\boldsymbol{h_i}(\hat{\boldsymbol{L}})$ such that

$$\boldsymbol{X}_{\mathbf{i}}(\hat{L})\ \mathbf{w}_{\mathbf{i}}(\hat{L}) = \boldsymbol{s_i}, i = 1, 2 \tag{5-4}$$

Accounting for noise, these equalizers $\boldsymbol{w_i}(\hat{\boldsymbol{L}})$ can be estimated $\widehat{\boldsymbol{w}}_{\boldsymbol{i}}(\hat{\boldsymbol{L}})$ as solution to following minimization problem

$$J_{eq}(\hat{L}) = \frac{\mathbf{1}}{\mathbf{2}\hat{\boldsymbol{L}}} \left\| \boldsymbol{X_1}(\hat{L})\widehat{\boldsymbol{w}}_1(\hat{L}) - \boldsymbol{X_2}(\hat{L})\widehat{\boldsymbol{w}}_2(\hat{L}) \right\|^{\mathbf{2}} \tag{5-5}$$

$$\boldsymbol{Subject\ to} \left\| \boldsymbol{X_1}(\hat{L})\widehat{\boldsymbol{w}}_1(\hat{L}) \right\|^{\mathbf{2}} = \left\| \boldsymbol{X_2}(\hat{L})\widehat{\boldsymbol{w}}_2(\hat{L}) \right\|^{\mathbf{2}} = \mathbf{1}$$

This technique estimates channel order of FIR based SIMO system by simultaneously minimizing blind identification cost function $J_{id}(\hat{L})$ and blind equalization cost function $J_{eq}(\hat{L})$. Hence, a new cost function $\mathrm{J}(\hat{L})$ for joint identification and equalization of the SIMO channel is defined

$$\mathrm{J}(\hat{L}) = J_{id}(\hat{L}) + J_{eq}(\hat{L}) \tag{5-6}$$

This method exploits the fact that $J_{id}(\hat{L})$ decreases while $J_{eq}(\hat{L})$ increases with estimated channel order. Also, $J_{id}(\hat{L})$ is expected to asymptotically flatten out when estimated channel order is greater than or equal to true channel order while $J_{eq}(\hat{L})$ is expected to be relatively constant for estimated channel order less than or equal to true one, i.e.

$$\begin{cases} J(\hat{L}) = 0, if\ \hat{L} = L \\ J(\hat{L}) > 0, if\ \hat{L} \neq L \end{cases} \tag{5-7}$$

Consequently, the cost function $J(\hat{L})$ is at its minimum value when estimated channel order is equal to the true channel order.

The algorithm utilizes an iterative approach to estimate optimum channel order. First, channel order is guessed and incremented 1 through $\hat{L}_{max}$ (maximum possible channel order). In our application of blind order estimation for blind aortic pressure estimation $\hat{L}_{max}$ was assumed to be 30. For each of these channel order value $J_{id}(\hat{L})$ and $J_{eq}(\hat{L})$ is computed. Final order estimate $\hat{L}$ is chosen as guessed order for which joint identification and equalization cost function, i.e. $J(\hat{L})$ is minimum. Arterial tree SIMO system FIR filter order was estimated using above mentioned algorithm and thus estimated channel order was then consumed for nonlinear MBSI based aortic pressure estimation.

5.2.2 Estimation of aortic pressure based on nonlinear MBSI

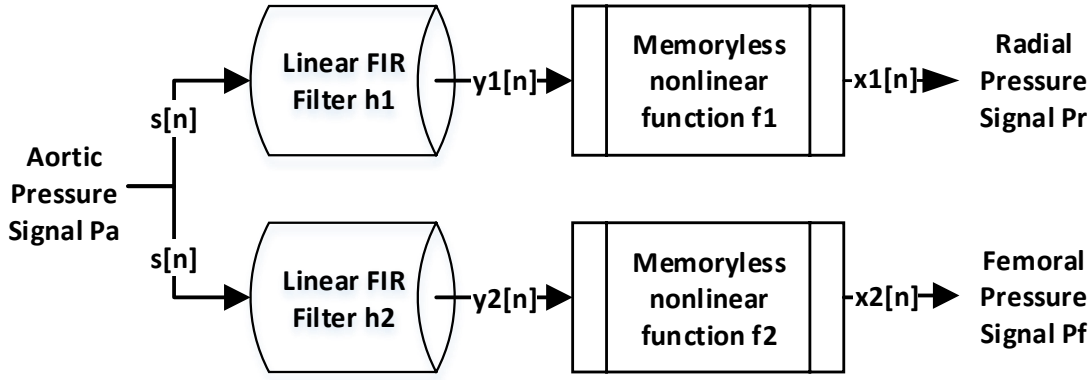

Fig. 5-2. A modified Single Input (aortic pressure) Multiple Outputs (radial and femoral arterial pressures) arterial system model.

Nonlinear MBSI for SIMO Wiener model as shown in Figure 5-2 with outputs: radial P_r and femoral P_f pressure signals and common input aortic pressure P_a was engaged for aortic pressure estimation. The representation of this input-output relation is given by

$$x_i[n] = f_i\left(\sum_{l=0}^{L-1} h_i[l]s[n-l]\right) \tag{5-8}$$

Where $f_i(.)$ is nonlinear memoryless function.

In particular, alternating Kernel canonical correlation analysis (AKCCA) method, introduced by Vaerenbergh et al. (Van Vaerenbergh et al., 2013), was employed. This method is explained in detail in our previous work (Patel et al., 2017). Here, high level algorithm of AKCCA based nonlinear MBSI is provided for P_a estimation. This method defines and solves the optimization problem. An iterative strategy was carried out that alternates between estimating linear channels $\widehat{\boldsymbol{h}}_{\boldsymbol{i}}$ and the nonlinearity estimates $\widehat{\boldsymbol{\alpha}}_{\boldsymbol{i}}$ until

the solution converges to minimize the error of estimation. SIMO Wiener model output P_r and P_f are input to this algorithm. Initially, nonlinear function is assumed to be unity and Canonical Correlation Analysis (CCA) is applied to estimate linear FIR filters $\widehat{\boldsymbol{h}}_{\boldsymbol{i}}$, where $i = 1, 2$ for two channel SIMO arterial tree. Next, nonlinear memoryless function is estimated using Kernel Canonical Correlation (KCCA) algorithm. These steps are repeated until the blind identification cost function converges. Similar to most of the other blind identification technique this algorithm loses the scale factor of estimates. The reconstructed aortic pressure was scaled such that mean peripheral pressure is same as mean aortic pressure. This step is justified by Poiseuille's law (Noordergraaf, 2011).

5.3 Experimental Results

5.3.1 Experimental Data

Table 5-1. Summary of Hemodynamic parameters

Data ID	PTT_a (ms)	PTT_a (ms)	$meanBP$ (mmHg)	dBP_a (mmHg)	sBP_a (mmHg)	dBP_f (mmHg)	sBP_f (mmHg)	dBP_r (mmHg)	sBP_r (mmHg)
1	60	80	61.38	47.65	79.39	46.14	92.66	50.12	77.66
2	50	80	70.49	49.6	98.8	48.98	106.5	51.47	103.3
3	70	110	49.53	43.93	69.05	43.49	80.96	44.54	74.18
4	130	100	59.81	46.59	78.1	45.32	98.88	48.95	75.08
5	50	100	58.58	43.27	82.58	42.26	98.57	46.61	78.25
6	50	70	65.98	46.39	94.85	44.82	117.2	52.5	84.52
7	60	70	51.55	36.94	86	35.9	115.4	42.48	78.52
8	70	100	65.96	53.92	87.61	51.99	100.1	56.22	85.13
9	50	90	59.1	46.64	78.67	44.83	103.1	51.85	72.74

PTT_{af}: pulse transit time between aorta and femoral artery, PTT_{ar}: pulse transit time between aorta and radial artery, $meanBP$: mean blood pressure, dBP: diastolic blood pressure and sBP: systolic blood pressure, *f*: femoral artery, *r*: radial artery.

With the modified and improved nonlinear model, aortic pressure was estimated based on 9 patient datasets previously acquired with IRB approval at the University of Alberta, and described in detail elsewhere (Rashedi et al., 2013). Briefly, beat-to-beat

blood pressure waveforms were simultaneously recorded in the radial artery (P_r) artery, the femoral artery (P_f) and the central aorta (P_a). The data were collected for 120 seconds and sampled at a rate of 1kHz in patients undergoing cardiopulmonary bypass surgery. These hemodynamic data are summarized in Table 4-4. In addition, pulse transit times (PTT) that are commonly used as an index of vascular stiffness is also calculated for aorta to femoral artery (PTT_{af}) and for aorta to radial artery (PTT_{ar}). A wide range of variations in pulse pressures and pulse transit times are seen and suitable for evaluation of the newly modified It has been recognized that pulse transit time can exert considerable influence on the arterial pulse transmission characteristics (Li, 2000),(Li, 2004; Sugimachi et al., 2001; Westerhof et al., 2007). These allow us to validate the present improved method at varying physiological conditions.

It should be pointed out that $meanBP$, dBP and sBP were calculated as the average values for a duration of 35 sec. Similar average values were obtained for PTT_{af} and for PTT_{ar}.

5.3.2 Signal Pre-processing and Signal Conditioning

35 second segments of measured pressure signals are extracted from each of the 120 sec long dataset. This ensures that these segments were free from any signal corruption. Since the original signals were sampled at 1 KHz, the aortic pressure, femoral and radial arterial pressures were subsequently downsampled to 100Hz. This is adequate, since the frequency contents of these signals are below 25 Hz. Arterial system identification problem can be isolated from phase delay (among P_a, P_r and P_f) identification problem. This is accomplished by having P_r and P_f advanced by PTT_{ar} and PTT_{af} respectively,

with respect to aortic pressure. The analysis was then applied to these 35 sec segments. The sampled waveforms P_a, P_r and P_f are shown in Figures 5-3, 5-4 and 5-5.

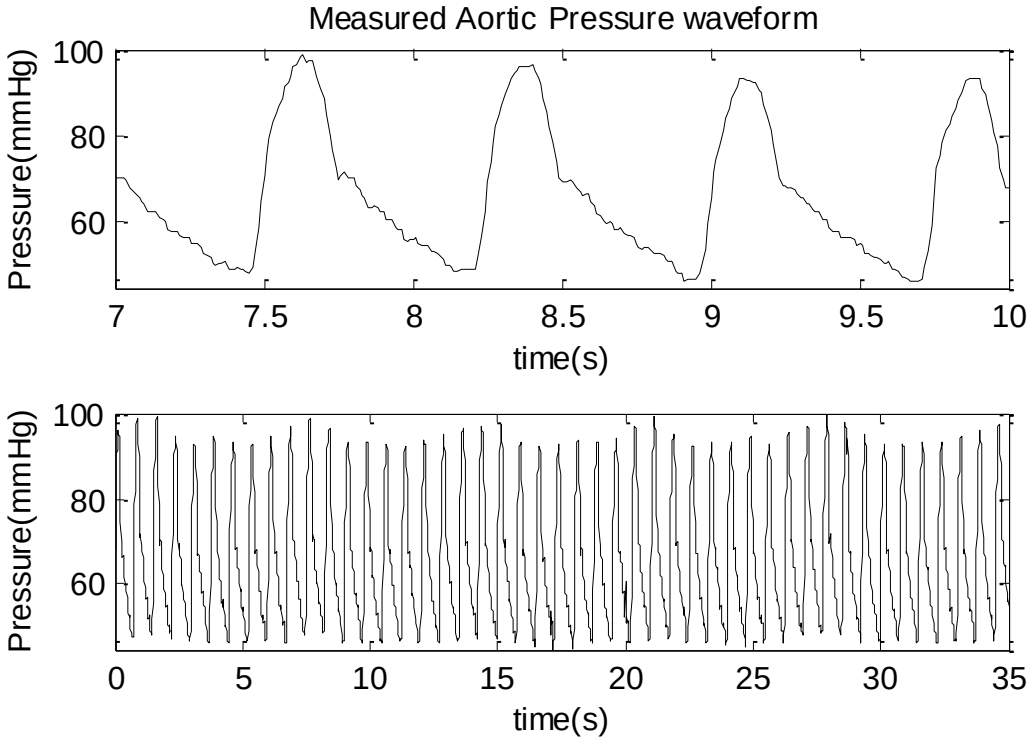

Fig. 5-3. Measured blood pressure waveforms in the aorta.

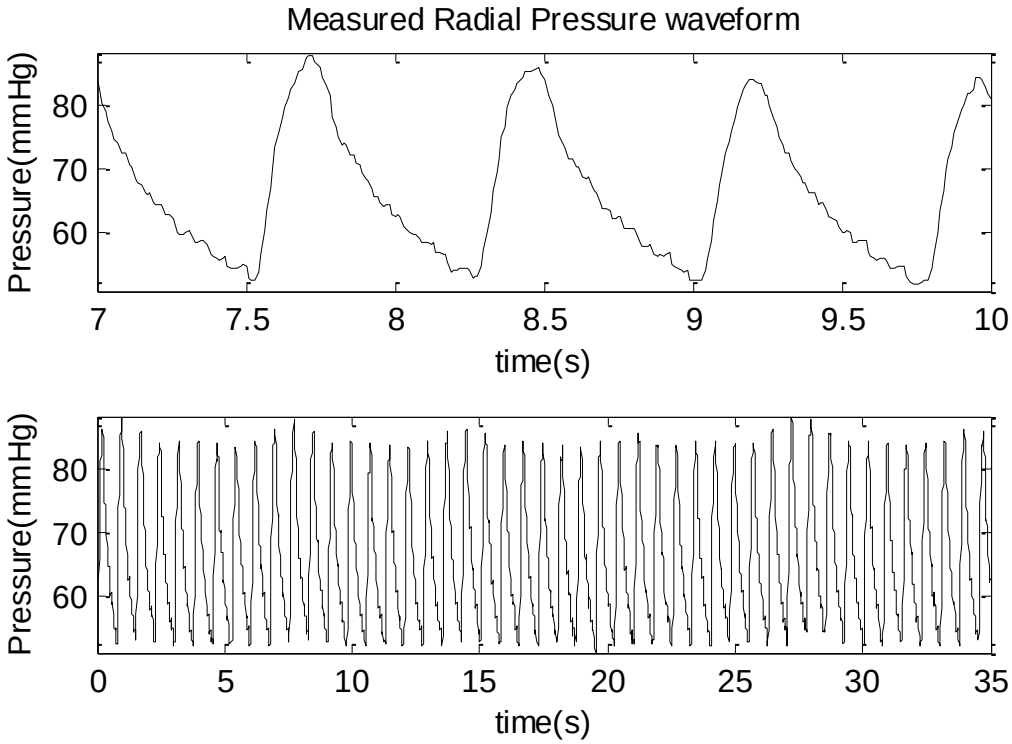

Fig. 5-4. Measured blood pressure waveforms in the radial artery

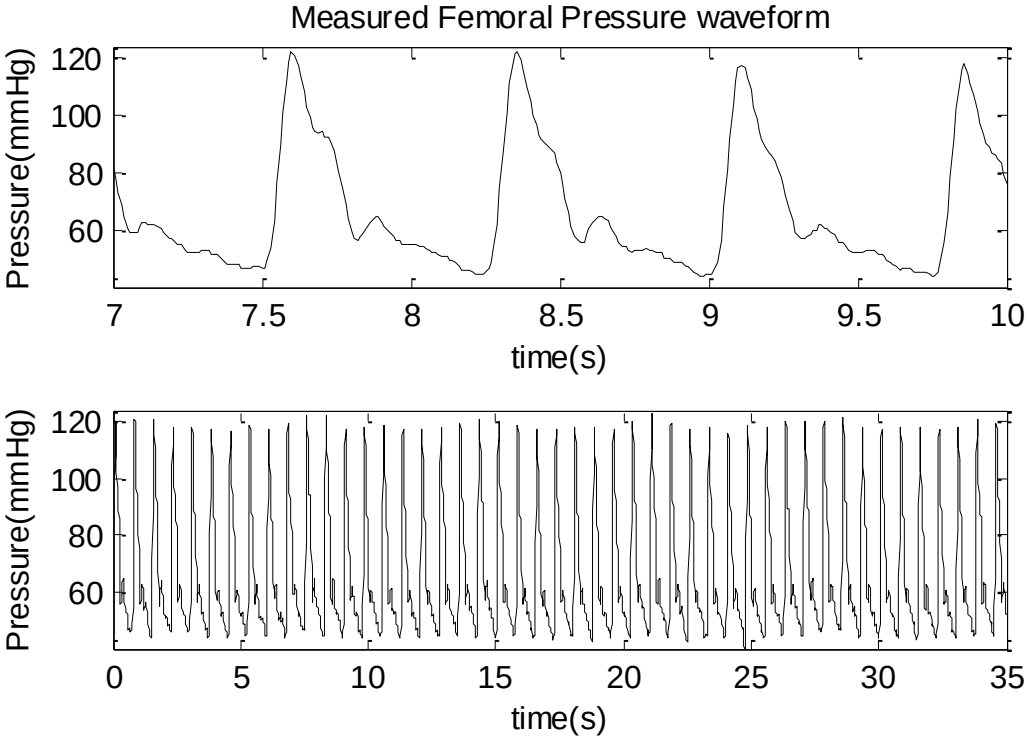

Fig. 5-5. Measured blood pressure waveforms in the femoral artery.

5.3.3 Aortic Pressure Estimation

5.3.3.1 Influence of FIR filter order on MBSI

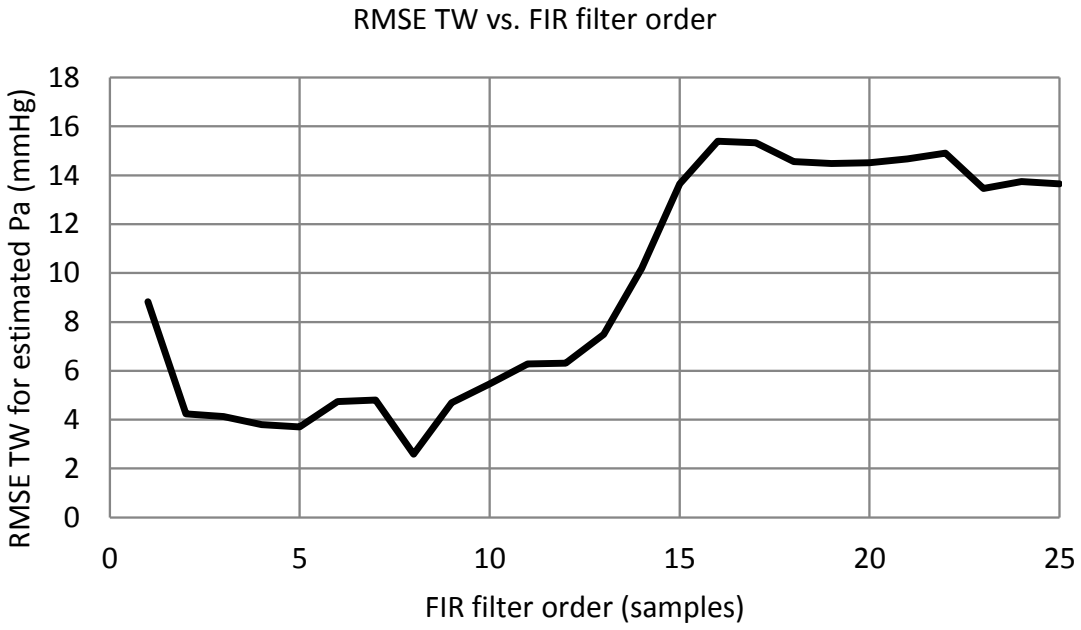

Fig. 5-6. Nonlinear MBSI estimated Aortic pressure TW RMSE vs. FIR filter order

In order to validate significance of proposed effort influence of FIR filter order was studied on MBSI and hence aortic pressure estimation, prediction error was computed as a function of filter order. Root mean squared error of total waveform was calculated between true P_a and P_a estimated using nonlinear MBSI with FIR filter order 1 through $\hat{L}_{max} = 25$. Figure 5-6 exhibits an example of $TW\ RMSE$ with respect to estimated Wiener model FIR filter order. Estimation error was found to be a convex function of channel order with minima occurring at effective channel order (8 in displayed example). In other words, if channel order is underestimated or overestimated aortic pressure

estimation accuracy is downgraded. MBSI performance is optimized with right choice of channel order.

5.3.3.2 Model Estimated vs Experimentally Measured Aortic Pressure Waveform

The performance of the newly formulated model with effective channel order (nonlinear MBSI-Gen2) for aortic pressure estimation was evaluated on each of the nine datasets. To demonstrate merit of the present approach, our previously utilized fixed order FIR filter (nonlinear MBSI-Gen1) for aortic pressure estimation was also applied to all 9 datasets. Waveforms estimated from both MBSI-Gen2 and MBSI-Gen1 were compared to those measured. MBSI-Gen1 and Gen2 resynthesized waveforms tended to be somewhat noisy and low-pass filtering was applied through three-tap average FIR filter. Figure 5-7 and 5-8 respectively illustrate reconstructed P_a signals using nonlinear MBSI-Gen2 (with estimated 8^{th} order FIR filter) and nonlinear MBSI-Gen1 (with fixed 10^{th} order FIR filter) along with measured aortic pressure for one of the 9 datasets. It is clear that nonlinear MBSI-Gen2 reconstructed P_a aligns better with measured P_a as compared to nonlinear MBSI-Gen1 reconstructed aortic pressure waveform.

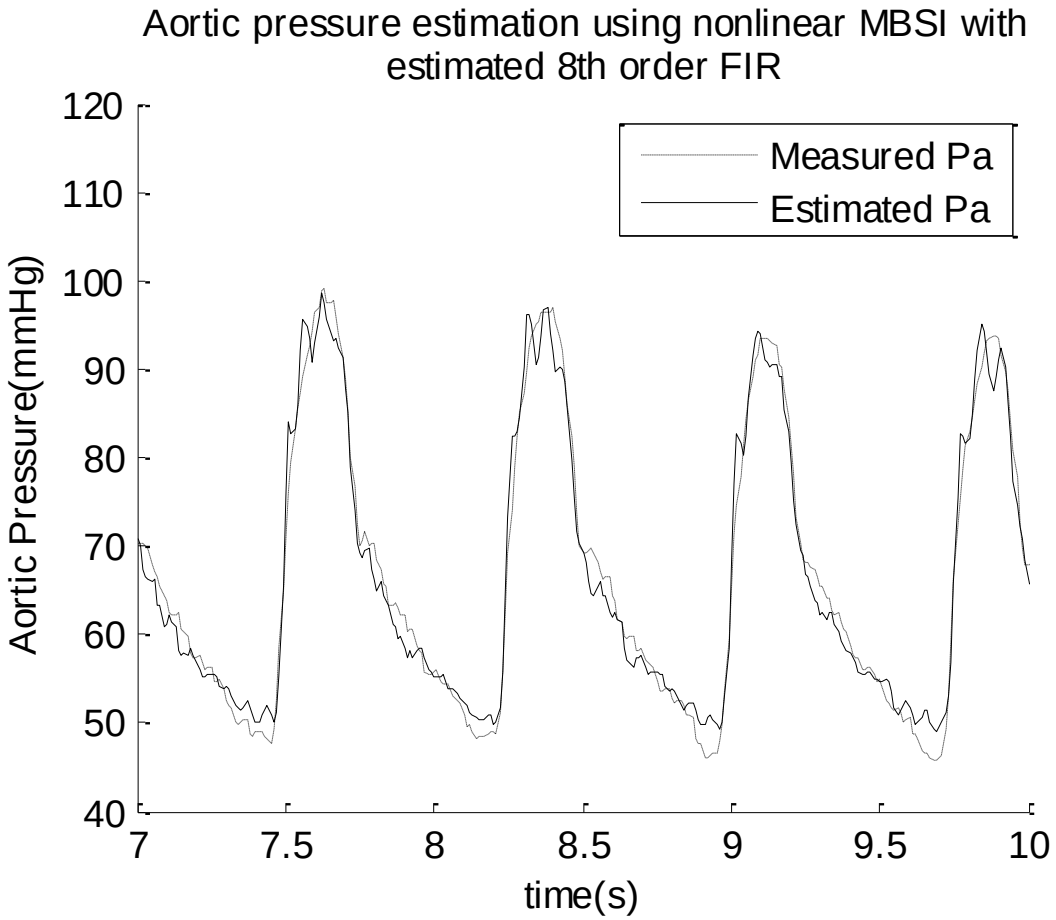

Fig. 5-7. Comparison of estimated and measured aortic pressure waveforms using nonlinear MBSI-Gen2

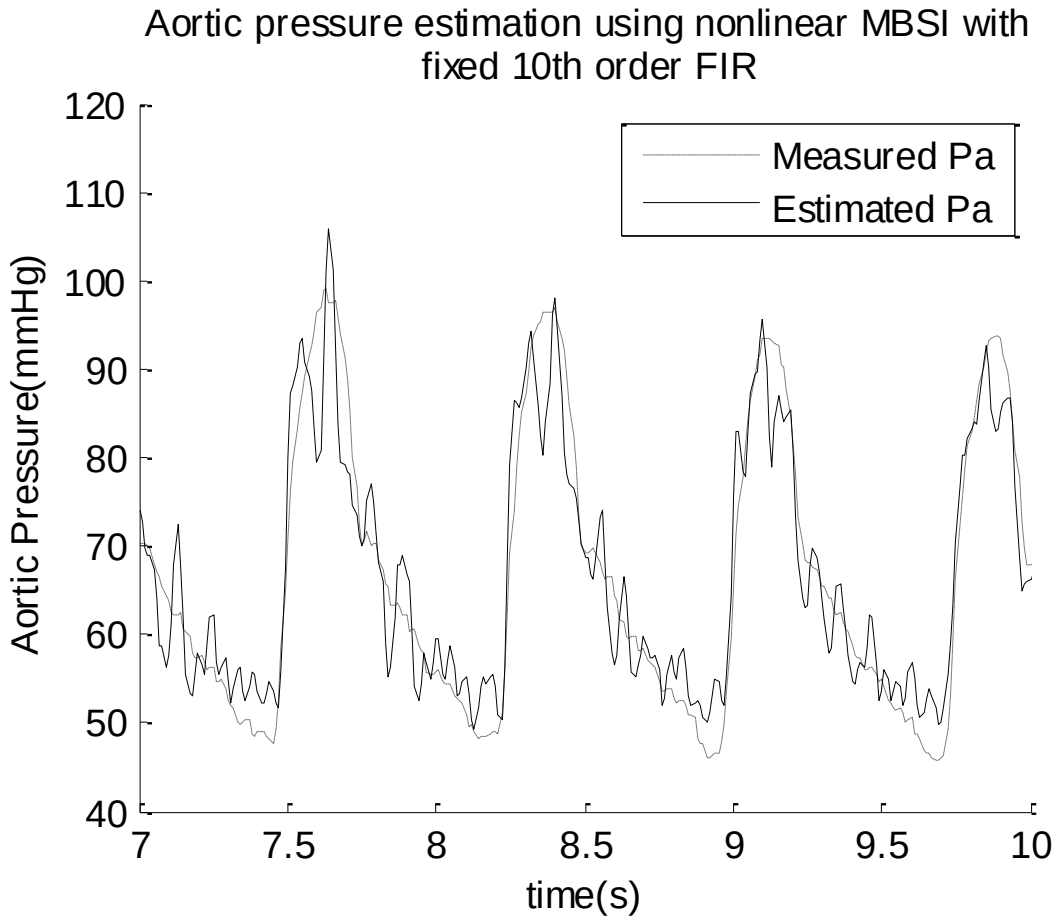

Fig. 5-8. Comparison of estimated and measured aortic pressure waveform using nonlinear MBSI-Gen1

5.3.3.3 Arterial linear channel identification

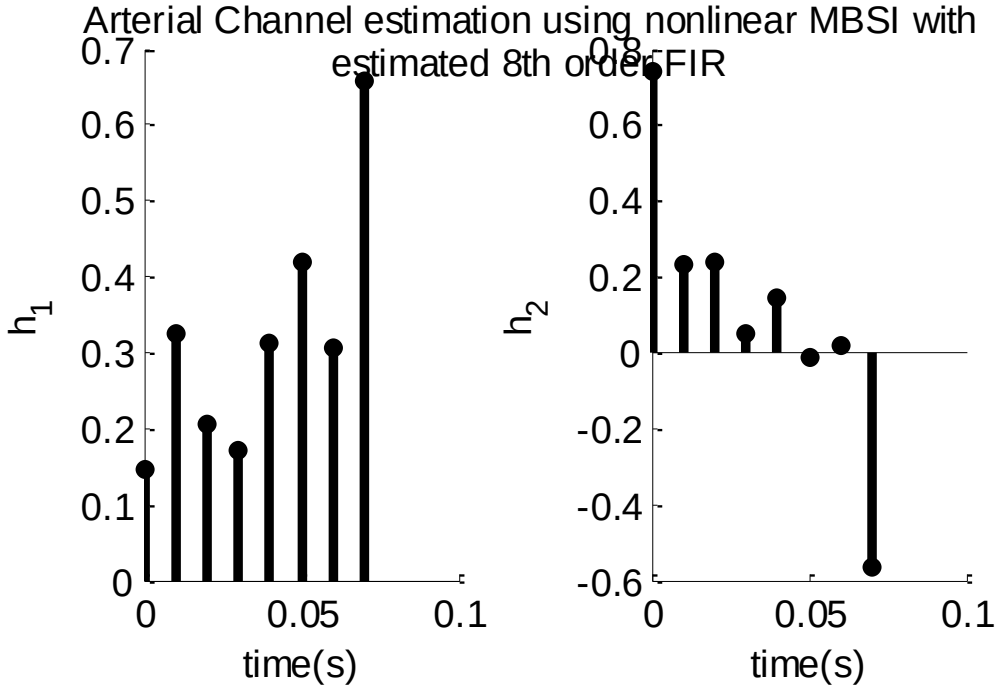

Fig. 5-9. Arterial pulse transmission path channel identification using nonlinear MBSI-Gen2 with estimated FIR filter order 8. h_1: aorta to radial artery pulse pressur transmission channel. h_2: aorta to femoral artery pulse pressure transmission channel.

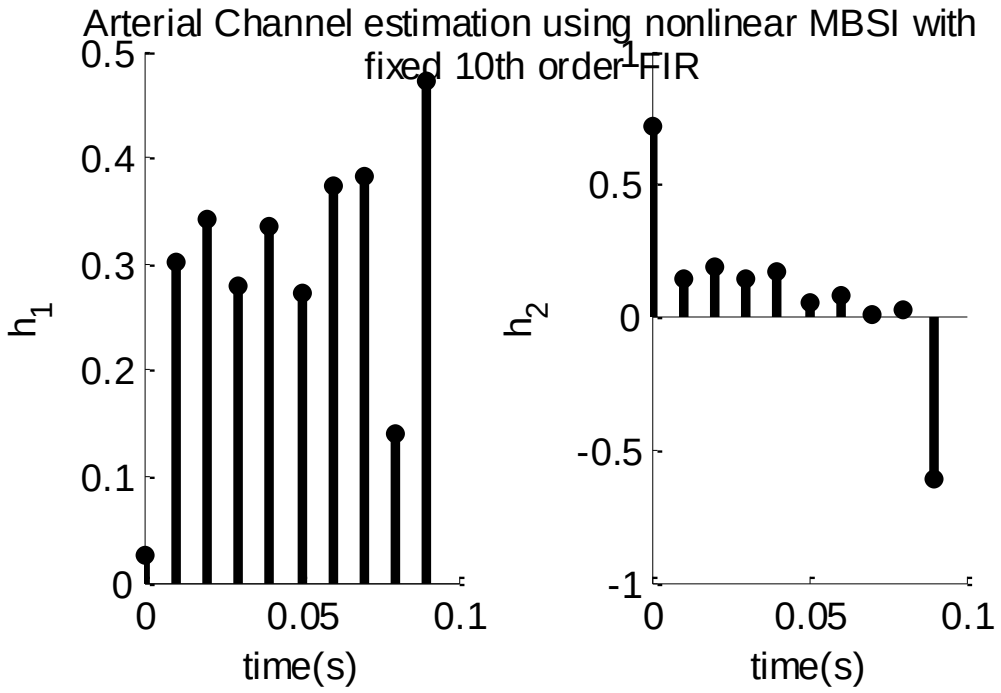

Fig. 5-10. Arterial pulse transmission channel identification using nonlinear MBSI-Gen1 with fixed FIR filter order 10. h_1: aorta to radial artery pressure pulse transmission channel. h_2: aorta to femoral artery pressure pulse transmission channel.

Examples of linear arterial channel identification using nonlinear MBSI-Gen2 (with estimated 8th order FIR filter) and nonlinear MBSI-Gen1 (with fixed 10th order FIR filter) approach respectively are shown in Figures 5-9 and 5-10. Here, h_1 represents aorta to radial artery pulse pressure transmission channel and h_2 represents aorta to femoral artery pulse pressure transmission channel.

5.3.3.4 Assessment by Pearson's Correlation and the Bland–Altman plot

To further assess the efficacy of MBSI-Gen2 for estimation of aortic pressure, correlation analysis and Bland-Altman plot are performed. The results are shown in

Figure 5-11. In correlation graphs, a linear fit with 0 intercept was implemented. The accuracy of the fit was quantified by r^2 (Pearson's approach), calculated along with slope of fitted line. RMSE (root-mean- squared error) between measured and estimated aortic pressure was computed to infer statistical significance in difference.

Element-by-element deviation of measured P_a from measured P_a was computed to produce Bland-Altman plots for nonlinear MBSI Gen1 as well as Gen2. Waveforms of data length $n = 3380$ were used to generate correlation and Bland-Altman plots. From this correlation study it was found that nonlinear MBSI-Gen2 generated P_a versus measured P_a presented higher correlation ($r^2 = 0.97$) as compared to nonlinear MBSI-Gen1 generated P_a versus measured P_a ($r^2 = 0.88$). $RMSE = 2.6mmHg$ in case of nonlinear MBSI-Gen2 produced P_a confirmed lower estimation error than in case of nonlinear MBSI-Gen1 $RMSE = 5.4mmHg$.

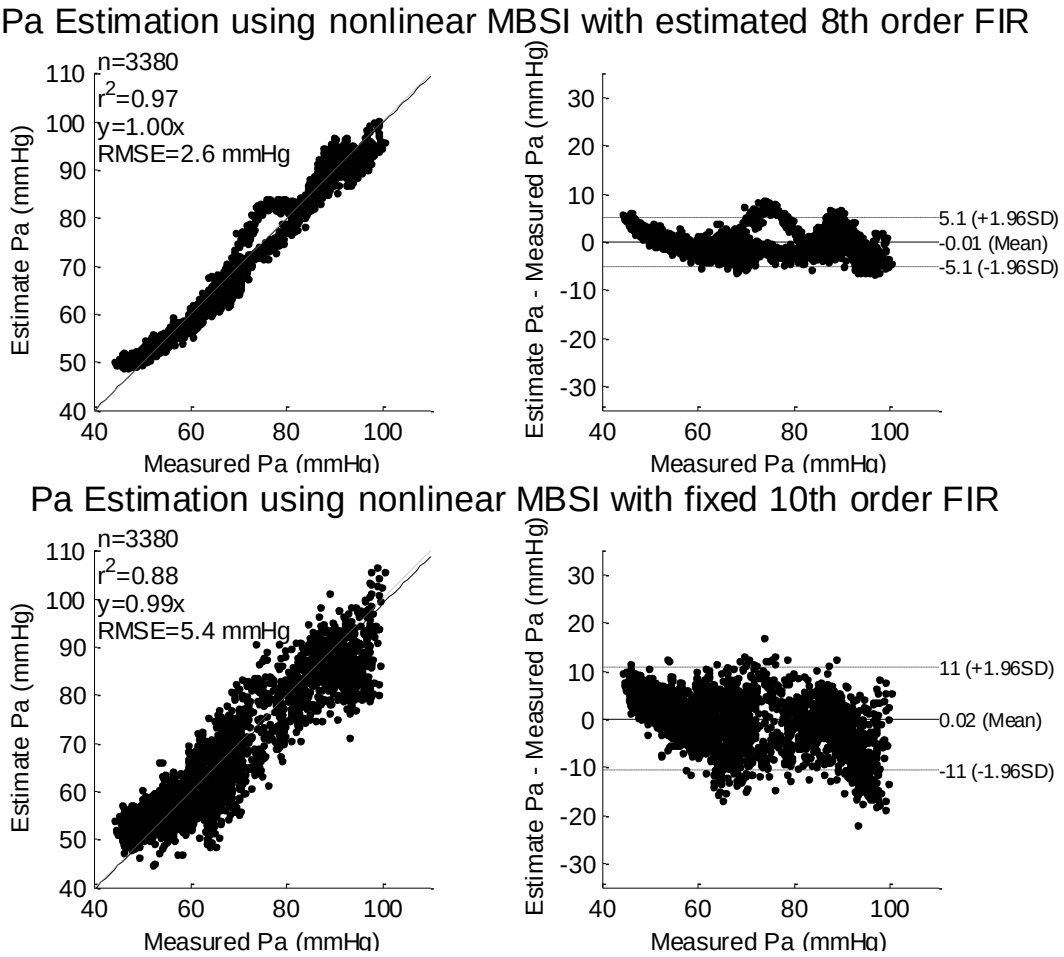

Fig. 5-11. Correlation obtained for measured versus estimated aortic pressure,using nonlinear MBSI-Gen2 (top-left) and Gen1 (bottom-left). Bland-Altman plots of aortic pressure estimation error with respect to measured aortic pressure for onlinear MBSI-Gen2 (top-right) and Gen1 (bottom-right). n: data points used for analysis. Dashed line represents coefficient of reproducibility ($\pm 1.96SD$) and solid line is mean of aortic pressure estimation error.

5.3.3.5 Data Analysis

Quantitative comparison between the measured and estimated aortic pressure waveforms betwen the present (nonlinear MBSI-Gen2) and previous (MBSI-Gen1)

methods was assessed RMS error, or RMSE. $RMSE$ was calculated for the total pulse pressure waveform (TW), systole pressure (sBP) and diastole pressure (dBP). Obviously, the lower the RMSE, the higher the correlation between estimated and measured aortic pressure waveforms. $TW\ RMSE$ is computed as sample-by-sample difference between estimated and measured aortic pressure waveforms for nonlinear and linear MBSI. Table 5-2 summarizes the findings. It is clear from the results that nonlinear MBSI-Gen2 demonstrated accurate estimation of aortic pressure waveform over differing physiological conditions of the acquired clinical datasets. The computed error metric of estimated aortic pressure demonstrated significantly improved correlation with the measured aortic pressure as compared to the previous Gen1 method. Nonlinear MBSI-Gen2 estimated aortic pressure was able to consistently reproduce TW, systolic and diastolic pressures more reliably than those from obtained from nonlinear MBSI-Gen1 method.

Table 5-2. Root mean squared error for aortic pressure estimated using nonlinear MBSI-GEN2 and GEN1 with respect to measured aortic pressure

Data ID	Estimated Aortic Pressure RMSE (mmHg) using nonlinear MBSI with estimated order FIR filter			Estimated FIR filter order	Estimated Aortic Pressure RMSE (mmHg) using nonlinear MBSI with fixed 10^{th} order FIR filter		
	TW	SP	DP		TW	SP	DP
1	1.71	1.03	2.81	8	1.95	1.03	3.04
2	3.77	2.35	3.44	7	4.70	2.36	3.54
3	1.96	3.18	1.12	7	2.30	3.49	2.83
4	4.84	0.58	4.34	12	5.15	0.74	4.65
5	3.09	0.74	2.78	7	4.76	1.63	5.51
6	2.58	1.50	3.38	8	5.45	4.07	4.66
7	2.67	2.30	3.72	6	3.94	2.68	4.35
8	2.37	1.51	2.47	7	4.99	4.43	3.51
9	2.29	2.95	1.02	13	3.00	3.62	1.12

Chapter 6: Discussion and Suggestions for Future Research

6.1 Discussion

Morphological changes in central aortic pressure waveform has been shown to reflect overall arterial system function and its interaction with the left ventricle (Li, 2010; Kerkhof et al., 2013). Thus, augmentation index, reduced large artery compliance and increased vascular stiffness and pulse wave reflections have targeted the aortic pressure waveforms as a compass in therapeutic applications. Derivation of central aortic pressure from peripheral arterial pressure such as the radial has been traditionally based on the model-based or generalized transfer function (Söderström et al., 2002; Fetics et al., 1999; Varanini et al., 2003; Karamanoglu and Feneley, 1997; Segers et al., 2000; Sugimachi et al., 2001). Several of these are based on linear system or constant compliance model assumptions. It requires calibration adjustment for diastolic pressure and mean blood pressure. As such, it is similar to the linear FIR filter model's g_1 shown in Chapter 3. Different approaches in the literature pose their own set of pros and cons; here some of these advantages and limitations of these approaches are highlighted:

6.1.1 Advantages and Limitations of previously presented methods:

6.1.1.1 Black Box System Identification

The generalized transfer function techniques with linear ARX (Chen et al., 1997) and nonlinear neural network ARX (Varanini et al., 2003) method exploit common filter design for aortic pressure estimation. The filter design in this type of methods is generic and do not change with respect to time, patient or biological condition. In contrary, this presumption results into identical estimated aortic pressure for all patients with identical

radial arterial pressure data independent regardless of their cardiovascular hemodynamic condition. Several studies have shown that arterial compliance and impedance, wave reflection and heart-artery interaction changes with age, medical condition (which could further deviate due to vasoactive drug therapy) (Nichols et al., 1985). Hence, it is desirable that the peripheral-to-aortic pressure transfer function accustom to inter-subject as well as intra-subject variability. Even Chen and Varanini's studies have admitted that aortic pressure estimation enhances upon using individual transfer function instead of generalized transfer function.

When compared the amplitude and phase plots of transfer function derived from different patient dataset differ considerably owing to differences in arterial compliance as well as phase and magnitude of reflected pressure waves. The relation between blood flow, pressure, arterial compliance and wave reflection differ from person to person and also with respect to vascular system dynamics (Li, 2000; Li, 2004). Also, a generalized transfer function is not truly an average of entire population as in practice only handful number of subjects data are normally used to derive generalized transfer function. Hence, in reality averaged transfer function has considerable error due to training data set selection bias.

6.1.1.2 Gray Box System Identification

The wave separation method (Stergiopulos et al., 1998) provides adequate per patient transfer function derivation. But, this method is based on several assumptions and hence bears some limitations. This approach assumes blood vessels to be a single frictionless uniform branch with linear arterial compliance. This can introduce errors if compliance varies greatly with pressure (Li et al., 1990), or if artery network has more than one large

arterial branch. Also, this method relies heavily on time delay between transmitted pressure signal and reflected signal. Small measurement error in time delay can result in unacceptable aortic pressure estimation. It may also be impractical to continually measure time shift to calibrate model on the fly to adapt to any temporal changeability in vascular properties.

The tube model method (Swamy et al., 2009) provides comprehensive adaptive transfer function technique. However, parallel tube model assumes that arterial compliance is time invariant and that there are no major branching in the arterial tree and wave reflection primarily arises at arterial termination due to large impedance. These could cost parametric modelling error which would then convolve with reconstruction algorithm to result in aortic pressure estimation discrepancy. Similar to the wave reflection method, this tube model algorithm extensively depends on delay time measurement of wave propagation. Good accuracy in time lag requires invasive measurement of travel time of pressure wave from start (aorta) to end (peripheral measurement site). Noninvasive time lag measurement techniques are necessary to calibrate the estimation model and a small measurement error in time delay can result in to significant modelling error. These constraints may render this approach rather impractical despite of its high performance and adaptive nature.

6.1.1.3 Blind System Identification

Blind system identification approach for aortic pressure estimation does not require any explicit calibration or personalized measurements (which in most cases are invasive measurements). Hence, this method by nature is self-calibrating to account for any inter-personal along with intra-personal vascular dynamics inconstancy. Another advantage of

this type of technique is that any measurement errors (e.g. two catheter systems) that are noncoprime i.e. common between the two measurand peripheral signals are cancelled out automatically as blind system identification can only detect coprimeness between the two measurands.

The FIR based MBSI method (Swamy et al., 2007) demonstrated outstanding performance to reconstruct aortic pressure by processing two or more peripheral pressure waveforms. However, their proposal is established on few assumptions. Each of the arterial branches to be modeled is assumed to be linear time invariant for each of 1 min segment of signals. Time invariance approximation can be rationalized by the argument that 1 min period is short enough for the arterial system to reach almost steady state. Nonetheless, neglecting nonlinearity of hemodynamics to entertain modelling simplicity can cost aortic pressure estimation error. Swamy's findings that estimated aortic pressure waveforms (with above mentioned assumptions) very closely mimicked measured aortic pressure could have been biased by their sample data. It is possible that the data set on which Swamy's FIR MBSI technique was verified might not have covered extreme cases with higher nonlinearity. Hence, these MBSI performance study results cannot be considered convincing enough to validate vascular properties linearity approximation.

Similar to the MBSI, the LaMBSI algorithm (McCombie et al., 2005) assumes the arterial network channels to be linear time invariant systems. Based on previous studies (Fruzzetti et al., 1997) it has been proven that cardiovascular system is neither linear nor time invariant. This has been mainly attributed to nonlinear terms in the Navier-Stokes equation and nonlinear time varying arterial compliance. To minimize modeling error due to these assumptions shorter segments of input signals are used for system modeling

which would warrant near steady state condition. As MBSI transfer function is computed for each of such small segmented signals continuously, the model is believed to adapt to vascular dynamics. In order to calculate larger number of FIR filter coefficient (desired for better accuracy of filter design) larger window of pressure data is needed (Xu et al., 1995). This turns out to be trade of between FIR filter size (larger the order higher is filter accuracy) and nonlinear/ time invariance (larger the FIR filter length higher would be the error due to nonlinearity and also time varying dynamic of the arterial system).

6.1.2 Contribution of current methodology

Correlation study presented in Chapter 3 validates the Wiener System based Arterial Transmission Channel model. In particular, comparison between linear FIR filter simulated radial (or femoral) pressure and measured radial (or femoral) pressure waveform showed that the fitting between $P_p^{simulated}$ and $P_p^{measured}$ is improved for higher order polynomial as compared to lower order polynomial. In general, it can be seen that 2nd and 3rd order term coefficients from $P_r^{simulated}$-to-$P_r^{measured}$ fitting are higher than those computed from $P_f^{simulated}$-to-$P_f^{measured}$ fitting. Hence, it can be inferred that arterial channel is more nonlinear for aortic-to-radial case as compared to aortic-to-femoral arterial channel. Besides, linear, quadratic or cubic polynomial fitted coefficients from Group 1 studies and Group 2 studies were found to be broadly uncorrelated with each other. Upon simulating Wiener model for the three cases it was observed that g_1 generated P_r and P_f underestimate systole pressures while g_2 or g_3 generated P_r and P_f did better job computing systole pressures. Based on the results, g_2 Wiener model demonstrated credible P_r and P_f estimation as compared to g_1 Wiener model (i.e. only linear FIR filter) over variety of clinical dataset. Error metric computed

on estimated P_r and P_f displayed further improved correlation for g_3 Wiener model simulated radial and femoral pressure waveforms. Wiener model with nonlinear functions g_2 and g_3 were able to consistently reproduce radial and femoral pressure waveforms of quality exceeding those from linear FIR model (g_1). Noteworthy feature of all of these three non-linear models is that they are all monotonic. In other words, they are all invertible functions. This aspect is pre-requisite for system identification technique used for aortic pressure estimation.

By fitting arterial pressure waveforms to Wiener system it is found that linear FIR filter in series with nonlinear memoryless function (preferably a higher order polynomial) exhibited higher accuracy arterial transmission channel model as compared to mere linear FIR filter. Also, aortic-to-radial channels were commonly seen to be more nonlinear than aortic-to-femoral channels. As computed nonlinear function is invertible, this validates the present black box system identification approach, which proves to be invaluable in studying arterial system characteristics. It can also be used to accurately simulate hemodynamic signals like aortic, radial and femoral pressure signals. In conclusion, our study validates the nonlinear Wiener model for aortic-to-radial and aortic-to-femoral arterial system– including the nonlinear function which can be further utilized for interpretation of underlying biomechanical properties.

With this Wiener System based model when nonlinear multichannel blind system identification is applied results (as shown in Chapter 4) demonstrate far superior P_a estimation than that from linear MBSI. It can be seen that the non-linear MBSI performs consistently well for all different patient datasets over variety of physiological conditions. Nonlinear MBSI estimated P_a was able to consistently reproduce TW, SP and DP of

quality exceeding those from radial BP, femoral BP along with linear MBSI generated P_a. Other interesting finding is that in case of non-linear MBSI estimation error reduces with increase in data length. While for linear MBSI estimation error grows with increase in data length. Thus, non-linear MBSI proves to be very robust and adaptive approach for aortic pressure estimation. Also, it provides personalized solution for human arterial system modelling, i.e. system dynamics identification for vascular channels. This accurately estimated aortic pressure waveform can be used to derive valuable clinical information to aid patient bed side assistance.

Key asset of blind system identification approach for aortic pressure estimation is that it does not require any explicit calibration or personalized measurements (which in most cases are invasive measurements). Hence, this method by nature is self-calibrating to account for any inter-personal along with intra-personal vascular dynamics inconstancy. Another advantage of this type of technique is that any measurement errors (e.g. two catheter systems) that are noncoprime, i.e. common between the two measurand peripheral signals, are cancelled out automatically as blind system identification can only detect coprimeness between the two measurands. Presented Blind Identification approach of single input multiple output non-linear Wiener systems for aortic pressure estimation was inspired by comparable research work in literature (Swamy et al., 2007; McCombie et al., 2005; Fazeli et al., 2014). However, their proposals assume the arterial network channels to be linear time invariant systems. Nonetheless, neglecting nonlinearity of hemodynamics to entertain modelling simplicity can cost aortic pressure estimation error. Based on previous studies (Fruzzetti et al., 1997) (Patel and Li, 2017)it has been proven that cardiovascular system is neither linear nor time invariant. This has been mainly

attributed to nonlinear terms in the Navier-Stokes equation (Li et al., 1981) and nonlinear time varying arterial compliance (Li, 2000; Li, 2004).

One of few drawbacks of using blind identification is channel order has to be known as priori. To entertain computational simplicity all the comparable research work on aortic pressure estimation using MBSI had used fixed FIR order across different patient datasets (Swamy et al., 2007; McCombie et al., 2005; Fazeli et al., 2014). It is known that considerable degradation is observed if the channel order is under or overestimated by blind system identification. In this regards, the present investigation proposed technique, perhaps for the first time, estimates channel order preceding arterial system identification. By using effective channel order for MBSI, system identification is optimized which then enhances aortic pressure estimation.

Results of the newly introduced multichannel blind system identification-Gen2 technique (Chapter 5) produced far more accurate estimation of aortic pressure waveform than our previous approach. The present technique performed consistently well for all different patient datasets studied under varied physiological conditions. The method was able to consistently reproduce accurately the systolic pressure, diastolic pressure, as well as the entire aortic pressure waveform. In addition, it is found that in the case of non-linear MBSI estimation error when plotted against Wiener model FIR filter order, it has a convex shape with least error at effective channel order. Thus, non-linear MBSI estimated aortic pressure is optimized by first estimating channel order and then executing MBSI for thus computed channel order. Arterial channel FIR order is expected to change inter and intra patient. As channel order is dynamically estimated before applying MBSI, the current approach can afford a desirable personalized solution for

modeling the hemodynamics of the patient's arterial system and in accurately providing the central aortic pressure waveform for personalized diagnosis and evaluation of therapeutic efficacy.

6.2 Efficacy of impulse responses estimated using blind system identification

6.2.1 Comparison of impulse responses estimated using Blind System Identification with ones estimated using "tfest"

- Aortic-to-radial and aortic-to-femoral impulse responses are computed using two methods:
    - Using blind identification technique (based on my Thesis proposed method): h1 and h2
    - Using MATLAB command "tfest": g1 and g2
- Blind estimated impulse responses were compared with "tfest" estimated impulse responses.
- Below please find aortic-to-radial and aortic-to-femoral impulse responses using these three methods for different patient datasets:

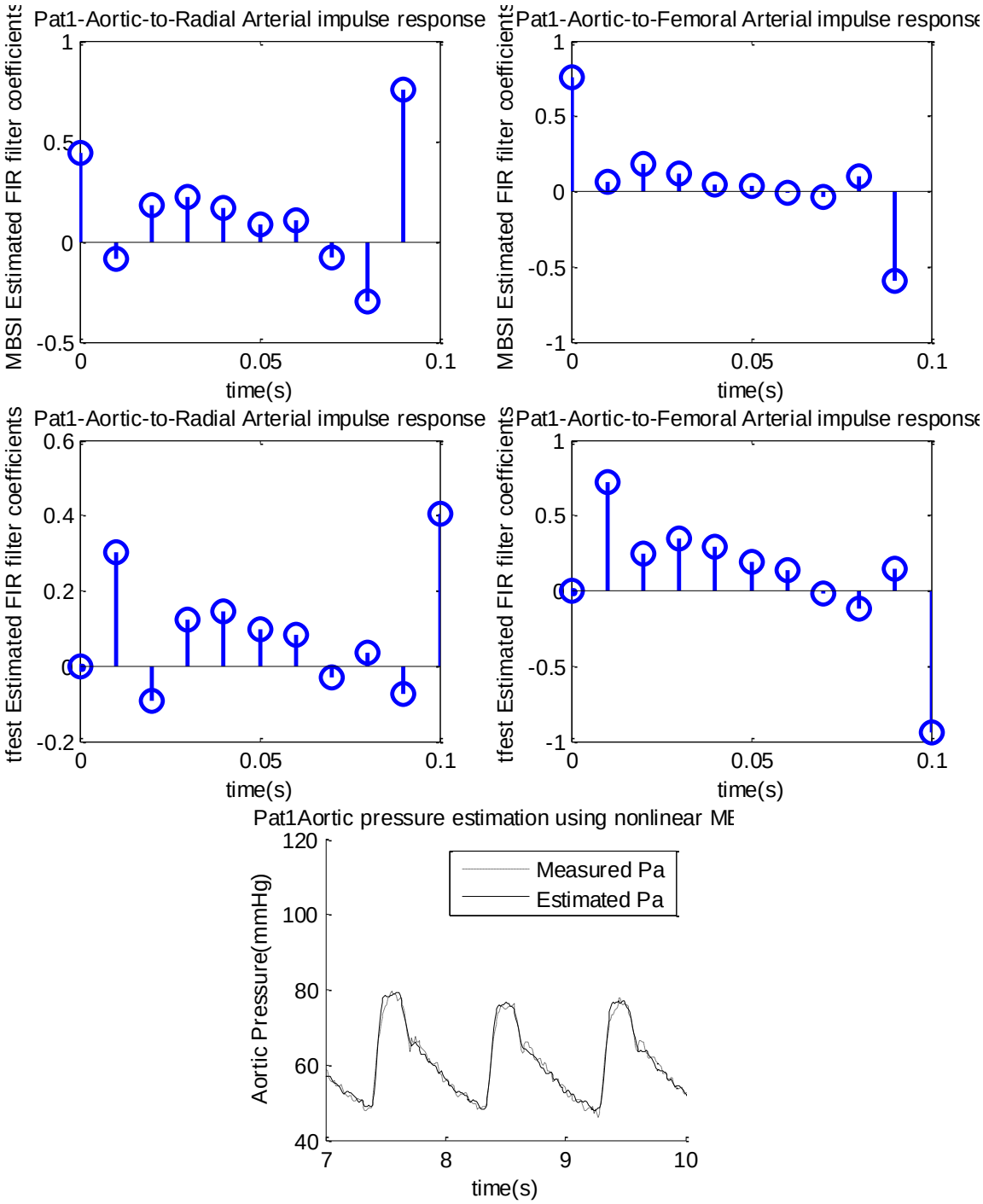

Fig. 6-1. Comparison of impulse responses estimated using MBSI and "tfest" MATLAB command for Dataset 1. Top-left: MBSI estimated h1. Top-right: MBSI estimated g1. Centre-left: MBSI estimated h2. Centre-right: MBSI estimated g2. Bottom: Measured vs. estimated aortic pressure waveform using MBSI

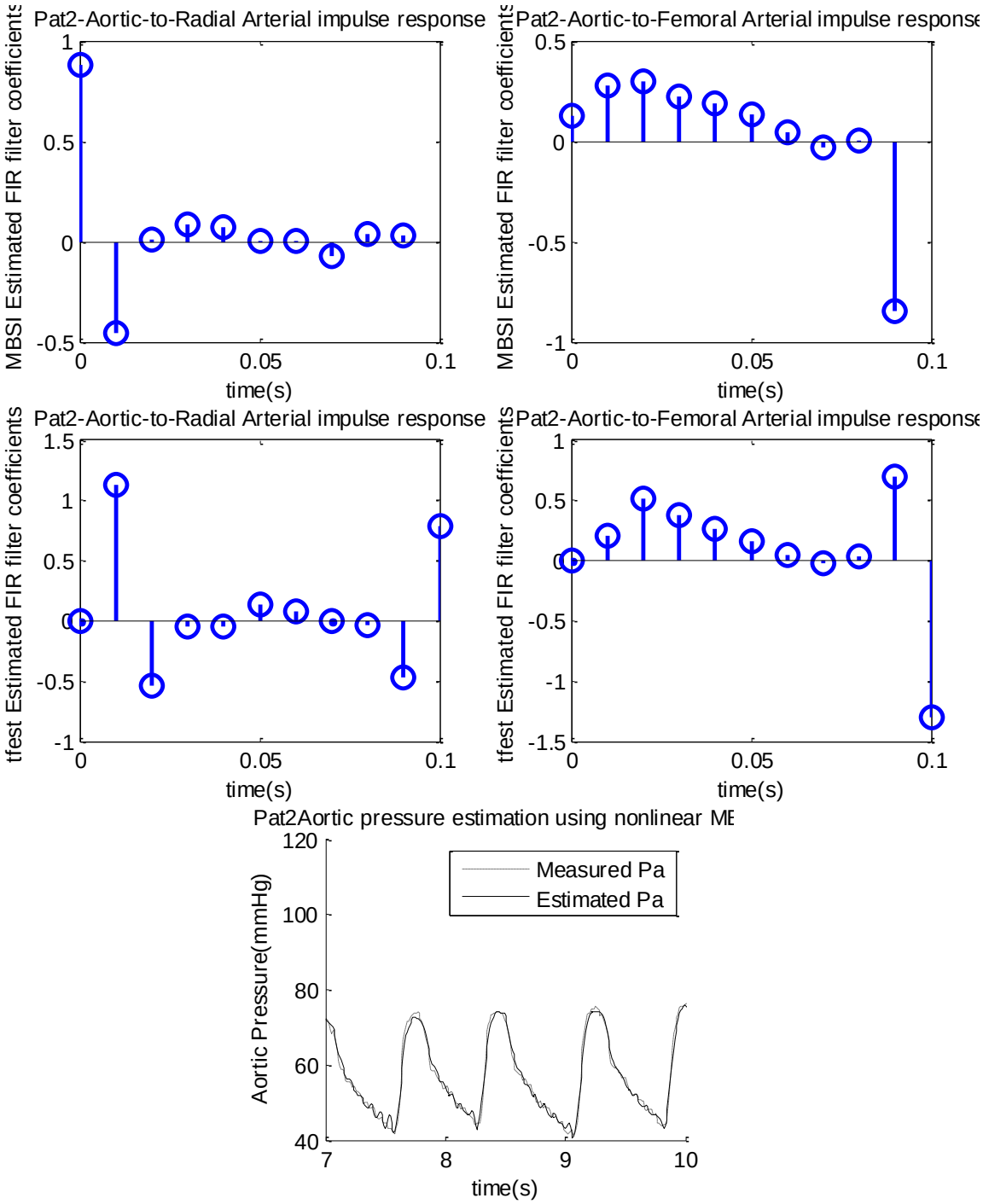

Fig. 6-2. Comparison of impulse responses estimated using MBSI and "tfest" MATLAB command for Dataset 2. Top-left: MBSI estimated h1. Top-right: MBSI estimated g1. Centre-left: MBSI estimated h2. Centre-right: MBSI estimated g2. Bottom: Measured vs. estimated aortic pressure waveform using MBSI

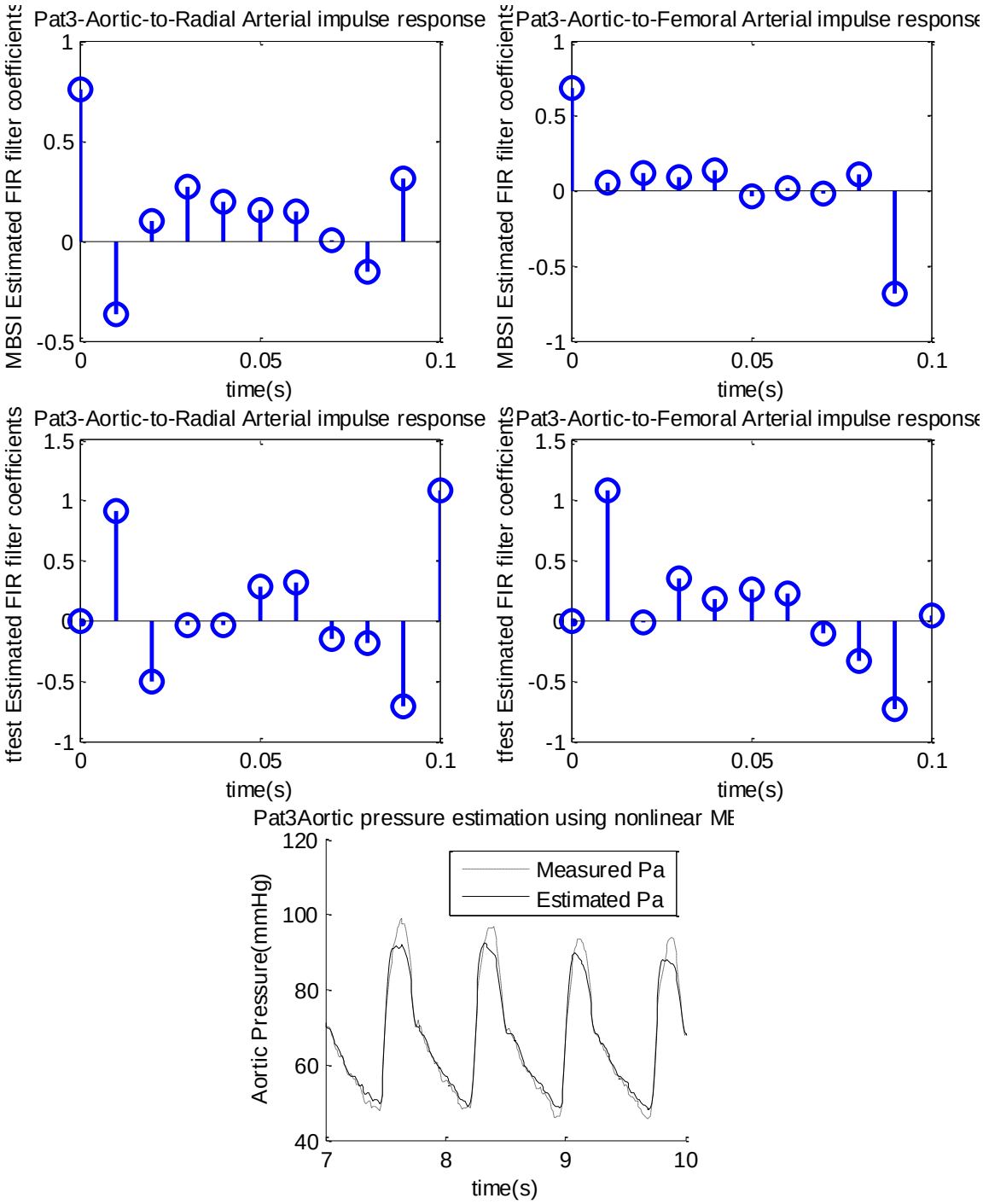

Fig. 6-3. Comparison of impulse responses estimated using MBSI and "tfest" MATLAB command for Dataset 3. Top-left: MBSI estimated h1. Top-right: MBSI estimated g1. Centre-left: MBSI estimated h2. Centre-right: MBSI estimated g2. Bottom: Measured vs. estimated aortic pressure waveform using MBSI

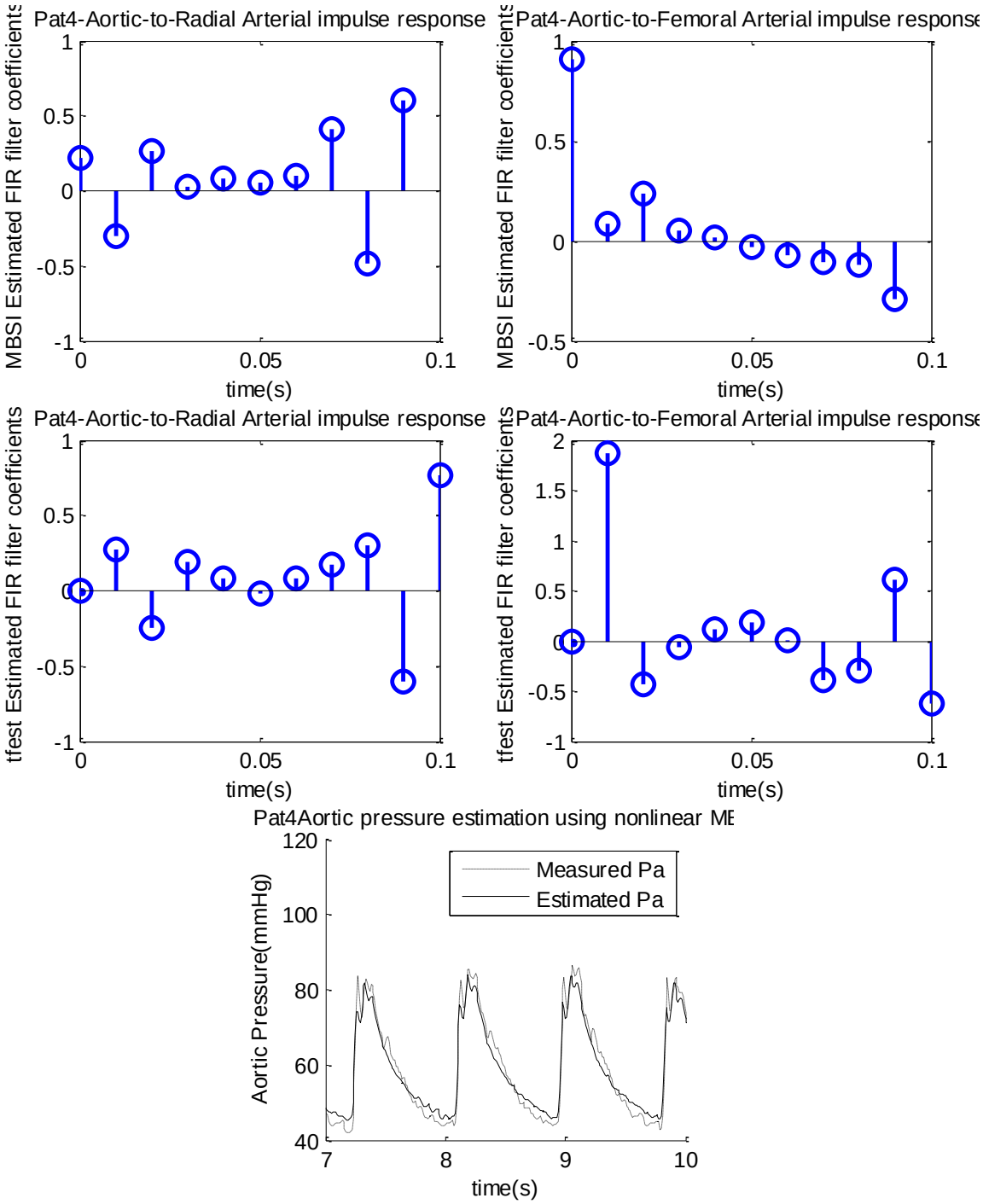

Fig. 6-4. Comparison of impulse responses estimated using MBSI and "tfest" MATLAB command for Dataset 4. Top-left: MBSI estimated h1. Top-right: MBSI estimated g1. Centre-left: MBSI estimated h2. Centre-right: MBSI estimated g2. Bottom: Measured vs. estimated aortic pressure waveform using MBSI

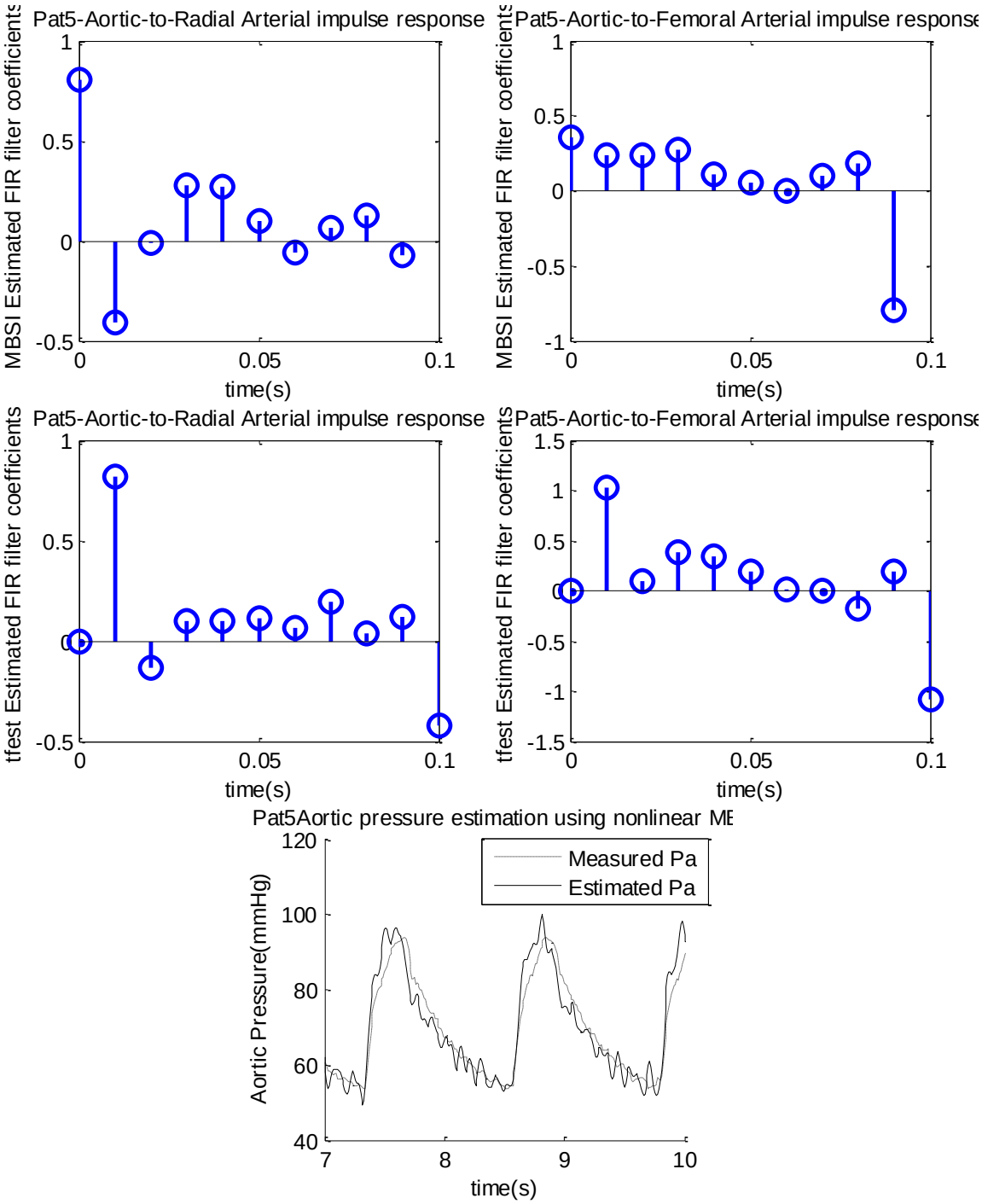

Fig. 6-5. Comparison of impulse responses estimated using MBSI and "tfest" MATLAB command for Dataset 5. Top-left: MBSI estimated h1. Top-right: MBSI estimated g1. Centre-left: MBSI estimated h2. Centre-right: MBSI estimated g2. Bottom: Measured vs. estimated aortic pressure waveform using MBSI

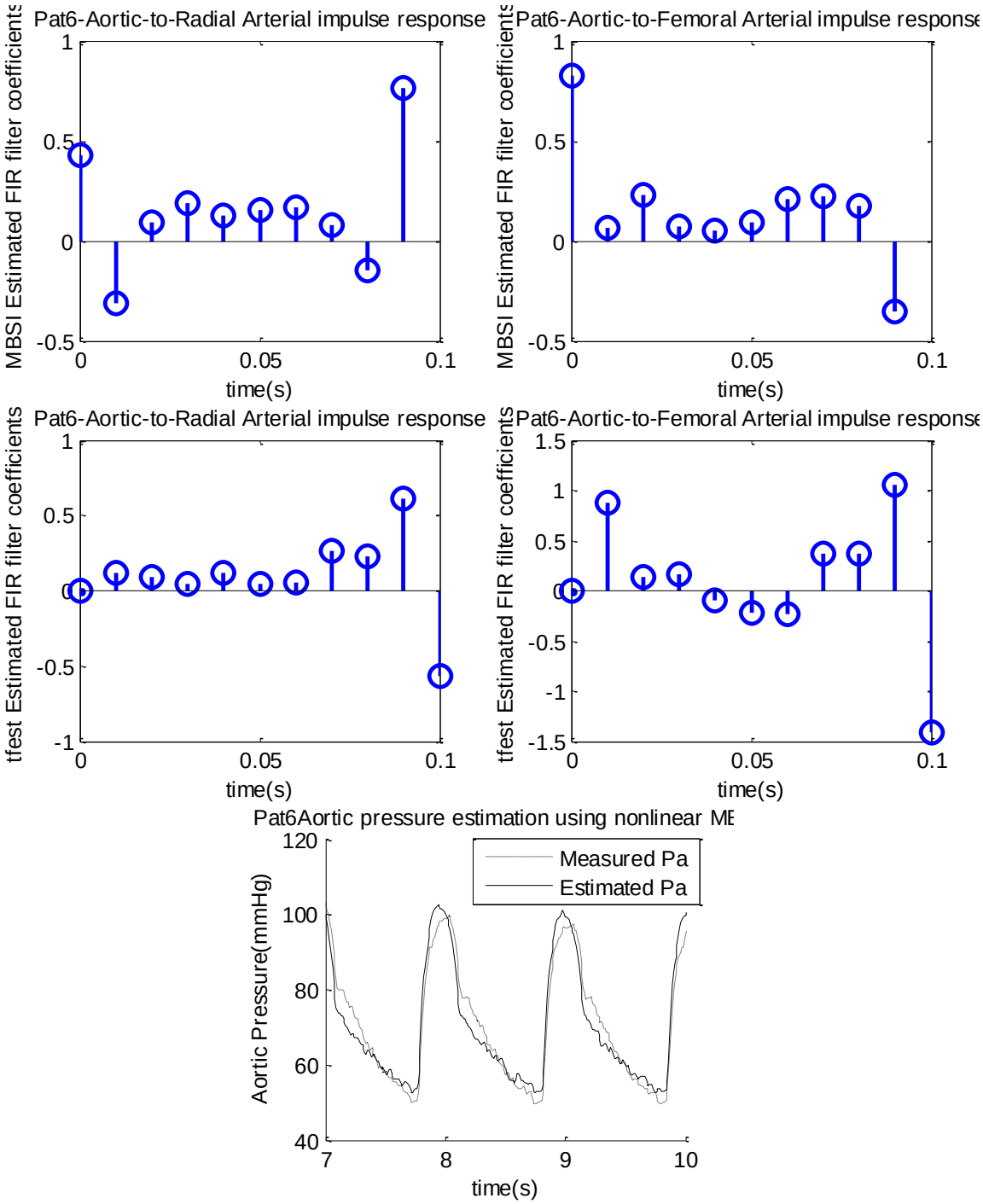

Fig. 6-6. Comparison of impulse responses estimated using MBSI and "tfest" MATLAB command for Dataset 6. Top-left: MBSI estimated h1. Top-right: MBSI estimated g1. Centre-left: MBSI estimated h2. Centre-right: MBSI estimated g2. Bottom: Measured vs. estimated aortic pressure waveform using MBSI

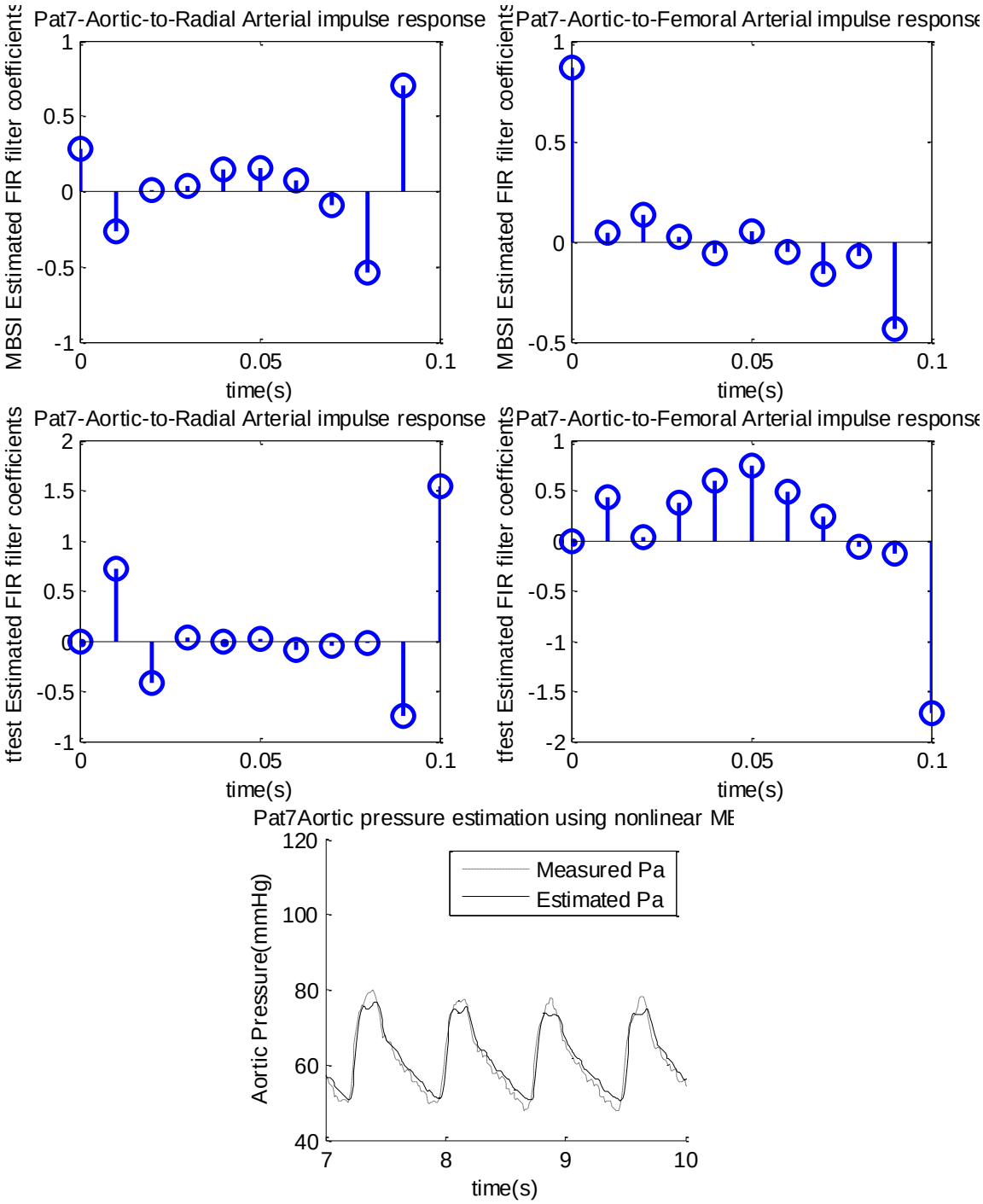

Fig. 6-7. Comparison of impulse responses estimated using MBSI and "tfest" MATLAB command for Dataset 7. Top-left: MBSI estimated h1. Top-right: MBSI estimated g1. Centre-left: MBSI estimated h2. Centre-right: MBSI estimated g2. Bottom: Measured vs. estimated aortic pressure waveform using MBSI

6.2.2 Discussion on comparison of impulse responses estimated using blind identification and "tfest" MATLAB command

- Please note that my model estimated filter coefficients are offset by one sample i.e. h1(0)=g1(1) and h2(0)=g2(1).

- Dataset 1: Overall shape of h1 and h2 is comparable with that of g1 and g2 respectively. for coefficients with mid ranges values in g1 are accurately identified by h1. g1 coefficients with neglible values like g1(7) and g1(8) are correctly identified in h1. first coefficient of g1 is correctly identified by h1. g2(2) through g2(9) seems to be scaled down in h2. Also g2(10) is scaled up in h2.

- Dataset 2: h1(0) through h1(7) looks identical to f(1) through f(8). g1(8) and g1(9) are not correctly identified in h1. g1(1) through f(8) are accurately identified in h1. But h1(8) is different from f(9). Also h1(9) is of lower value than g1(10).

- Dataset 3: g1(1) and g1(2) are identical to h1(0) and h1(1). g1(3), g1(4), g1(7) and g1(8) has identification error in h1(2), h1(3), h1(6) and h1(7). g1(5) and g1(6) seems to be identified well by h1(4) through h1(5) . g1(9) and g1(10) are scaled down in h1(8) through h1(9) . g2(1) through g2(7) seems to be scaled down in h2. g2(9) is shifted by one sample in h2(9) instead of h2(10).

- Dataset 4: g1 looks very identical to h1. g2(1) and g2(10) are scaled to about half value in h2(0) and h2(9). g2(2) and g2(9) are not correctly identified in in h2. Rest all coefficients in g2 are negligible and so is the case in h2.

- Dataset 5: g1(1) is correctly identified by h1(0). g1(2) through g1(9) looks similar to h1(1) through h1(8) except they are scaled up. g1(10) is scaled down in h1(9). g2(1) weight is distributed between h2(0) and h2(1). g2(3) through g2(10) have values similar to that of h2(2) through h2(9).

- Dataset 6: Values of coefficients g1(1) and g1(2) are re-distributed such that g1(1)+g1(2)=h1(0)+h1(1). g1(8) through g1(10) coefficient weights are re distributed in h1(7) through h1(9). Rest of the coefficients in g1 are negligible. g2(1) is similar to h2(0). Coefficients g2(2) through g2(6) are not correctly identified in h2(1) through h2(5). g2(7) and g2(8) look similar to h2(6) and h2(7). g2(9) and g2(10) are scaled up in h2(8) and h2(9).

- Dataset 7: g1(1) and g1(2) are scaled down in h1(0) and h1(1). The coefficients are negligible for g1(3) through g1(8) and also for h1(2) through h1(7). g1(9) and g1(10) are scaled down in h1(8) and h1(9). g2 looks quite different from h2. g2(10) has identical trend h2(9) except that it is scaled down.

- Summary of differences

    - In general it was found that impulse response coefficient with negligible values were not accurately identified by blind system identification.

    - In particular when leading or trailing coefficients are negligible they resulted in system identification error.

    - In some cases it can be seen impulse response with two or more taps/ coefficients with small values were estimated as two consecutive taps with

opposite polarity. In most of the case this type of estimation error (consecutive coefficients with opposite polarity) should not affect as blood pressure waveforms donot have any frequency components more than about 10Hz. But these opposite polarity coefficient could potentially be more susceptible to high frequency noise (say measurement noise).

- Possible reasons for errors in the blind aortic pressure estimations
    - In some of the datasets it is possible the two peripheral sites where pressure waveforms are obtained from are not coprime enough. For example these sites are not distant enough. In this case arterial channel dynamics might have common zeros which is violation to blind system identification technique and hence would result into aortic pressure estimation error.
    - Another potential source of error can be if the catheters used to acquire two peripheral pressure signals have dynamics that are coprime (are not identical) could potentially result in error in Aortic pressure waveform estimation using multi-channel blind system identification technique.

6.2.3 Nonlinear MBSI estimated aortic pressure with same peripheral pressure waveform

- Wiener system model was simulated with same peripheral pressure signal (i.e same radial pressure signal instead of radial and femoral pressure waveform); the aortic pressure estimation method is expected to fail when same peripheral pressures are used.

a. Using same radial pressure signal for multi-channel blind identification for aortic pressure estimation

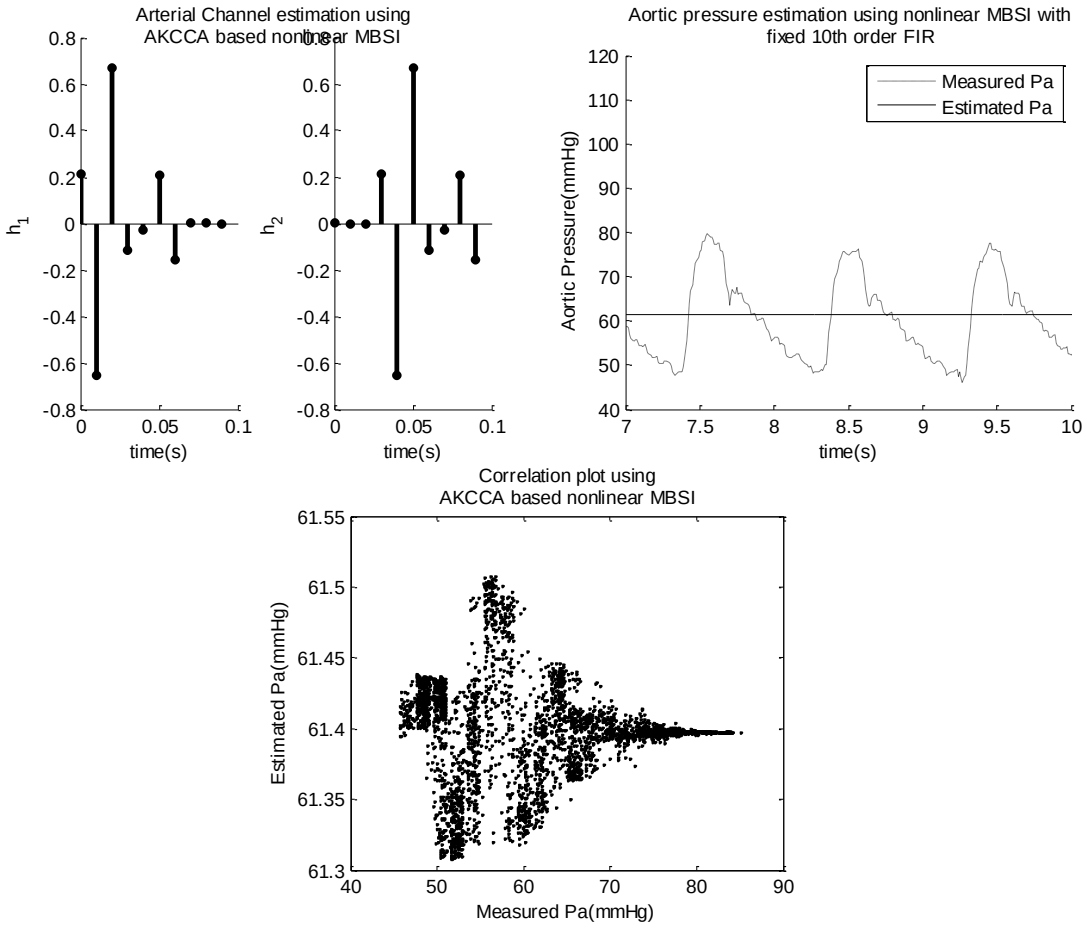

Fig. 6-8. Nonlinear multi-channel blind aortic pressure estimation with same radial pressure signal. Top-left: Nonlinear MBSI estimated arterial channel identification. Top-right: Measured vs. estimated aortic pressure waveform using MBSI. Bottom: Correlation graph for measured versus estimated P_a using nonlinear MBSI

b. Using same femoral pressure signal for multi-channel blind identification for aortic pressure estimation

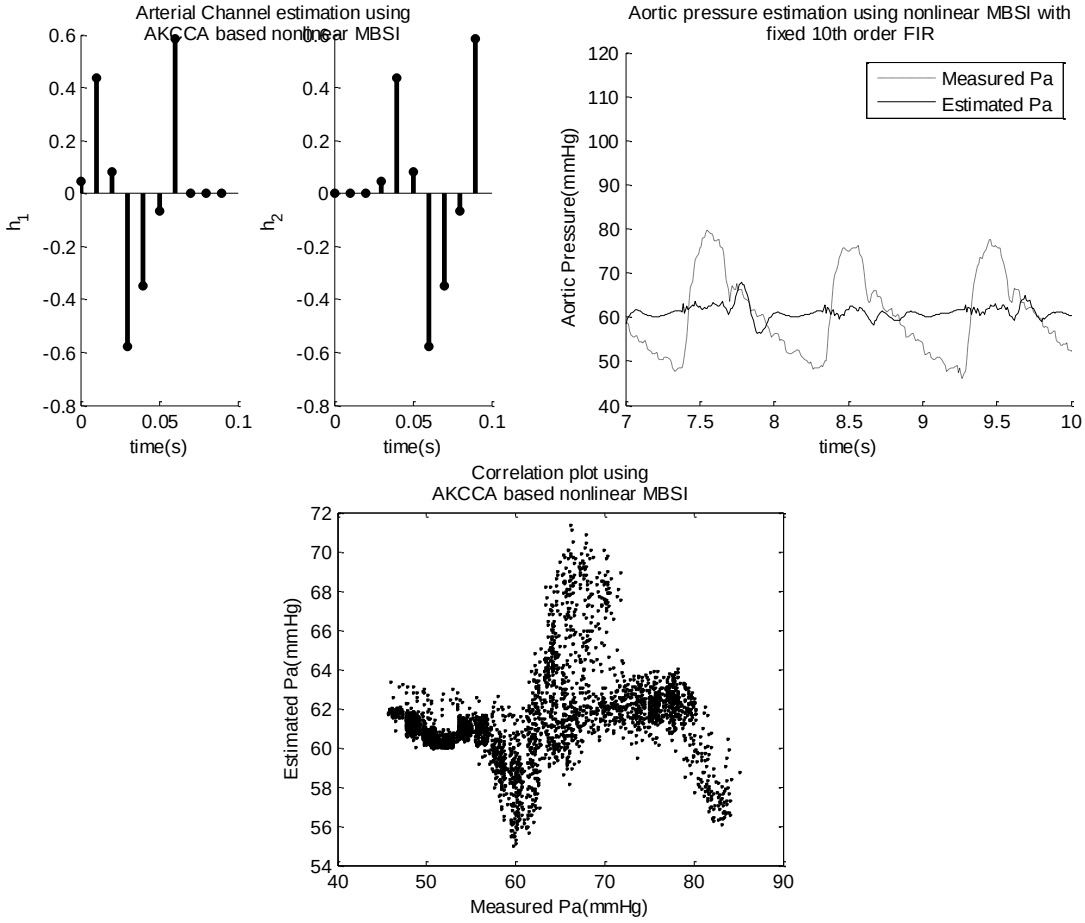

Fig. 6-9. Nonlinear multi-channel blind aortic pressure estimation with same radial pressure signal. Top-left: Nonlinear MBSI estimated arterial channel identification. Top-right: Measured vs. estimated aortic pressure waveform using MBSI. Bottom: Correlation graph for measured versus estimated P_a using nonlinear MBSI

6.2.4 Clinical Significance of Aortic Pressure waveform

Traditional methodology for clinical diagnosis relies on deriving central aortic pressure based on blood pressure measurement at a single peripheral arterial site, i.e. the radial artery pressure. The derivation is based on traditional transfer function approach,

i.e. tfest and that only single pulse transmission path is utilized. The new approach of the thesis utilizes Single Input Multiple Output (SIMO) technique, i.e. aortic pressure is derived based on two peripheral pressure measurement sites, namely, the femoral arterial pressure and the radial arterial pressure. This provides a more comprehensive description of the pulse transmission paths. In particular, the aorta-to-femoral path encompasses the entire transmission path of the aorta. In addition, the thesis has shown that MBSI technique derived aortic pressure is more accurate when compared with traditional transfer function measured aortic pressure.

The MBSI FIR response is characterized by an initial amplitude and a rapid decline (impulse). Deviations from this may signal a diseased state, i.e. interrupted pulse transmission. A severely hypertensive patient may have a very stiff aorta, as such the difference in aorta and femoral pressures may not be too different and impulse amplitude could be drastically reduced. This aspect was proposed as a future study in the thesis.

Since clinical diagnostic indices such as large artery compliance, aortic augmentation index and wave reflections are based on central aortic pressure waveform, the accuracy of MBSI derived aortic pressure demonstrated here, provides the physicians the confidence for computing their diagnostic indices mentioned above and in turn for assessing the state of their patients or their drug effectiveness.

6.2.5 Assumption and Limitation of proposed blind system identification method for aortic pressure estimation

- Full characterization of $\widehat{\boldsymbol{h}}_{\boldsymbol{i}}$ is only possible if the two channels are co-prime or in other words don't have common zeros (Xu et al., 1995).

- Left and right Radial (or Femoral or Carotid) pressures cannot be used as inputs at same time as they are similar.

- Two input pressures on the same transmission path cannot be used for blind aortic pressure estimation, e.g. Left or Right Brachial and Radial arteries.

- Input pressures need to be finite distance apart to allow sufficient resolution (pulse transit time) and waveform differences.

- In general, if any of above mentioned assumption/ limitation is violated could result in estimation error.

6.2.6 Reliability of blind system identification based aortic pressure estimation

- As in any other Blind system identification technique, presented method assumes that the two channels (aortic-to-femoral and aortic-to radial) are well defined by finite impulse response and they are coprime with each other (i.e. their Z transforms don't have any common zeros or poles). From all the test results it can be inferred that this assumption holds in most of the cases as it was demonstrated that estimated aortic pressure waveform aligned very accurately with measured aortic pressure waveform.

- If the catheters used to acquire two peripheral pressure signals have dynamics that are coprime (are not identical) could potentially result in error in Aortic pressure waveform estimation using multi-channel blind system identification technique.

- For the purpose of establishing the methodology and its validation the presented study was performed on only 14 datasets (7 aortic-to-radial and 7 aortic-to-

femoral) collected during cardiac surgery. Preliminary study of proposed blind system identification based aortic pressure estimation demonstrated promising results. However, intensive clinical assessment of this method is suggested for future work. Also, presented approach can be extended to other arterial branches, e.g. aortic-to-carotid.

- Cardiovascular properties are known to vary with time and physiological conditions. It would be worthwhile investigating change in Wiener model with time and also the impact of differing cardiovascular differing interventions.

6.3 Suggestions for Future Work

For the purpose of establishing the methodology and its validation the presented study was performed on only 14 datasets (7 aortic-to-radial and 7 aortic-to-femoral). It would be interesting to perform this study on larger datasets. Presented approach can be extended to other arterial branches, e.g. aortic-to-carotid. Cardiovascular properties are known to vary with time and physiological conditions. It would be worthwhile investigating change in Wiener model (especially nonlinear function) with time and also the impact of differing cardiovascular differing interventions. Higher order polynomial along with other nonlinear functions like exponential and sigmoidal fitting can be employed to further improve Wiener system based model of arterial pulse transmission channel.

The current study can be extended to explore the nonlinear aortic pressure estimation performance at various other cardiovascular conditions. In the presented analysis only two pressure signals were used for multi-channel (two channels) blind system

identification. It would be worthwhile to investigate nonlinear MBSI reconstructed aortic pressure using more than two distinct pressure signals. Also, present studies assumed the memoryless invertible nonlinear function for SIMO Wiener system to be identical for both the channels. Nonlinear blind identification algorithm should be challenged to perform blind system identification for non-identical nonlinear functions for the two channels of arterial system.

References

World Health Organization-International Society of Hypertension Guidelines for the Management of Hypertension. Guidelines Subcommittee. J Hypertens. 1999;17(2):151-183.

Abed-Meraim K, Qiu W, Hua Y. Blind system identification. Proceedings of the IEEE 1997;85(8):1310-1322.

Abed-Meraim K, E Moulines, P Loubaton. Prediction error method for second-order blind identification. IEEE Transactions on Signal Processing 1997;45(3):694-705.

Berger D, Li J K-J. Temporal relationship between left ventricular and arterial system elastances. IEEE Trans Biomed Eng. 1992;39(4):404-410.

Boutouyrie P, Achouba A, Trunet P, Laurent S, EXPLOR Trialist Group. Amlodipine-valsartan combination decreases central systolic blood pressure more effectively than the amlodipine-atenolol combination the EXPLOR Study. Hypertension 2010;55(6):1314-1322.

Chen CH, Nevo E, Fetics B, Pak PH, Yin FC, Maughan WL, Kass DA. Estimation of central aortic pressure waveform by mathematical transformation of radial tonometry pressure validation of generalized transfer function. Circulation 1997;95(7):1827-1836.

Chen CH, Ting CT, Nussbacher A, Nevo E, Kass DA, Pak P, Wang SP, Chang MS, Yin FC. Validation of carotid artery tonometry as a means of estimating augmentation index of ascending aortic pressure. Hypertension 1996;27(2):168-175.

Collins R, Peto R, MacMahon S, Hebert P, Fiebach N, Eberlein K, Godwin J, Qizilbash N, Taylor J, Hennekens C. Blood pressure, stroke, and coronary heart disease. Part 2, Short-term reductions in blood pressure: overview of randomised drug trials in their epidemiological context. Lancet. 1990;335(8693):827-838.

Drzewiecki GM, Melbin J, Noordergraaf A. Arterial tonometry: review and analysis. Journal of biomechanics 1983;16(2):141-152.

Fazeli N, Kim C, Rashedi M, Chappell A, Wang S, MacArthur R, McMurtry M, Finegan B, Hahn J. Subject-specific estimation of central aortic blood pressure via system identification: preliminary in-human experimental study. Med Biol Eng Comput. 2014;52(10):895-904.

Fetics B, Nevo E, Chen CH, Kass D. Parametric model derivation of transfer function for noninvasive estimation of aortic pressure by radial tonometry. Biomedical Engineering, IEEE Transactions on 1999;46(6):698-706.

Fogliardi R, Di Donfrancesco M, Burattini R. Comparison of linear and nonlinear formulations of the three-element windkessel model. American Journal of Physiology-Heart and Circulatory Physiology 1996;271(6):H2661-H2668.

Fruzzetti K, Palazoğlu A, McDonald K. Nolinear model predictive control using Hammerstein models. Journal of process control 1997;7(1):31-41.

Gao M, Cheng HM, Sung SH, Chen CH, Olivier NB, Mukkamala R. Estimation of Pulse Transit Time as a Function of Blood Pressure Using a Nonlinear Arterial Tube-Load Model. IEEE Transactions on Biomedical Engineering 2016;PP(99):1-1.

Guala A, Camporeale C, Ridolfi L, Mesin L. Non-invasive aortic systolic pressure and pulse wave velocity estimation in a primary care setting: An in silico study. Medical Engineering \& Physics 2017;42:91-98.

Guanghan Xu, Hui Liu, Lang Tong, T Kailath. A least-squares approach to blind channel identification. IEEE Transactions on Signal Processing 1995;43(12):2982-2993.

Gürelli MI, Nikias CL. EVAM: An eigenvector-based algorithm for multichannel blind deconvolution of input colored signals. Signal Processing, IEEE Transactions on 1995;43(1):134-149.

Hardoon DR, Szedmak S, Shawe-Taylor J. Canonical correlation analysis: An overview with application to learning methods. Neural computation 2004;16(12):2639-2664.

Hotelling H. Relations between two sets of variates. Biometrika 1936;28(3/4):321-377.

Imholz BP, Wieling W, van Montfrans GA, Wesseling KH. Fifteen years experience with finger arterial pressure monitoring. Cardiovascular research 1998;38(3):605-616.

Jeon YJ. Estimation of an Aortic Pressure Waveform from Radial Pulse using ARX Model. *World Congress on Medical Physics and Biomedical Engineering 2006: August 27 -- September 1, 2006 COEX Seoul, Korea ``Imaging the Future Medicine''*. Springer Berlin Heidelberg; 2007:783-786.

Karaaslan F, Denizhan Y, Kayserilioglu A, Gulcur H. Long-term mathematical model involving renal sympathetic nerve activity, arterial pressure, and sodium excretion. Ann Biomed Eng. 2005;33(11):1607-1630.

Karakutuk S, T E Tuncer. Channel Matrix Recursion for Blind Effective Channel Order Estimation. IEEE Transactions on Signal Processing 2011;59(4):1642-1653.

Karamanoglu M, Feneley MP. On-line synthesis of the human ascending aortic pressure pulse from the finger pulse. Hypertension 1997;30(6):1416-1424.

Karamanoglu M, Gallagher DE, Avolio AP, O'Rourke MF. Pressure wave propagation in a multibranched model of the human upper limb. American Journal of Physiology-Heart and Circulatory Physiology 1995;269(4):H1363-H1369.

Kelly R, Karamanoglu M, Gibbs H, Avolio A, O'Rourke M. Noninvasive carotid pressure wave registration as an indicator of ascending aortic pressure. J Vasc Med Biol 1989;1:241-247.

Kerkhof PLM, Yasha Kresh J, Li J K-J., Heyndrickx GR. Left ventricular volume regulation in heart failure with preserved ejection fraction. Physiol Rep 2013;1(4):e00077.

Khoo, Wiley-IEEE Press: Physiological Control Systems: Analysis, Simulation, and Estimation - [Internet]. [updated 2017; cited 4/7/2017]. Available from: http://www.wiley.com/WileyCDA/WileyTitle/productCd-0780334086,miniSiteCd-IEEE2.html

Lang Tong, Qing Zhao. Joint order detection and blind channel estimation by least squares smoothing. IEEE Transactions on Signal Processing 1999;47(9):2345-2355.

Leeson C, Whincup P, Cook D, Mullen M, Donald A, Seymour C, Deanfield J. Cholesterol and arterial distensibility in the first decade of life: a population-based study. Circulation. 2000;101(13):1533-1538.

Li J K-J. Pulse Pressure, Arterial Compliance and Wave Reflection Under Differential Vasoactive and Mechanical Loading. Cardiovascular Engineering 2010;10(4):170-175.

Li J K-J., Cui T, Drzewiecki G. A nonlinear model of the arterial system incorporating a pressure-dependent compliance. IEEE Trans Biomed Eng. 1990;37(7):673-678.

Li J K-J., Melbin J, Riffle R, Noordergraaf A. Pulse wave propagation. Circ Res. 1981;49(2):442-452.

Li J K-J., Van B, Noordergraaf A. Fluid-filled blood pressure measurement systems. J Appl Physiol. 1976;40(5):839-843.

Li J K-J., Zhu J, Nanna M. Computer modeling of the effects of aortic valve stenosis and arterial system afterload on left ventricular hypertrophy. Comput Biol Med. 1997;27(6):477-485.

Li J K-J. Time domain resolution of forward and reflected waves in the aorta. IEEE transactions on biomedical engineering 1986;8(BME-33):783-785.

Li J K-J. A new description of arterial function: The compliance-pressure loop. Angiology 1998;49(7):543-548.

Li J K-J. The Arterial Circulation: Physical Principles and Clinical Applications. Springer Science & Business Media; 2000. 271 p.

Li J K-J. Dynamics of the vascular system. World scientific; 2004.

Li J K-J. Zhu Y. Arterial compliance and its pressure dependence in hypertension and vasodilation. Angiology 1994;45(2):113-117.

Liavas A, Regalia P. On the behavior of information theoretic criteria for model order selection. IEEE Transactions on Signal Processing 2001;49(8):1689-1695.

Liavas A, Regalia P, J P Delmas. Blind channel approximation: effective channel order determination. IEEE Transactions on Signal Processing 1999;47(12):3336-3344.

Liavas A, Regalia P, Delmas JP. On the robustness of the linear prediction method for blind channelidentification with respect to effective channelundermodeling/overmodeling. IEEE Transactions on Signal Processing

MacMahon S, Peto R, Cutler J, Collins R, Sorlie P, Neaton J, Abbott R, Godwin J, Dyer A, Stamler J. Blood pressure, stroke, and coronary heart disease. Part 1, Prolonged differences in blood pressure: prospective observational studies corrected for the regression dilution bias. Lancet. 1990;335(8692):765-774.

Marchais SJ, Guerin AP, Pannier BM, Levy BI, Safar ME, London GM. Wave reflections and cardiac hypertrophy in chronic uremia. Influence of body size. Hypertension 1993;22(6):876-883.

Martin H, Hu J, Gennser G, Norman M. Impaired endothelial function and increased carotid stiffness in 9-year-old children with low birthweight. Circulation. 2000;102(22):2739-2744.

McCombie DB, Reisner AT, Asada HH. Laguerre-model blind system identification: cardiovascular dynamics estimated from multiple peripheral circulatory signals. Biomedical Engineering, IEEE Transactions on 2005;52(11):1889-1901.

Mohiaddin R, Underwood S, Bogren H, Firmin D, Klipstein R, Rees R, Longmore D. Regional aortic compliance studied by magnetic resonance imaging: the effects of age, training, and coronary artery disease. Br Heart J. 1989;62(2):90-96.

Moulines E, P Duhamel, J F Cardoso, S Mayrargue. Subspace methods for the blind identification of multichannel FIR filters. IEEE Transactions on Signal Processing 1995;43(2):516-525.

Murgo JP, Westerhof N, Giolma JP, Altobelli SA. Aortic input impedance in normal man: relationship to pressure wave forms. Circulation 1980;62(1):105-116.

Nichols WW, O'Rourke MF, Avolio AP, Yaginuma T, Murgo JP, Pepine CJ, Conti CR. Effects of age on ventricular-vascular coupling. The American journal of cardiology 1985;55(9):1179-1184.

Noordergraaf A. Circulatory System Dynamics. 1978;

Noordergraaf A. Blood in Motion. 1 ed. Springer Science & Business Media; 2011. 323 p.

O'Rourke M, Kelly R, Avolio A. The Arterial Pulse, Lea & Febiger. Philadelphia, PA 1992;

Papaioannou TG, Karageorgopoulou TD, Sergentanis TN, Protogerou AD, Psaltopoulou T, Sharman JE, Weber T, Blacher J, Daskalopoulou SS, Wassertheurer S, others.

Accuracy of commercial devices and methods for noninvasive estimation of aortic systolic blood pressure a systematic review and meta-analysis of invasive validation studies. J Hypertens 2016;34(7):1237-1248.

Patel A, Li J K-J. Validation of a novel nonlinear black box Wiener System model for arterial pulse transmission. Comput Biol Med 2017;88:11-17.

Patel A, Li J K-J., Finegan B, McMurtry M. Aortic Pressure Estimation using Blind Identification Approach on Single Input Multiple Output Non-linear Wiener systems. IEEE Trans Biomed Eng. 2017;:10.

A neural network for estimation of aortic pressure from the radial artery pressure pulse. 2001 Conference Proceedings of the 23rd Annual International Conference of the IEEE Engineering in Medicine and Biology Society; 2001. 239 vol.1 p.

Rashedi M, Fazeli N, Chappell A, Wang S, Macarthur R, Sean M, Finegan B, Hahn J. Comparative study on tube-load modeling of arterial hemodynamics in humans. J Biomech Eng. 2013;135(3):31005.

Salomaa V, Riley W, Kark J, Nardo C, Folsom A. Non-insulin-dependent diabetes mellitus and fasting glucose and insulin concentrations are associated with arterial stiffness indexes. The ARIC Study. Atherosclerosis Risk in Communities Study. Circulation. 1995;91(5):1432-1443.

Schölkopf B, Herbrich R, Smola AJ. A generalized representer theorem. Computational learning theory 2001;:416-426.

Segers P, Carlier S, Pasquet A, Rabben S, Hellevik L, Remme E, De Backer T, De Sutter J, Thomas J, Verdonck P. Individualizing the aorto-radial pressure transfer function: feasibility of a model-based approach. American Journal of Physiology-Heart and Circulatory Physiology 2000;279(2):H542-H549.

Shimizu M, Kario K. Review: Role of the augmentation index in hypertension. Therapeutic advances in cardiovascular disease 2008;2(1):25-35.

Söderström S, Nyberg G, O'Rourke M, Sellgren J, Ponten J. Can a clinically useful aortic pressure wave be derived from a radial pressure wave?†. British journal of anaesthesia 2002;88(4):481-488.

Stergiopulos N, Segers P, Westerhof N. Use of pulse pressure method for estimating total arterial compliance in vivo. Am J Physiol. 1999;276(2 Pt 2):H424-H428.

Stergiopulos N, Westerhof BE, Westerhof N. Physical basis of pressure transfer from periphery to aorta: a model-based study. American Journal of Physiology-Heart and Circulatory Physiology 1998;274(4):H1386-H1392.

Stok WJ. Evaluation of aortic blood pressure waveform using an adaptive peripheral pressure transfer function.

Sugimachi M, Shishido T, Miyatake K, Sunagawa K. A new model-based method of reconstructing central aortic pressure from peripheral arterial pressure. Jpn J Physiol. 2001;51(2):217-222.

Sugimachi M, Shishido T, Miyatake K, Sunagawa K. A new model-based method of reconstructing central aortic pressure from peripheral arterial pressure. The Japanese journal of physiology 2001;51(2):217-222.

Swamy G, Ling Q, Li T, Mukkamala R. Blind identification of the aortic pressure waveform from multiple peripheral artery pressure waveforms. American Journal of Physiology-Heart and Circulatory Physiology 2007;292(5):H2257-H2264.

Swamy G, Xu D, Olivier NB, Mukkamala R. An adaptive transfer function for deriving the aortic pressure waveform from a peripheral artery pressure waveform. American Journal of Physiology-Heart and Circulatory Physiology 2009;297(5):H1956-H1963.

Van Vaerenbergh S, Via J, Santamaria I. Blind identification of SIMO Wiener systems based on kernel canonical correlation analysis. Signal Processing, IEEE Transactions on 2013;61(9):2219-2230.

Varanini M, Massoni M, Marraccini P, Kozakova M, Djukic G, Bamoshmoosh M, Testa R, Vittone F, Palombo C. Non-invasive estimation of central aortic pressure from radial artery tonometry by neural networks. Computers in Cardiology, 2003 2003;:501-504.

Via J, Santamaria I, Perez J. Effective channel order estimation based on combined identification/equalization. Signal Processing, IEEE Transactions on 2006;54(9):3518-3526.

Waddell TK, Dart AM, Medley TL, Cameron JD, Kingwell BA. Carotid pressure is a better predictor of coronary artery disease severity than brachial pressure. Hypertension 2001;38(4):927-931.

Wesseling K, Jansen J, Settels J, Schreuder J. Computation of aortic flow from pressure in humans using a nonlinear, three-element model. Journal of applied physiology 1993;74(5):2566-2573.

Westerhof BE, Guelen I, Stok WJ, Wesseling KH, Spaan JA, Westerhof N, Bos WJ, Stergiopulos N. Arterial pressure transfer characteristics: effects of travel time. American Journal of Physiology-Heart and Circulatory Physiology 2007;292(2):H800-H807.

Xiao H, Qasem A, Butlin M, Avolio A. Estimation of aortic systolic blood pressure from radial systolic and diastolic blood pressures alone using artificial neural networks. J Hypertens 2017;35(8):1577-1585.

Xu G, Liu H, Tong L, Kailath T. A least-squares approach to blind channel identification. Signal Processing, IEEE Transactions on 1995;43(12):2982-2993.